Investigations on Performance Analysis of Universal Filtered Multicarrier System

Submitted in partial fulfillment of the requirements
for the award of the degree of
DOCTOR OF PHILOSOPHY

by

VIJAYA DURGA CHINTALA

(Roll No: 718146)

Supervisor:

Dr. S. Anuradha
Associate Professor

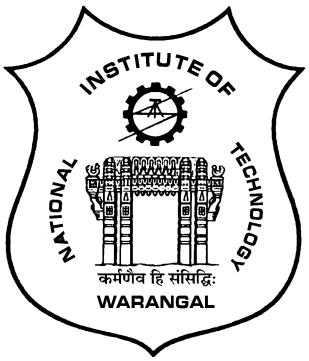

DEPARTMENT OF ELECTRONICS AND COMMUNICATION ENGINEERING
NATIONAL INSTITUTE OF TECHNOLOGY WARANGAL
TELANGANA STATE-506004, INDIA

2021

Dedicated to

My family & Gurus

DECLARATION

This is to certify that the work presented in the thesis entitled "**Investigations on Performance Analysis of Universal Filtered Multicarrier System**" is a bonafide work done by me under the supervision of **Dr. S. Anuradha**, Assosciate Professor, Department of Electronics and Communication Engineering, National Institute of Technology Warangal, India and was not submitted elsewhere for the award of any degree.

I declare that this written submission represents my ideas in my own words and where others' ideas or words have been included, I have adequately cited and referenced the original sources. I also declare that I have adhered to all principles of academic honesty and integrity and have not misrepresented or fabricated or falsified any idea / data / fact / source in my submission. I understand that any violation of the above will be a cause for disciplinary action by the Institute and can also evoke penal action from the sources which have thus not been properly cited or from whom proper permission has not been taken when needed.

Vijaya Durga Chintala

(Roll No: 718146)

Date: .....

DEPARTMENT OF ELECTRONICS AND COMMUNICATION ENGINEERING

NATIONAL INSTITUTE OF TECHNOLOGY WARANGAL

TELANGANA STATE-506004, INDIA

CERTIFICATE

This is to certify that the thesis entitled "**Investigations on Performance Analysis of Universal Filtered Multicarrier System**", which is being submitted by **Ms. Vijaya Durga Chintala (Roll No: 718146)**, in partial fulfillment for the award of the degree of Doctor of Philosophy to the Department of Electronics and Communication Engineering of National Institute of Technology Warangal, is a record of bonafide research work carried out by him under my supervision and has not been submitted elsewhere for any degree.

Dr. S. Anuradha
(Supervisor)
Associate Professor
Department of E.C.E.
N.I.T. Warangal
Warangal - 506004, India

ACKNOWLEDGEMENTS

First of all, I would like to express my sincere gratitude to my supervisor Dr. S. Anuradha for her guidance and support. Her extreme energy, encouragement, and immense knowledge that resolved all my queries have always been a constant source of motivation throughout my Ph.D. study and research. Her passion and enthusiasm for teaching, sharing his knowledge and motivating students have not only inspired me, but has also made every individual an ardent academic disciple who has been taught by her. Being student-responsive and an effective mentor, her guidance helped me throughout thick and thin periods of my research, for which I am honestly indebted and thankful throughout my career and lifetime.

I am also grateful to Prof. L. Anjaneyulu, Head of the department, Department of Electronics and Communication Engineering, NIT Warangal for his valuable suggestions and support that he shared during my research tenure.

Besides my supervisor, I take this privilege to thank Doctoral Scrutiny Committee members, Dr. D. Vakula, Associate professor, Department of Electronics and Communication Engineering, NIT Warangal, and Dr. A. Benerji Babu, Associate Professor, Department of Mathematics, NIT Warangal for their continuous support, suggestions and advices during my research period whenever required.

It is my pleasure to show my indebtedness to my co-scholars at NIT like K Shriram Tej, D Srikar, S Subba Rao, and P Raveendra for their help during the course of this work.

I find no words inadequate to express any form of acknowledgment to my father, mother, husband, son, daughter, and sisters for their love, support and patience for making my dream come true.

Finally, I thank God, for filling me every day with new hopes, strength, purpose and faith.

ABSTRACT

Universal filtered multi carrier (UFMC), a promising 5G waveform, is being widely employed in short burst communications. The UFMC waveform merges the simplicity of orthogonal frequency division multiplexing (OFDM) and robustness of filter bank multi carrier (FBMC). The FBMC is also one of the popular 5G waveforms but suffers from long filter length. The UFMC utilizes per sub-band filtering, whereas FBMC utilizes per sub-carrier filtering. Hence, the UFMC system does not demand long filter length and successfully eliminates the out-of-band (OOB) radiations. Also, UFMC does not use cyclic prefix like OFDM. So, UFMC provides high spectral efficiency when compared to OFDM. Additionally, UFMC systems are more attractive since they provide relaxation to carrier frequency offset.

In this thesis, we first analyze the performance of channel estimation techniques for UFMC system. A comb type pilot-aided channel estimation that has pilot tones at the periodically-located subcarriers is employed for UFMC system. The least-square (LS) and minimum-mean-square-error (MMSE) techniques are applied to estimate channel characteristics at the receiver. The MMSE technique can provide better estimation accuracy and BER performance than LS technique. Although UFMC has attractive features, it suffers from high peak-to-average power ratio (PAPR) like other multi carrier techniques. High PAPR reduces the efficiency of the power amplifier and may cause degradation in the system performance. This problem is more important in the uplink since efficiency of a power amplifier is critical due to limited battery power in a mobile terminal. Hence, high PAPR increases energy consumption. Since energy efficiency is one of the essential requirements of 5G, energy consumption should be minimum. Therefore, there is a need to reduce PAPR in 5G UFMC systems.

An optimal hybrid transform is employed to reduce the PAPR of the UFMC system. The proposed hybrid transform is the combination of modified exponential companding (MEC) and clipping scheme. The MEC scheme employs two companding levels and one threshold parameter. Therefore, it can offer more design flexibility than other companding schemes. Moreover, the performance analysis of various companding schemes for UFMC system is investigated. The companding scheme that transforms the statistical distribution of UFMC amplitude signals into quasiuniform distribution offers enhanced system performance when compared to other companding schemes. Moreover, the combination of proposed companding and clipping further reduces the PAPR of UFMC system. Additionally, the UFMC system with the proposed hybrid schemes are verified by employing wireless open-access research platform (WARP) as hardware over real time channel.

A pilot-based time domain channel estimation (CE) along with PAPR reduction is proposed for UFMC system. The pilots that are inserted in time domain not only estimate the channel behavior but also can be used in the reduction of PAPR. For PAPR reduction, a linear companding scheme, which can treat amplitudes of the UFMC signal separately with a different scale, is proposed. The proposed companding scheme offers more design flexibility and better performance gains by using two inflexion points. However, the proposed companding scheme requires side information (SI) to perform de-companding at the receiver. The transmission of SI decreases the data efficiency, so a pilot-assisted UFMC system that can perform both data recovery and PAPR reduction without the requirement of SI transmission is proposed. Furthermore, a hybrid transform, which improves PAPR performance by employing clipping scheme to the linear companded signal, is proposed. Moreover, the proposed joint time domain CE with hybrid PAPR reduction scheme of UFMC system are validated over real time by employing WARP board.

The UFMC waveform is combined with the massive multi-user multiple-input and multiple output (MU-MIMO) technology to meet the desired needs of future wireless networks. A nonlinear quantized precoder called squared-infinity norm Douglas-Rachford splitting (SQUID), which generates signals with constant envelope, is proposed. The proposed SQUID precoder reduces the power consumption and MUI of UFMC based massive MU-MIMO systems. Moreover, a piecewise linear companding (PLC) scheme, which further reduces the PAPR by employing two threshold values and one companding parameter, is also proposed. The proposed UFMC based massive MU-MIMO with quantized nonlinear SQUID precoding provides better performance than quantized linear precoders.

Contents

List of Figures

List of Tables

List of Abbreviations

3GPP 3rd Generation Partnership Project

ACE Active Constellation Extension

ACI Adjacent Channel Interference

AWGN Additive White Gaussian Noise

BER Bit Error Rate

CCDF Complementary Cumulative Distribution Function

CDF Cumulative Distributive Function

CE Channel Estimation

CP Cyclic Prefix

CR Clipping Ratio

CSI Channel State Information

DCT Discrete Cosine Transform

DFT Discrete Fourier Transform

EC Exponential Companding

FBMC Filter Bank Multiple Carrier

FDE Frequency Domain Equalization

FFT Fast Fourier Transform

FMT Filtered Multi Tone

FIR Finite Impulse Response

GFDM Generalized Frequency Division Multiplexing

HPA High Power Amplifier

IBO Input Back-Off

ICI Inter Carrier interference

IFFT Inverse Fast Fourier Transform

ISI Inter Symbol Interference

LC Linear Companding

LTE Long Term Evolution

LS Least Square

MCM Multi Carrier Modulation

MEC Modified Exponential Companding

MIMO Multiple Input Multiple Output

MMSE Minimum Mean Square Error

MSE Mean Square Error

MU Multi User

NDC No De-Companding

OFDM Orthogonal Frequency Division Multiplexing

OFDMA Orthogonal Frequency Division Multiple Access

OOB Out-Of-Band

PA Power Amplifier

PAPR Peak-to-Average Power Ratio

PDF Probability Density Function

PLC Piecewise Linear Companding

PSD Power Spectral Density

PTS Partial Transmit Sequence

QAM Quadrature Amplitude Modulation

SC-FDMA Single Carrier Frequency Division Multiple Access

SI Side Information

SLM SeLective Mapping

SNR Signal to Noise Ratio

SQUID Squared-Infinity norm Douglas-Rachford splitting

SSPA Solid State Power Amplifier

TI Tone Injection

TR Tone Reservation

UFMC Universal Filtered Multicarrier

WARP Wireless open Access Research Platform

SLM SeLective Mapping

Chapter 1

Introduction

1.1 Single carrier transmission

In wireless communication, the data can be transmitted by employing single carrier (SC) modulation schemes and multi-carrier modulation schemes. The SC modulation schemes have a long history and can be widely employed in various wireless communication standards, such as 1G, 2G, 3G, and uplink of 4G systems. Moreover, low PAPR can be achieved by implementing these schemes; consequently, design complexity decreases. Thus, inexpensive devices can be utilized for the design implementation. Also, SC schemes are less sensitive to carrier frequency offsets, thus making time and frequency synchronization easy in wireless communication systems, particularly in point-to-point communications. Besides, the use of single-tap equalizers makes the channel equalization simple at the receiver [1]. Hence, the SC transmission schemes are still used in SC-FDMA (single carrier frequency division multiple access) system, which is a promising 4G technology and can be employed in the uplink transmission of LTE (long term evolution) standard.

In single carrier transmission scheme, the minimum bandwidth required to support the symbol rate of R_s symbols per second is Nyquist bandwidth, i.e., $R_s/2$. It indicates that large bandwidth is necessary to achieve high data rates in SC transmission schemes. Also, the channel effect is compensated to a great extent by using equalizer at the receiver. However, large signal bandwidth is required in this SC transmission scheme when symbol rate increases. When the signal bandwidth of a wireless channel exceeds the coherence bandwidth, the channel suffers from multi-path fading, thus resulting in inter-symbol interference (ISI). Adaptive equalizers are

commonly used to address the ISI caused due to the time-varying multi-path fading channel. It can be employed by the FIR (finite impulse response) filters with adaptive tap coefficients that can be varied to minimize the effect of ISI. As the data rate increases, the equalizer requires more taps to minimize ISI, thus increasing the complexity of the equalizer. Therefore, the SC transmission scheme may be inappropriate to attain high data rates due to high complexity of the equalizer in the receiver.

1.2 Multi carrier transmission

The multi-carrier transmission is a fine approach to attain high data rates and reduce the complexity of the equalizer [2, 3]. In multi-carrier transmission, entire frequency band is divided into many subcarriers and the wide-band signal is analyzed by splitting into a number of narrow-band signals at the transmitter and synthesized at the receiver. Consequently, the frequency selective wide-band channel is approximated as multiple frequency-flat narrow-band channels, which in turn reduces the complexity of the equalizer at the receiver. Besides, as long as the sub-channels are orthogonal, the inter-carrier interference (ICI) can be suppressed, thus leading to distortion-free transmission. If each sub channel in the multi-carrier scheme is band limited, it becomes a filtered multi-tone (FMT) transmission.

The FMT scheme, which is one of the multichannel systems, is used to separate the subbands by employing filters to reduce the adjacent channel interference (ACI) at the cost of spectral efficiency (SE) [4, 5]. Since there is no need of guard band in FMT, the number of subcarriers is less than 64, so better SE can be achieved. The FMT scheme can handle the frequency selectivity of the channel by employing individual higher quality filters, oscillators, and more encoders/decoders for each sub channel. So, the implementation of FMT transmission becomes hard when the number of subcarriers increases. The FMT can be employed as a transmission technique in Terrestrial Trunked Radio II (TETRA-II) standard in the ETSI (European Telecommunications Standards Institute).

Orthogonal frequency division multiplexing (OFDM), which is a well established multi carrier modulation (MCM) scheme, offers a high data rate and ensures effective communication over frequency selective fading channels [6, 7]. The design complexity of the receiver in conventional communication systems becomes high to handle the communication over frequency selective fading channels. The OFDM efficiently handles this situation by converting the frequency selective fading channel into narrow bandwidth flat fading channels. The flat

fading channels make the receiver design simple to combat ISI by utilizing simple equalization schemes. Unlike FMT, OFDM does not employ individual oscillators and band limited filters for each sub channel. Moreover, the optimum spectral efficiency (SE) is accomplished by overlapping the sub-carriers that are orthogonal to each other over the symbol period. With these attractive features, OFDM has been a popular scheme for wideband digital communications [8, 9]. It is being implemented in WiMAX (IEEE 802.16), wireless LAN (IEEE 802.11a and 11g), and third generation partnership project (3GPP) long term evolution downlink systems.

Massive MIMO is a promising technology to improve the capacity, spectral efficiency, and energy efficiency (EE) of multiuser networks by employing several hundreds of antennas at the base station (BS). The capacity of the massive MIMO can be increased on the order of 10 times or more and the radiated energy efficiency can be improved on the order of 100. The massive number of BS antennas can be successfully employed to serve tens of user equipments (UEs) simultaneously in the same frequency band.

1.3 Motivation

The 4G multi carrier OFDM is being employed in various applications in most of the countries across the world. However, in the recent years, the data traffic is grown exponentially due to the rapid growth of laptops, tables, smart phones, and other wireless devices, which cannot be handled even by 4G. The demand for wireless data traffic would be even more in future. The OFDM suffers from certain drawbacks, such as low bandwidth efficiency because of the use of cyclic prefix (CP) per OFDM symbol, synchronization problems due to the orthogonality mismatch, high out-of-band (OOB) radiations due to the utilization of rectangular filters, and high peak to average power ratio (PAPR) because of multiple subcarriers that are added through IFFT operations. Hence, OFDM may be inappropriate to meet the requirements of 5G. The 5G technology demands mobile data that is 1000 times more than the data required for 4G and latency that is $\frac{1}{5}^{th}$ of the latency of 4G [10]. Besides, it demands high energy efficiency, low signaling overhead, better security, and relaxed synchronization [11].

The 5G system is essential for providing significant wireless connectivity in Internet of Things (IoT) and machine-type communication applications [12]. Hence, some alternate waveform contenders are required to serve 5G and beyond 5G (B5G) communications. Some of the promising contenders are generalized frequency division multiplexing (GFDM), filter bank multicarrier (FBMC), and universal filtered multicarrier (UFMC).

The FBMC employs per subcarrier filtering, which reduces OOB emissions and eliminates inter-carrier interference significantly [13]. Furthermore, FBMC need not require strict synchronization and is also spectrally efficient since there is no use of cyclic prefix. However, it requires long filter length due to the narrowband frequency response of a filter. Therefore, it is not suitable for IoT and short burst communications [14]-[16]. UFMC, an alternative to both OFDM and FBMC, is simple like OFDM and robust like FBMC. The spectral efficiency and relaxation to carrier frequency offset are the attractive features of UFMC system. UFMC system employs per sub-band filtering unlike FBMC. Hence, it does not require long filter length and also reduces OOB radiations. So, it suits well for short burst communications [17]. The performance of UFMC system is evaluated in terms of mean square error, bit-error-rate, and PAPR.

1.4 Problem statement

The design of channel estimators is very crucial in wireless communications since the mean square error (MSE) performance has a direct impact on receiver's throughput in terms of system BER performance. Hence, channel estimation should be carried out for UFMC system in order to enhance the system BER performance.

High PAPR has always been a drawback in multicarrier systems as it reduces the efficiency of power amplifier (PA) in the system. Power amplifier efficiency is an important parameter that is directly related to PAPR. So, PA efficiency can be enhanced by diminishing the PAPR of the UFMC signal to save power and cost of the system. Therefore, the PAPR of the UFMC system should be reduced by employing novel PAPR reduction schemes.

Since massive MIMO is a potential technology to enhance the capacity, energy efficiency (EE), and SE of multiuser networks by using more number of antennas at the base station, it is expected that the combination of massive MIMO with multicarrier waveform schemes would enhance the robustness of the system against the multipath fading channels. Hence, the UFMC system is combined massive MIMO technology to attain the benefits of both UFMC and massive MIMO systems.

1.5 Research objectives

The main objectives of this thesis can be summarized as follows:

1. **Channel estimation in UFMC system:** To study and analyze the performance of various channel estimation techniques. To extract the channel information by inserting a known symbols into the data symbols using a comb type pilot arrangement. To propose least square (LS) and minimum mean square error (MMSE) techniques in order to enhance the MSE and BER performances of UFMC system.

2. **Optimal hybrid schemes for PAPR reduction in UFMC system:** To study and analyze the performance of various companding schemes for PAPR reduction of UFMC system. To propose a modified exponential companding (MEC) technique that transforms the Rayleigh distributed UFMC signals into uniform distribution in order to reduce the PAPR without increasing the average power of the signal. To propose an optimal hybrid transform, in which clipping is employed on the MEC signal to further reduce the PAPR. Also, to propose a new companding scheme that transforms the UFMC amplitude signals from statistical distribution to quasi uniform distribution.

3. **A joint time domain CE with PAPR reduction in UFMC system:** To propose a joint pilot-based time domain CE with hybrid PAPR reduction scheme for UFMC system. Also, to present a linear companding (LC) scheme for reducing the PAPR of the UFMC system.

4. **A joint quantized precoding and PAPR reduction in massive MIMO-UFMC system:** To propose a UFMC based Massive MIMO systems in order to meet the requirements of future generation wireless networks (5G and Beyond 5G). To propose a nonlinear phase-quantized precoder called SQUID-UFMC that addresses the high PAPR problem of massive MU-MIMO-UFMC downlink systems. Also, to present a PLC scheme to further reduce PAPR of the proposed quantized massive MU MIMO-UFMC system.

1.6 Thesis organization

The thesis is structured into seven chapters. This section describes the outline of all.

1. **Chapter 1** This chapter illustrates the introduction, motivation, problem statement and objectives of the research.

2. **Chapter 2** In this chapter, an overview of UFCM system is discussed. The basics of channel estimation in UFMC system are defined and an overview of different channel estimation and interpolation approaches in conventional OFDM system is presented. Besides, the PAPR of the UFMC is described and the impact of PAPR on high power amplifiers is illustrated. The generalized PAPR reduction schemes in traditional OFDM system are also presented. Moreover, the basics of massive MIMO system are discussed. The precoding and quantization methods in massive MIMO and OFDM based massive MIMO systems are summarized.

3. **Chapter 3** In this chapter, pilot based-channel estimators are analyzed. In pilot assisted CE, different pilot arrangements are discussed and examined to choose an appropriate pilot pattern for UFMC transmission. The comb type LS and MMSE techniques are introduced for UFMC system.

4. **Chapter 4** In this chapter, the nonlinear companding transforms to reduce PAPR in UFMC system are investigated. A modified exponential companding transform, which can use two companding levels based on a threshold value, is proposed. Moreover, an optimal hybrid transform is also proposed to improve PAPR performance, where clipping operation is employed on MEC signal based on an appropriate clipping threshold. Besides, a companding technique based on error function is proposed and its performance is evaluated and compared with various companding transforms, such as μ-law, A-law, advanced rooting, hyperbolic tangent, and proposed companding technique. The performance of the proposed system is verified by considering real-time indoor channel by employing WARP hardware.

5. **Chapter 5** This chapter introduces pilot-based time domain channel estimation (CE) along with PAPR reduction for UFMC system. A linear companding transform that can treat amplitudes of the UFMC signal separately with a different scale is proposed. Furthermore, a clipping scheme is employed on the LC signal to further mitigate the PAPR of the proposed system. The performance of the proposed system is verified by considering real-time indoor channel by employing WARP hardware.

6. **Chapter 6** This chapter proposes a combination of UFMC system with massive MIMO technology to attain the benefits of both UFMC system and massive MIMO technology. Also, a nonlinear quantized precoding that mitigates the PAPR of the proposed UFMC based massive MIMO system is proposed. The mathematical modelling of the proposed

quantized precoding of the massive MIMO-UFMC system is done. A piece wise linear companding scheme is employed to further reduce the PAPR of the massive MIMO-UFMC system.

7. **Chapter 7** This chapter illustrates the conclusions of the work and summarizes the results of all the objectives discussed in the earlier chapters and discusses the future scope of this research concisely.

Chapter 2

Literature Survey

2.1 Introduction to Universal Filtered Multi Carrier System

The UFMC, a promising 5G waveform candidate, is a compromise between OFDM and FBMC systems. It is simple like OFDM and robust like FBMC. The OFDM is not suitable for cognitive radio applications due to the high OOB radiations in OFDM [18, 19]. Hence, the reduction of OOB radiation by a factor of 100 is one of the significant performance indicators of 5G technology. The UFMC employs per sub-band filtering that reduces OOB radiation effectively [20]. The use of CP in OFDM to deal the multipath fading ISI reduces the spectral efficiency, which is also one of the key requirements of 5G. Whereas high SE is achieved in UFMC system due to the absence of CP. The strict synchronization of OFDM is also a drawback of OFDM. The relaxation to carrier frequency offset is an attractive feature of UFMC system [21]. Hence, the UFMC system efficiently addresses the shortcomings of OFDM.

The FBMC is also a potential 5G candidate that offers low OOB radiations, robust against multipath fading. But the long filter impulse response makes the system more complex and prevents its usage in tight latency constraints and sporadic traffics. The sub-band filtering in UFMC has short filter impulse response, so system complexity decreases. Hence, UFMC can be employed in short burst communications. Finally, it can be concluded that UFMC overcomes the drawbacks of OFDM and FBMC effectively [22, 23].

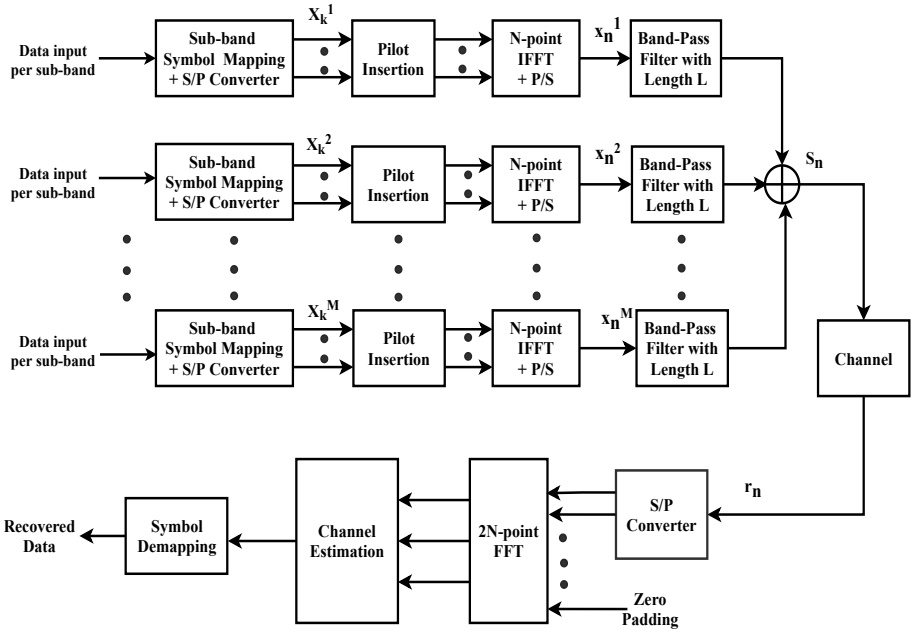

Figure 2.1: UFMC system model

2.2 UFMC system model

The block diagram of UFMC system model is shown in Fig. 2.1. Unlike OFDM systems, the total bandwidth of UFMC system with N subcarriers is separated into M sub-bands. Each sub-band of this model carries consecutive subcarriers. An orthogonal relationship is maintained between the subcarriers of each sub-band, which can suppress OOB emissions. Each sub-band is modulated with relevant modulation schemes like PAM, PSK, QAM, etc. After modulation, N-point IFFT operation is applied to convert the frequency domain signal into time-domain signal. The mathematical representation of the above process is given in the following.

For an arbitrary p^{th} sub-band B^p, where $p\ \varepsilon(1:M)$, the frequency domain signal X_k^p is transformed to the time domain signal x_n^p by the IFFT operation, and the expression is

$$x_n^p = \frac{1}{N}\sum_{k\epsilon B^p} X_k^p \exp^{j\frac{2\pi}{N}nk} \qquad 0 \le n \le N-1 \tag{2.1}$$

Then the time domain signal x_n^p is passed through a Dolph-chebyshev band pass filter with filter length L. The filtering operation in UFMC system eliminate OOB emissions effectively. Now the UFMC signal is obtained by applying linear convolution between the time domain signal x_n^p and filter impulse response f_l. Therefore the length of UFMC symbol becomes $N+L-1$. Then

the transmitted UFMC signal at the transmitter can be denoted as

$$s_n = \sum_{p=1}^{M} b_n^p \qquad 0 \leq n \leq N + L - 1 \tag{2.2}$$

where M is total number of sub-bands and b_n^p is the p^{th} sub-band signal which can be given as

$$b_n^p = \sum_{l=0}^{L-1} x_{n-l}^p f_l^p \qquad 0 \leq n \leq N - 1 \tag{2.3}$$

where x_n^p is the time domain N-IFFT signal given in (2.1) and f_l^p is the l^{th} filter coefficient can be written as

$$f_l^p = f_l \exp^{\frac{j2\pi l C^p}{N}} \qquad 0 \leq l \leq L - 1 \tag{2.4}$$

where N indicates IFFT size, f_l is l^{th} reference filter coefficient and C^p denotes center sub-carrier index of p^{th} sub-band.

Finally, the UFMC signal at the transmitter end is obtained by incorporating eq(2.3) and eq(2.4) in eq(2.2) is

$$s_n = \frac{1}{N} \sum_{p=1}^{B} \sum_{l=0}^{L-1} \sum_{k=B^p} X_k^p f_l^p \exp^{\frac{j2\pi(n-l)k}{N}} \qquad 0 \leq n \leq N + L - 1 \tag{2.5}$$

Now the UFMC signal has been transmitted through a wireless channel. Then the received signal r_n can be expressed as

$$r_n = s_n + w_n \tag{2.6}$$

where w_n is the channel noise with mean zero and variance one. The received UFMC signal is transmitted through $2N$-point FFT block to convert the time domain signal into the frequency domain. Then frequency domain CE and MMSE equalization is employed for each subcarrier to estimate the channel and eradicate inter-symbol interference, respectively. Finally, de-mapping is performed on equalized output to retrieve the data bits.

2.3 Channel estimation

The channel estimation is one of the key performance parameters of any wireless communication system [24]. As the transmitted signals are propagated through the channel, they are altered by the three physical effects, such as reflection, diffraction, and scattering. Hence,

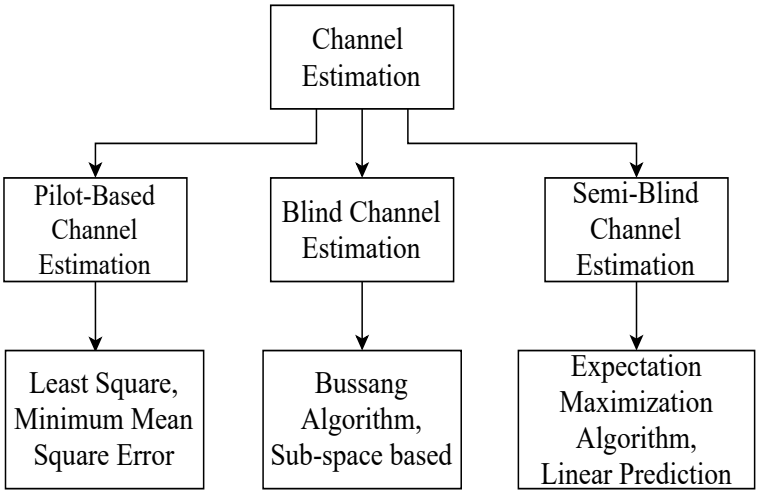

Figure 2.2: Classification of channel estimation schemes

these signals arrive at the receiver from two or more paths. When signals coming from different paths have same delay, they are added either constructively or destructively, thus resulting in fading. When they have different delays, they emerge as signal echoes. The channel changes over time due to the mobility of the transmitter, the receiver, and the scattering objects. So, the received signal is distorted by the channel characteristics. Therefore, the estimation of channel state information (CSI) becomes a requirement in the receiver in order to compensate the channel effect and retrieve the transmitted data bits [25]. The accuracy of CSI estimation at receiver significantly influences the overall UFMC system performance.

Channel estimation can be categorized into three types as shown in Fig. 2.2. They are training based, blind method, and semi blind method. Different aspects like computational complexity, accuracy, and spectral efficiency must be considered to choose a proper channel estimation type in multicarrier systems. The training based methods are simple and offer a good system performance in terms of accuracy [26, 27]. However, these methods consume bandwidth due to the frequent transmission of training data (i.e., pilots) to estimate the CSI at the receiver. The use of more pilots improves the accuracy of the system but decreases the spectral efficiency.

The blind type channel estimation techniques mostly depend on second order and higher order statistics. It does not employ training symbols to estimate the channel impulse response. Therefore, it offers better spectral efficiency when compared to the former one [28, 29]. However, the blind estimation methods are very complex and have slow convergence speed, large computation, and poor portability. The semi blind estimation has the advantages of both training based and blind estimation [30]. It employs pilot symbols as well as statistical properties of channel. Moreover, it offers better accuracy and spectral efficiency.

2.4 Literature on channel estimation

In [31], the modified LS and MMSE estimators with the knowledge of channel statistics for OFDM system in slow fading channels were proposed. The results show that the MMSE estimate provides SNR gain ranging from 10-15 dB for the same MSE of LS estimate. But the complexity of the MMSE estimate is more when compared to LS estimate.

In [32], a block oriented linear MMSE technique using only frequency correlation was employed for OFDM system. It offers less complexity than the estimator with both time and frequency correlation. The complexity of the LMMSE was further reduced by employing a low-rank approximation scheme to LMMSE estimator. The simulation results confirm that the MSE of the LMMSE with low-rank approximation is 1.5 times less than that of the LMMSE with Wiener filter estimator of equal complexity.

In [33], a comb type optimal low-rank estimator was employed to reduce the complexity of MMSE. Moreover, linear interpolation and second-order interpolation were employed to estimate the data symbols at the receiver [34]. Results show that the second-order interpolation offers better performance than linear interpolation.

In [35], a complete analysis of both comb type and block type pilot arrangements for estimating the channel was provided. The performance of block type pilot arrangement was evaluated by employing decision feedback equalizer in slow fading channel. The comb type structure allows the tracking of fast fading channel. The LS and LMS (least mean square) methods were employed to estimate channel at pilot carriers. Different interpolation techniques, such as linear, spline, low-pass, and time domain were employed to estimate the channel at data frequencies. Results show case that the comb type structure with low-pass interpolation provides better performance than all other CE algorithms.

In [36], a sub-space based blind method was employed to estimate the channel. The CP is used in OFDM transmitter to combat ISI. This redundant CP is used in order to estimate the channel blindly. Therefore, there is no need of any further modifications in the OFDM transmitter to estimate the CSI. Moreover, the performance of blind method is further improved by employing training symbols. Since blind and training based methods are combined, the proposed technique is called semi-blind method. Simulations prove that the sub-space methods offer better performance, especially in time domain.

In [37], a semi blind method, which employs first order statistics to estimate the impulse response of the multipath fading channel, was proposed. A periodic training sequence is superimposed on the data sequence in each OFDM block to estimate the channel. Results confirm that the semi blind method provides better MSE performance when compared to sub-space method and LS scheme.

In [38], a robust channel estimator that uses the frequency domain and time domain correlation functions to estimate the CSI in OFDM systems was proposed. The simulations show that the robust estimator provides increase in SNRs of 2.5 dB and 1.5 dB at Doppler frequencies of 40 Hz and 200 Hz, respectively.

The interpolation that is employed to estimate the channel at data frequencies in training based methods, was proposed [35]. The Wiener interpolator provides good MSE performance that depends only on the pilot density but not the pilot pattern. On the other hand, the Wiener scheme may not be employed in practical scenarios due to high complexity. The linear and spline interpolators are simple and can be used in practical scenarios. [39, 40]. The performance of these interpolators depends on both pilot density and pilot pattern [41]-[44]. For instance, when the channel fluctuates rapidly with a small delay spread, the insertion of more pilots in time domain is more desirable than in frequency domain, and vice versa [45].

In [46], a time domain CE is performed for OFDM systems. It employs circular cross-correlation to estimate channel impulse responses using training symbols. To improve the accuracy of synchronization and channel estimate, a CIR search window approach was also presented. The search window's output can also be used to calculate channel's delay spread. The proposed CE offers near-ideal accuracy with low computational complexity.

A pilot based time domain channel estimator was employed for OFDM systems [47]. The channel state information is accurately measured in time domain by employing cross correlation between pilot carriers and received signal. Besides, the pilot pre FFT CE can accurately evaluate the CIR at low SNR. The MSE of this pilot based time domain channel estimator is better than conventional frequency domain LS and MMSE estimators.

A time domain CE model was developed for FBMC system [48]. The CIR is evaluated in time domain by using frequency domain pilots. Two time domain estimators like weighted least square and LMMSE were presented to improve the CE performance of the FBMC systems. In comparison to traditional frequency domain approaches, the results confirm that the proposed channel estimators are more robust to time synchronization errors.

2.5 Peak to average power ratio (PAPR)

PAPR is a performance metric that can be used to evaluate the amplification efficiency of PAs. High PAPR is one of the serious shortcomings of multi-carrier systems. It demands high resolution quantizers, which increase the complexity at the receiver front end. Since high PAPR may drive the transmit PA into saturation region, the power amplifier (PA) needs large input backoff (IBO) to ensure the linear amplification [49]-[51]. As IBO increases, the PA requires high power consumption, thus resulting in degradation of performance of PA. As a result, high PAPR does not meet the energy efficiency requirement of 5G systems. So mitigation of PAPR is one of the challenging problems in UFMC system. For continuous-time signal s_t, the PAPR is nothing but the ratio of the maximum instantaneous power to the average power. The PAPR of the discrete time UFMC signal s_n can be given as

$$PAPR = \frac{\max_{n\epsilon[0,1,2.....N+L-1]} \left\{|s_n|^2\right\}}{E\left[|s_n|^2\right]} \tag{2.7}$$

where $E[.]$ denotes the expectation operator.

The PAPR has a significant impact on the performance of power amplifiers. Theoretically, transmit power efficiency and PAPR [dB] are related as follows [52, 53].

$$\eta = \eta_{max} 10^{-PAPR/20} \tag{2.8}$$

Here, η and η_{max} denote the efficiency of PA and maximum efficiency of PA, respectively. The maximum power efficiency of class A and class B power amplifiers are 50% and 78.5%, respectively [54]. It is shown from Fig. 2.3 that high PAPR reduces the efficiency of power amplifier. In practice, the PAPR is assessed using the empirical complementary cumulative distribution function (CCDF). The amount of CCDF reduction obtained decides the decrease in PAPR. CCDF is nothing but the probability for which PAPR is greater than a specific PAPR threshold $PAPR_0$ (i.e., $(P_r\{PAPR > PAPR_0\})$).

2.6 Non-linear power amplifier model

The PA is one of the most important components of wireless communications. It compensates for the attenuation induced by free-space propagation. But, it is an analog component

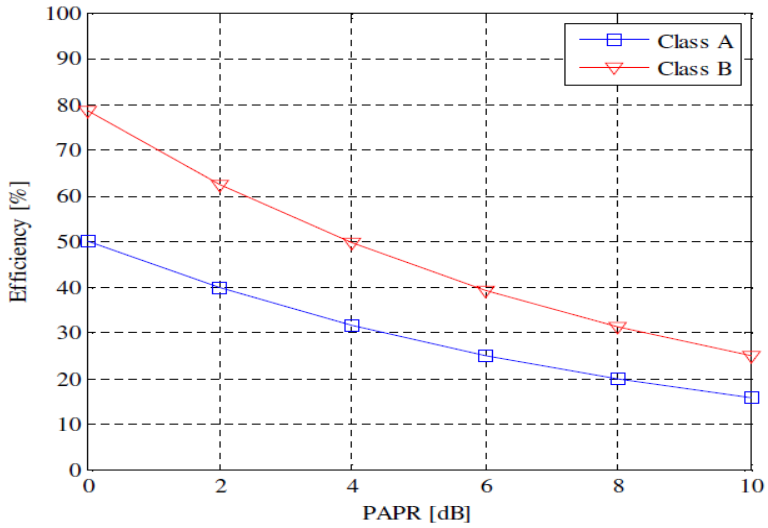

Figure 2.3: Relationship between PAPR and transmit PA efficiency.

and is naturally non-linear (NL) as the amplifier circuits are composed of active elements like transistors, which are NL in nature.

Most of the radio systems have employed HPAs in the transmitter to achieve required transmit power. The SSPA is one of the widely accepted models of HPAs and is advantageous due to the utilization of Gallium Arsenide (GaAs) device technology. The GaAs based devices employed in SSPA offer high power handling capability than Silicon based devices due to the large energy band gap of GaAs material. According to the model [55], the complex envelope of the SSPA input signal can be expressed as

$$g_n(t) = |g_n(t)|\, e^{j\theta_n(t)} \tag{2.9}$$

and the output signal is expressed as

$$g_{no}(t) = \frac{a\,|g_n(t)|}{\left[1 + \left(\frac{|g_n(t)|}{A_{sat}}\right)^{2p_a}\right]^{\frac{1}{2p_a}}} e^{j\theta_n(t)} \tag{2.10}$$

where, A_{sat} denotes the saturation level, a represents the amplifier gain, and p_a is a random positive integer that controls the nonlinearity of the amplifier. The SSPA produces only the AM/AM conversion and no phase distortion ($\theta_n(t)$=0). So, substituting $\theta_n(t)$=0 in eq(2.10) gives eq(2.11)

$$g_{no}(t) = \frac{a\,|g_n(t)|}{\left[1 + \left(\frac{|g_n(t)|}{A_{sat}}\right)^{2p_a}\right]^{\frac{1}{2p_a}}} \tag{2.11}$$

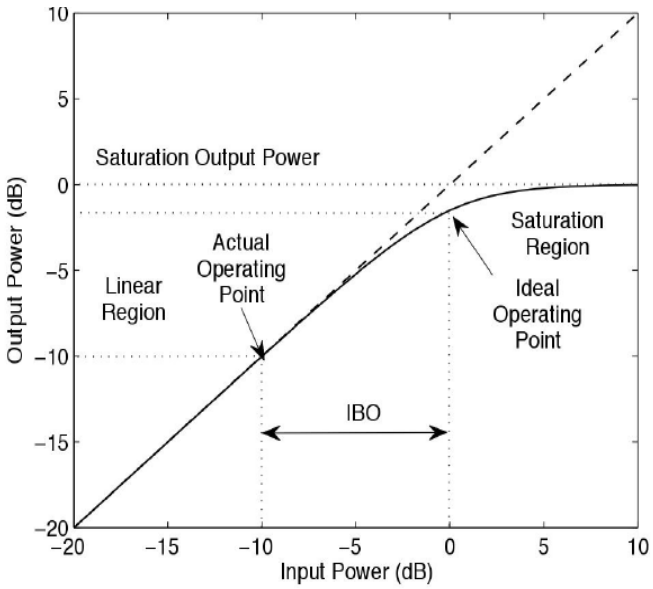

Figure 2.4: Relation between input and output power characteristics curve

The operating point of the PA is to be kept below the saturation level. However, high peaks of the transmitted UFMC signal switches the HPA into saturation region. Consequently, IBO is required to shift the operating point from saturation region to linear region, as shown in Fig. 2.4. The IBO, which reduces nonlinear distortions in the transmitted signal can be represented as

$$IBO = \frac{A_{sat}^2}{P_{in}} \tag{2.12}$$

where $P_{in} = E\left[|g_n(t)|^2\right]$ is the average power of the input signal. On the other hand, the higher IBO lowers the SSPA efficiency. Hence, the IBO must be chosen carefully to achieve better BER performance without degrading power amplifier efficiency since there is a tradeoff between low distortion and high SSPA efficiency.

2.7 PAPR reduction techniques

Several techniques have been employed to reduce PAPR in multi-carrier systems. The PAPR reduction schemes can be mainly classified into different types, such as signal distortion, multiple signaling and probabilistic, and coding techniques, as shown in Fig. 2.5 [56]-[58].

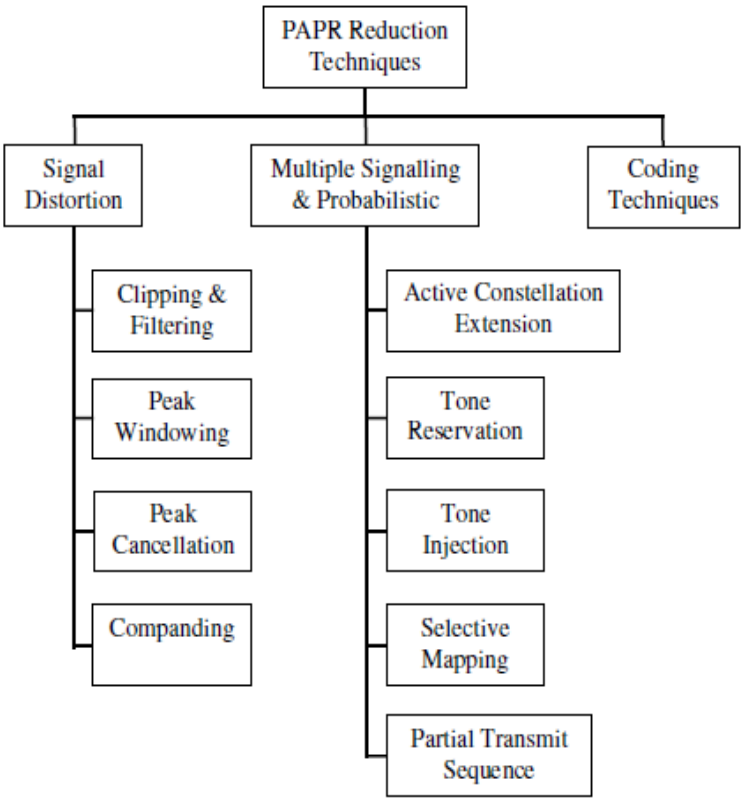

Figure 2.5: Classification of PAPR reduction schemes

2.7.1 Signal distortion techniques

The signal distortion techniques, such as clipping and filtering [59, 60], peak windowing [61], companding [62, 63], and peak cancellation [64] mitigate the PAPR by distorting the UFMC signal s_n before it transmits through the PA. These techniques significantly reduce the PAPR, but they cause both in-band and OOB distortion, thus resulting degradation in BER. Therefore, PAPR could be decreased at the cost of a tolerable increase in BER.

2.7.2 Multiple signaling and probabilistic techniques

Multiple signaling and probabilistic schemes function in two different ways. One way is to produce multiple permutations of UFMC signal and broadcast the one with the lowest PAPR. Another way is modifying the UFMC signal by shifting constellation points or introducing phase shifts and adding peak reduction carriers. The probabilistic schemes, such as partial transmit sequence (PTS) [65]-[67], selective mapping (SLM) [68, 69], tone injection (TI) [70, 71], and tone reservation (TR) [72, 73] schemes mitigate PAPR without degradation in BER

and OOB distortion. However, these schemes need side information (SI), which decreases the SE and increases the complexity of the sysetm as the number of subcarriers increases.

2.7.3 Coding techniques

The coding techniques aim to choose code words that can reduce or minimize PAPR. These techniques do not suffer from in-band and OOB distortions but suffer from SE as the code rate is reduced. Also, they increase the computational complexity of the system to determine the best codes and include Golay complementary sequence [74], M-sequence or Hadamard code, and Reed Muller code [75].

2.8 Literature on conventional PAPR reduction schemes

In [76], a uniform distribution method was employed to mitigate the PAPR of OFDM signals. Also, a Lagrange multiplier (LM) optimization was used to reduce the number of iterations that involved in the adaptive approach. Three different schemes, which employs clipping followed by filtering, were employed to reduce the PAPR. Simulation outcomes show that the proposed schemes with LM optimization provide better PAPR reduction than the adaptive iterative clipping and filtering schemes without LM optimization.

In [77], the PAPR of OFDM signals was mitigated by employing two new peak windowing techniques. In first method, the asymmetric windows for every peak are formed by varying the window length sequentially. These asymmetric peak windows added together to smooth the overall window function. In other one, the weighting coefficients for every peak were optimally designed by employing the convex optimization algorithm. Simulations confirm that these two approaches provide enhanced performance when compared to the existing schemes.

In [78], the peak cancellation schemes to mitigate PAPR of OFDM signals were theoretically analyzed. Also, the performance of peak cancellation was analyzed in terms of in-band and OOB distortions. The analytical approach presented in this paper was validated by the simulation outcomes.

In [79], a precoding based advanced rooting companding scheme was presented to diminish the PAPR of UFMC signals. The precoding, which is also called pulse shaping technique,

can effectively mitigate the PAPR. Hence, the combination of precoding with companding provides better PAPR reduction with slight degradation in BER. Various precoding schemes, such as DFT, DCT, DHT, and DST, were employed to reduce the PAPR. The DFT-ARCT provides improved performance characteristics in terms of PAPR and BER among these schemes.

In [80], a companding transform, which mitigates the PAPR of OFDM signals, was presented. A sophisticated theoretical performance analysis was carried out for OFDM systems. Results confirm that the companding transform is simple and efficient scheme to reduce the PAPR of multi carrier systems. However, the authors only considered the effect of quantization noise and ignored the performance of power amplifier.

In [81], a companding scheme that transforms the statistical distribution of amplitude signals into quasi uniform distribution to reduce the PAPR of OFDM system with constant average power level was proposed. Also, the performance of this transform was verified while considering the effect of solid state power amplifier (SSPA). Simulation outcomes show that the companding transform offers good performance metrics in terms of PAPR reduction and BER, even in the presence of SSPA.

In [82], a hyperbolic tangent (HT) companding that enlarges the small amplitudes and reduces the peak amplitudes of OFDM signal was presented. The transfer curve of the companding was expressed by a hyperbolic tangent function. It is noticed that the HT transform provides better PAPR reduction, but it degrades the BER performance.

In [83], four companding schemes, such as linear nonsymmetrical transform (LNST), linear symmetrical transform (LST), nonlinear nonsymmetrical transform (NLNST), and nonlinear symmetrical transform (NLST), were proposed for OFDM system. Among these, LNST offers better BER characteristics and better PAPR reduction. However, LNST degrades the power spectrum performance.

The SLM schemes are suffered from high computational complexity. To minimize the complexity, a modified SLM technique was proposed to reduce PAPR of OFDM signal [84]. The time-domain signals are segmented and processed by utilizing Fourier transform properties to provide large number of candidates with fewer IFFT blocks. As a result, the modified SLM technique generates $4M^4$ candidates from M-IFFT operations. Results showcase that the modified SLM technique provides better PAPR reduction than other existing techniques. Besides, the proposed SLM technique offers low computational complexity when compared to Swapped SLM and CSLM schemes.

In [49], a low-complexity PTS technique that significantly minimizes the computational complexity was proposed to reduce the PAPR of OFDM signals. The dominant time-domain samples were selected on the basis of rotating samples of IFFT (inverse fast Fourier transform) sub-blocks to the local area, where the first block of IFFT was placed. Furthermore, the computational complexity of PTS scheme was reduced by pre-excluding the phase rotating vectors using the time-domain sample rotation method. Results show case that the proposed PTS techniques offer approximately similar PAPR performance as that of the traditional PTS technique with less computational complexity.

In [85], a low-complexity PTS technique was presented for PAPR reduction of UFMC signals. The sub-bands in the UFMC system were divided into multiple sub-blocks. To reduce the complexity of the PTS scheme, the minimum peak amplitude that can be treated as a threshold value was found out. Later, the signal samples that had amplitudes below the threshold were canceled. This reduces the amount of time-domain samples that must be multiplied by the appropriate phase-rotating vectors, and it can also be used to estimate the PAPR. Results prove that the modified PTS technique provides nearly equivalent PAPR performance as that of the traditional PTS scheme while significantly reducing the computational complexity.

In [86], an ACE technique, where convex optimization schemes and subcarrier grouping are implemented for PAPR reduction of OFDM systems, was proposed. Unlike the conventional ACE scheme, which involves intensive FFT/IFFT computation, the proposed ACE scheme is realized simply to yield the optimal solution at a time. Consequently, the complexity of the proposed ACE offers less complexity than conventional ACE schemes.

In [87], a TR scheme, which reduces the PAPR of the multicarrier system by using unused or reserved tones, was proposed. Since an active set method converges quickly to an optimum solution, it leads to low computational complexity. Tone injection is a potential candidate to reduce the PAPR of OFDM system [88]. However, the injected signal raises the power of the transmitted signal. Therefore, a hexagonal constellation method is employed to mitigate the PAPR of OFDM signal without raising the signal power in the TI scheme.

The SLM scheme reduces the PAPR, but it needs the SI that increases the complexity and reduces the SE. In [89], a blind SLM technique was proposed for OFDM system. In the proposed scheme, the SI is obtained from pilot sub-channel responses. A low complexity SI detection technique can efficiently perform data decoding and required SI is obtained from a decision metric. Results confirm the proposed SI decoding scheme offers BER characteristics similar to that of the ML decoding scheme.

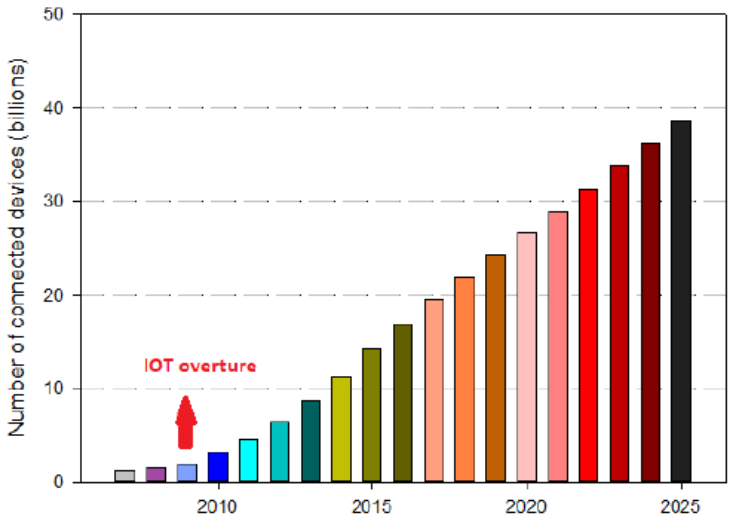

Figure 2.6: The Global growth of the number of active connected devices in the wireless services

2.9 Introduction to Massive MIMO System

In wireless communication, the transmitted signals are attenuated by fading, which occurs due to multipath propagation. Also, they are affected by shadowing, which occurs due to the existence of large obstacles between the transmitter and receiver. Hence, achieving good reliability is a common challenge in communications. It is well known that a popular diversity technique called MIMO is used to improve the reliability of the communication. Furthermore, multiple streams can be sent out by using with multiple antennas; therefore, we can obtain a multiplexing gain that significantly improves the communication capacity [90]. Moreover, the use of multiple antennas at the transceivers can increase the SE, which is directly related to the wireless throughput (bits/s) [91]. The throughput is nothing but the product of bandwidth and SE of the system.

Nowadays, data traffic is growing exponentially because of the rapid growth of tablets, smart phones, laptops, and other wireless data consuming devices, as shown in Fig. 2.6. By the end of 2025, the number of connected devices will significantly increase and may reach around 39 billion. So, high capacity, high SE, high data rates, and high EE will be required [92]. Consequently, the future generation communication systems may demand new technologies in the context of the MIMO schemes.

The massive MIMO, a large-scale MU - MIMO, is a potential technology for future wireless communications [93] and its model is shown in Fig. 2.7. The key concept in massive MIMO is to equip more number of BS antennas that are employed to serve many users simulta-

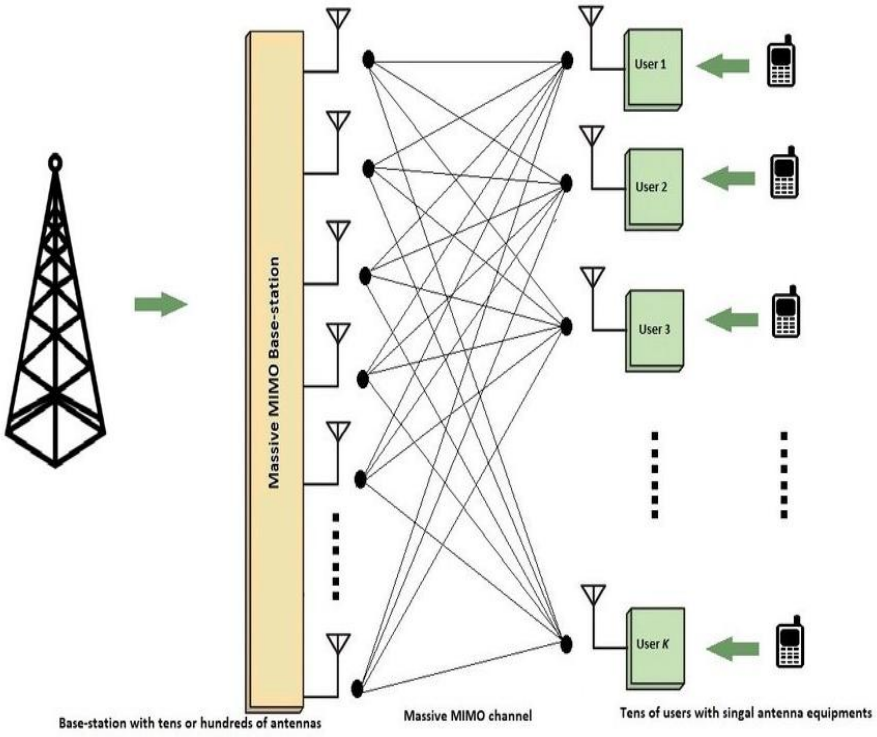

Figure 2.7: Massive MIMO system architecture

neously in the same frequency resource with no severe inter-user interference. Hence, Massive MIMO fulfills all the requirements of 5G and B5G communications [94].

In massive MIMO, high data rates can be attained by employing an aggressive spatial multiplexing with no need of additional spectrum. Moreover, the implementation of large number of antennas offers high spectral efficiency and large array gain. Since large array gain increases the received signal strength, better coverage can be achieved [95]. Besides, each antenna at the BS is implemented with an inexpensive hardware that requires simple signal processing schemes and a low-power amplifier. Additionally, the use of precoding techniques can attain near-optimal performance.

2.10 Precoding

Precoding is a beam forming concept in which multiple antennas facilitate multi-stream transmission. It is an imperious method in massive MIMO systems to increase the throughput and reduce the effects of path-loss and interference [96]. The precoding schemes are categorized into two types, such as linear precoding and nonlinear precoding.

2.10.1 Linear precoding

The basic linear precoder multiplies the transmitted signal S with the precoding matrix Q_B. The linear precoding schemes include zero-forcing (ZF) [97, 98], maximum ratio transmission (MRT), Wiener precoding (WF), and minimum mean square error (MMSE) precoding.

(i): ZF Precoding

The ZF precoding, one of the basic precoding techniques of massive MIMO system, is a counterpart of channel inversion method. The ZF scheme reduces the interference caused by the other users by pointing the transmitted signal beam into the intended user equipment while nullifying directions of other located UEs. The ZF precoding is employed by multiplying the transmitted data with the ZF precoding matrix that can be given as

$$Q_B^{ZF} = \sqrt{\beta_a} H^* \left(G_g^{-1}\right) \tag{2.13}$$

where $G_g = H^T H^*$ denotes the Gram matrix, which becomes an identity matrix when the BS antennas increases to infinity. As a result, computational complexity reduces.

$$y^{ZF} = \sqrt{\beta_a}\sqrt{P_{ant}} H^T H^* \left(G_g^{-1}\right) s + w, \quad y \epsilon \mathbb{C}^{U\times 1} \tag{2.14}$$

The performance of ZF precoder is close to optimal as the noise is trivial compared to the interference. The ZF precoder is very simple to implement, but it doesn't provide the optimal results when noise is very high. However, it attains good performance metrics when SNR is very high.

(ii): MRT Precoding

The MRT mainly aims to maximize the transmitted signal gain into a specific receive user terminal and is the counterpart of the MF precoding and conjugate beamforming. The precoding matrix of MRT scheme is represented as

$$Q_B^{MRT} = \sqrt{\beta_a} \left(H^*\right) \tag{2.15}$$

where H^* is the complex conjugate of H matrix and β_a is a precoded factor. Then, the received signal is given as

$$y^{MRT} = \sqrt{\beta_a}\sqrt{P_{ant}}H^T H^* s + w, \quad y \epsilon \mathbb{C}^{U\times 1} \tag{2.16}$$

where P_{ant} represents the per antenna transmit power. The performance of MRT precoding is close to optimal as the interference is trivial compared to noise. Besides, each BS antenna in MRT performs signal processing locally. Therefore, it allows a decentralized construction, thus leading to offer a more flexibility.

(iii): MMSE Precoding

The MMSE utilizes both the benefits of ZF and MRT schemes. So, it is a compromise between them. The MMSE precoding reduces the MSE between the transmitted signal at the BS and the received signal at the user terminal, thus achieving a better performance. The precoding matrix of MMSE scheme is represented as

$$Q_B^{MMSE} = \sqrt{\beta_a}H^* \left(G_g + V + \lambda I_N\right)^{-1} \tag{2.17}$$

The parameter λ and matrix V denote the positive regularizing factor and Hermitian non-negative matrix, respectively. The parameter λ depends on the channel characteristics and system dimensions. The matrix V decides the performance of the MMSE precoder. The received signal of MMSE precoder is given as

$$y^{MMSE} = \sqrt{\beta_a}\sqrt{P_{ant}}H^T H^* \left(G_g + V + \lambda I_N\right)^{-1} s + w, \quad y \epsilon \mathbb{C}^{U\times 1} \tag{2.18}$$

Although the linear precoders are low complex, precoding accuracy is not so good, especially when B/U is close or equal to one. The ML precoder is the optimal precoder when compared to other precoders, but its complexity increases exponentially when number of BS antennas (i.e., B) increases. Therefore, the ML precoders are not suitable to implement in massive MIMO systems. The non linear precoding techniques include dirty-paper coding (DPC), tomlinson-harashima (TH), vector perturbation (VP) precoding, and lattice reduction aided (LR) precoding.

A massive MIMO system with more number of antennas increases the power consumption and hardware cost when costly PAs are employed. Hence, it is essential to find a practical solution to implement massive MU-MIMO systems [99, 100]. The massive MIMO systems are

practically implemented by employing efficient nonlinear HPAs. Consequently, the PAPR of the massive MIMO should be low to reduce the effect of amplifier non-linearity.

2.10.2 Literature on precoding techniques in Massive MIMO

The precoders in massive MIMO reduce interference, but it increases the PAPR of the system. Since high PAPR reduces the efficiency of the HPA, low-PAPR precoders are desirable to increase the efficiency of the HPA. In [101], low-PAR precoders were implemented for massive MIMO systems to increase the power efficiency. Moreover, the proposed low-PAPR precoding was compared with the various precoders, such as ZF, regularized ZF, MRT, and constant-envelope (CE) precoding schemes.

As the number of BS antennas increases, the complexity of the massive MIMO systems increases, so the implementation of massive MIMO systems is a challenging task. Hence, 1-bit digital-to-analog converters (DACs) were considered in [102] for the downlink massive MIMO systems to attain low complex systems. It is the first work that consider 1-bit DACs along with OFDM for massive MU-MIMO over frequency-selective channels. Also, the impact of the quantization effects was analyzed. The low-complexity MRT technique was employed for user separation and requires less signal processing operations than singular value decomposition and zero forcing techniques. Results confirm that the nonlinear distortion levels decrease when the number of BS antennas increases. Consequently, good performance is achieved even with 1-bit DACs.

In [103], the authors mostly concentrated on the computational complexity of massive MIMO systems. Hence, 1-bit quantized ZF precoding was employed for massive MIMO system in order to reduce complexity and power consumption. With large number of antennas and an accurate CSI, the proposed method generates received signals, which are perfectly detected like the desired symbols at each UE. Results showcase that the proposed method provides better performance than ML encoder, particularly at low to moderate SNRs.

A mathematical analysis of 1-bit quantized linear precoders for massive MU-MIMO downlink systems was presented. The use of 1-bit DACs reduces the power consumption and computational complexity at BS [104]. Bussgang theorem was used to analyze the performance of 1-bit linear precoders, specifically the 1-bit quantized ZF precoder was analyzed. A simple asymptotic expression, which indicates SER at each terminal, was derived for 1-bit quantized linear ZF precoder. Simulations confirm that the proposed scheme achieves slightly better

performance when compared to non-linear least squares encoder for low to moderate SNRs. Moreover, a modified quantized ZF precoder that provides lower SERs at high SNR was also proposed.

The performance of linear precoders like MRT and ZF, subject to coarse quantization was analyzed [105]. A closed-form approximation was derived by employing Bussgang's theorem that can be used to analyze the 1-bit ADC massive MIMO systems. The results show that the performance of massive MIMO with infinite-resolution DACs is comparable to the DACs with 3-4 bits resolution. Moreover, a novel nonlinear precoding scheme with 1-bit quantization was proposed for massive MIMO system. The proposed precoding provides better performance than linear precoders, but it increases the computational complexity. In particular, the proposed nonlinear precoding suffers only a 3 dB penalty when compared to the infinite-resolution case at BER of 10^{-3}, while it is about 8 dB in case of linear precoders.

In [106], an OFDM based down link massive MIMO systems were investigated. The multi carrier OFDM system causes high PAPR that requires expensive RF components at the BS. Therefore, low PAPR massive MU-MIMO-OFDM systems are desirable to reduce the complexity and cost. So, a novel PMP scheme that jointly performs the multi user precoding, modulation (OFDM), and PAPR reduction was employed. The proposed PMP scheme maintains a trade-off between SNR and PAPR performance for the OFDM based massive MU-MIMO downlink systems. Numerical results show that PMP reduces PAPR by more than 11 dB when compared to traditional precoding schemes with no significant OOB interference.

The constant envelope precoders are more favorable for massive MIMO systems to attain high energy efficiency, especially when large number of antennas is used at base station. The constant envelope approach reduces the MUI by varying the phases of the transmit signal. In [107], a novel scheme that employs the cross-entropy optimization (CEO) technique to reduce the MUI of the constant envelope algorithm was proposed. Simulation outcomes confirm that the CEO technique provides better performance gains than the conventional constant envelope precoding schemes and linear zero-forcing precoding scheme. On the other hand, the proposed CEO technique suffers from high computational complexity than the sequential gradient descent research scheme.

In [108], the constant envelope precoder was employed for massive MU-MIMO systems. A computationally efficient optimization algorithm was employed to obtain the constant envelope precoded samples that reduce the PAPR of the massive MIMO signal. Besides, the performance of the proposed scheme was analyzed by considering the power amplifiers. The

results prove that the proposed precoder offers better performance in terms of signal to interference plus noise ratio than ZF precoder by up to 5-6 dBs, when the power amplifiers are operated in the saturation region.

The optimization problem of the non-linear mapping technique is shown as non-convex due to 1-bit quantization. Hence, the conversion of non-convex optimization problem to convex optimization problem is the primary goal in non-linear schemes. Thereafter, an element-wise normalization was employed on convex constraints to assure 1-bit DAC transmission. In [109], a symbol scaling approach, which provides low complexity and selects 1-bit quantized massive MIMO signal from each antenna element, was proposed. In massive MIMO, all precoding schemes offer low BER due to the large number of antennas at the base station. Generally, the non-linear precoding techniques achieve low BER than linear precoding schemes. The results confirm that the proposed approach attains an equivalent performance to the non-linear optimization based algorithms. Additionally, the proposed symbol scaling method offers less computational complexity than non-linear precoding techniques. The proposed scheme is more flexible as there is a trade-off between performance and computational complexity.

2.11 Conclusion

From the literature survey discussed in above sections, Chapter 2 can be concluded with a few major observations as follows:

The UFMC, a promising 5G technology, is a compromise between OFDM and FBMC. The channel estimation and PAPR are the key performance indicators of any wireless communication system. Hence, the performance of UFMC system is analyzed by employing channel estimation schemes and PAPR reduction schemes. The channel effect is estimated and compensated by using pilot based CE schemes, which are simple and provides better estimation accuracy when compared to blind channel techniques. The PAPR of the UFMC system is reduced by employing companding transforms, which are simple and don't require any side information, but they affect the system performance. Consequently, the design of companding transforms is the crucial task since trade-off exists among PAPR, BER and spectral regrowth. Moreover, the combination of massive MIMO with UFMC system is a possible solution to meet the desired requirements of future wireless communications (5G and beyond 5G). Besides, the computational complexity and power consumption in massive MIMO systems are reduced by employing the quantized pecoding schemes.

Chapter 3

Performance Analysis of Channel Estimation Techniques

3.1 Introduction

Channel estimation is one of the fundamental design issues of wireless communication system. In general the received signal is affected by channel characteristics. Hence, CSI derived from CE is essential for receivers to perfectly recover the transmitted signals. The CSI is efficiently extracted by employing known training symbols called pilot symbols that are known to both transmitter and receiver. The pilot symbols that are inserted into the data symbols can be used for CE.

Two popular pilot structures can be employed based on the arrangement of pilots as block type and comb-type. In block type, the pilot symbols are inserted in few UFMC symbols on all subcarriers periodically as shown in Fig. 3.1. The time domain interpolation is employed to estimate the CSI along time axis. Whereas in comb type, pilot tones are inserted in few subcarriers of all UFMC symbols periodically as shown in Fig. 3.2. The frequency domain interpolation is employed to estimate the CSI along frequency axis.

The contents of this contribution are ordered as follows. The proposed UFMC system model with CE is discussed in section 3.2. The proposed channel estimation schemes and interpolation schemes are described in section 3.3. The simulation results of the proposed system and conclusions are discussed in section 3.4 and section 3.5, respectively.

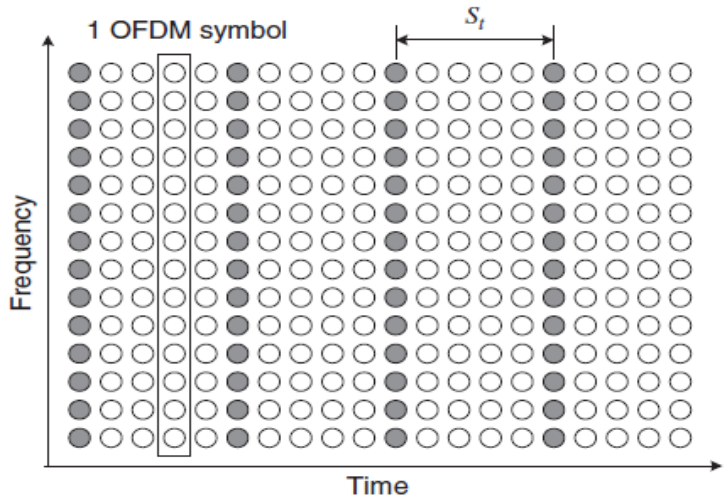

Figure 3.1: Block type pilot structure.

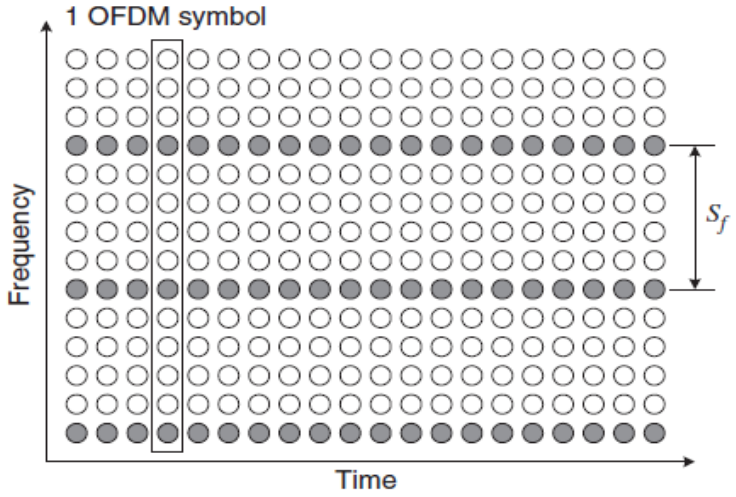

Figure 3.2: Comb type pilot structure.

3.2 UFMC system model with channel estimation

The UFMC system with CE is described in Fig. 3.3. The entire bandwidth with N subcarriers of UFMC system is separated into M number of sub-bands. Each sub-band includes consecutive subcarriers, which are modulated by employing QAM as a modulation scheme. Then, the pilots are inserted in the frequency domain by employing comb-type pilot arrangement to estimate the CSI at the receiver.

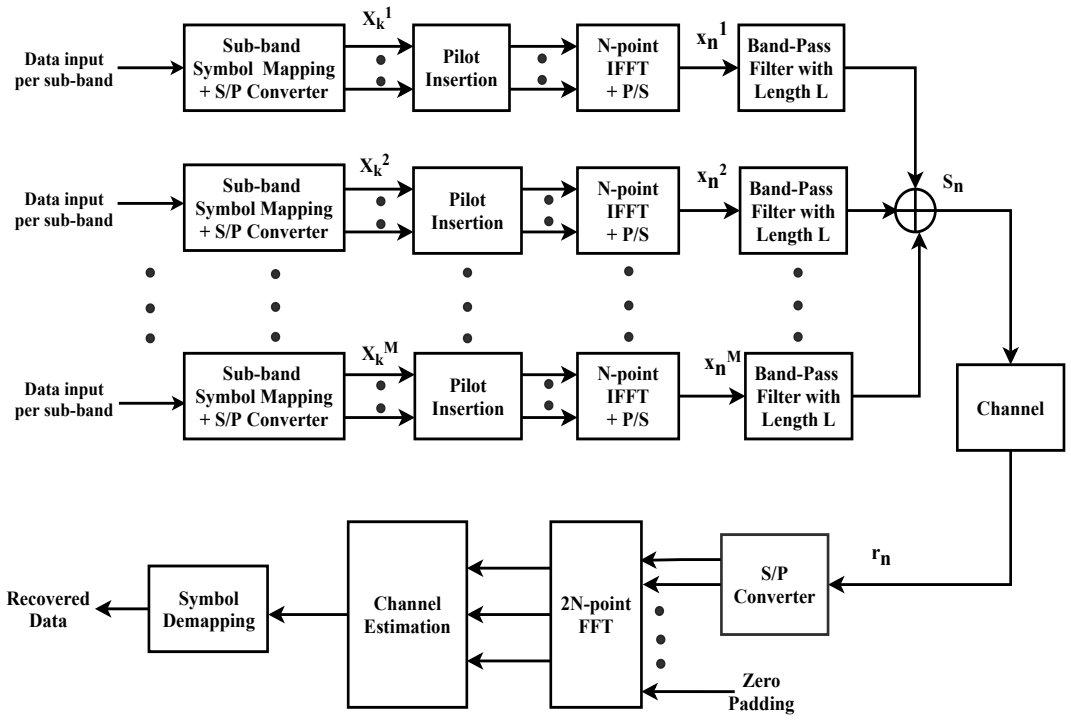

Figure 3.3: UFMC system with channel estimation.

In each sub-band, the N_q pilot symbols are inserted uniformly into the modulated signal X_k based on the following eq(3.1).

$$X_k = X_{[mN_f+d]} = \begin{cases} x_q(m), & d = 0 \\ \text{data}, & d = 1, 2, ...N_f - 1 \end{cases} \tag{3.1}$$

Where, X_k is the parallelized data, N_f denotes the pilot insertion frequency, m = 0, 1, 2,...,N_q-1, N_q is the number of pilot subcarriers that can be obtained as $N_q = \frac{N}{N_f}$, and N represents the number of subcarriers.

The pilot aided frequency domain signal is passed through the N-IFFT block to attain the time domain signal. For an arbitrary p^{th} sub-band B^p, where $p \, \varepsilon (1 : M)$, the frequency domain signal X_k^p is transformed to the time domain signal x_n^p by the IFFT operation, and the expression is

$$x_n^p = \frac{1}{N} \sum_{k \epsilon B^p} X_k^p \exp^{j\frac{2\pi}{N}nk} \qquad 0 \leq n \leq N-1 \tag{3.2}$$

Later, the signal x_n^p is transmitted through a band pass filter (BPF). Here, Dolph-chebyshev filter with filter length L is employed as a BPF. The filtering in the UFMC system eradicates OOB radiations successfully. The UFMC signal with $N + L - 1$ symbol length is attained by employing linear convolution between the filter impulse response f_l and the IFFT signal x_n^p.

Then the UFMC signal can be mathematically expressed as

$$s_n = \frac{1}{N} \sum_{p=1}^{B} \sum_{l=0}^{L-1} \sum_{k=B^p} X_k^p f_l^p \exp^{\frac{j2\pi(n-l)k}{N}} \qquad 0 \leq n \leq N + L - 1 \tag{3.3}$$

where f_l^p denotes the l^{th} filter coefficient. Afterwards, the UFMC signal is passed through a wireless channel. The received signal r_n is written as

$$y_n = s_n * h_n + w_n \tag{3.4}$$

where w_n denotes channel noise with mean of 0 and variance of 1. The time domain signal is passed through the $2N$-FFT block to obtain the frequency domain signal. After the FFT operation the received output signal at the k^{th} subcarrier can be represented as

$$Y_k = X_k F_k H_k + W_k \tag{3.5}$$

where X_k, F_k, H_k, and W_k denotes the transmitted UFMC signal, Chebyshev filter response, frequency response of channel, and channel noise of the k^{th} subcarrier, respectively. The signal represented in the above eq(3.5) is a generalized representation of multi-carrier system. The frequency domain channel estimation and equalization is performed for each subcarrier to eliminate inter symbol interference in the signal. Finally the equalized output is de-mapped to retrieve the data bits.

3.3 Channel estimation in UFMC

The received UFMC signal represented in eq(3.5) is almost same as the OFDM received signal after FFT operation except FIR filter response in UFMC signal (i.e., it becomes a OFDM received signal if F_k =1). The CE and equalization schemes of OFDM are applicable to UFMC, except that the filter response in UFMC is additionally equalized. Hence, the filter response is compensated immediately after $2N$-FFT and then without any modification performs the channel estimation techniques similarly as in OFDM system, as shown in Fig. 3.4. Now the filter response in eq(3.5) has to be compensated to get the channel estimates. Then the compensated received signal is represented as

$$Y = XH + W \tag{3.6}$$

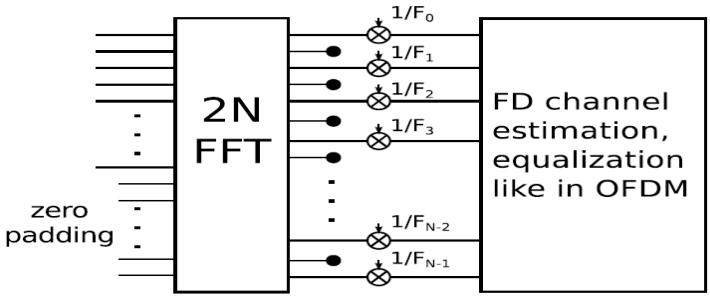

Figure 3.4: Channel estimation in UFMC.

3.3.1 Least square channel estimation

Least squares method is one of the channel estimation techniques to measure the channel parameters at the pilot carriers. If the pilots are arranged properly then we can get the better estimation in terms of mean square error. With respect to some performance measures the equally spaced and equally powered pilot symbols gives the optimal performance. In eq(3.6), W represents the noise that is random in nature and can be modeled as Additive White Gaussian Noise (AWGN) with mean zero and variance σ^2. Therefore, Y is also random with mean XH and variance σ^2. The log likelihood function $L(Y;H)$ given the least square cost function as

$$L(Y;H) = \|Y - XH\|^2 \tag{3.7}$$

$$\begin{aligned} \|Y - XH\|^2 &= (Y - XH)^H (Y - XH) \\ &= \left(Y^H - H^H X^H\right)(Y - XH) \\ &= Y^H Y - Y^H XH - H^H X^H Y + H^H X^H Y + H^H X^H XH \\ &= Y^H Y - 2Y^H Y + H^H X^H XH \quad (\because Y^H XH = H^H X^H Y) \end{aligned} \tag{3.8}$$

The LS estimate is obtained by minimizing the least square cost function i.e., min $\|Y - XH\|^2$. The minimum value is calculated by derivative the least square cost function with respect to true channel parameter H and equate it to zero.

$$\frac{\partial \|Y - XH\|^2}{\partial H} = 0 \tag{3.9}$$

Finally the estimate of LS technique is obtained as

$$H^{LS} = \left(X^H X\right)^{-1} X^H Y = X^{-1} Y \tag{3.10}$$

From eq(3.10), it clearly depicts that LS estimation is the simple division of the pilot tones at output, affected by channel over pilot tones inserted at input. LS channel estimate of each component is represented as H_k^{LS}, where k = 0,1,2...,N-1. The channel estimate of LS at each subcarrier is obtained by

$$H_k^{LS} = \frac{Y_k}{X_k} \tag{3.11}$$

Channel parameters are estimated at the pilot subcarriers using eq(3.11). Besides, the interpolation techniques are employed to get the channel estimates at data subcarriers. The MSE of the LS estimator is given by

$$\begin{aligned} MSE^{LS} &= E\left\{\left(H - \hat{H}^{LS}\right)^H \left(H - H^{LS}\right)\right\} \\ &= E\left\{\left(H - X^{-1}Y\right)^H \left(H - X^{-1}Y\right)\right\} \\ &= E\left\{\left(X^{-1}W\right)^H \left(X^{-1}W\right)\right\} \\ &= \frac{\sigma_w^2}{\sigma_x^2} \end{aligned} \tag{3.12}$$

where σ_w^2 and σ_x^2 denote the variance of the channel and transmitted UFMC, respectively. The MSE of LS estimatior in eq(3.12) is inversely proportional to signal to noise ratio (i.e., SNR=$\frac{\sigma_x^2}{\sigma_w^2}$) that increases the noise, particularly when the channel is in a deep null. However, the LS technique is widely employed for CE due to its simplicity.

3.3.2 Minimum mean square error channel estimation

The accuracy of LS estimate reduces when noise is high as MSE is inversely proportional to signal to noise ratio. Hence, MMSE is employed that minimizes the estimation error between the true value and the estimated value. The error of the estimator is represented as

$$e = H - \hat{H} \tag{3.13}$$

where H and $\hat{H}$ are the true value and estimated values of the channel impulse response (CIR).

From Fig. 3.5, the estimated value of CIR is given in eq(3.14) as

$$\hat{H} = W_m \tilde{H} \tag{3.14}$$

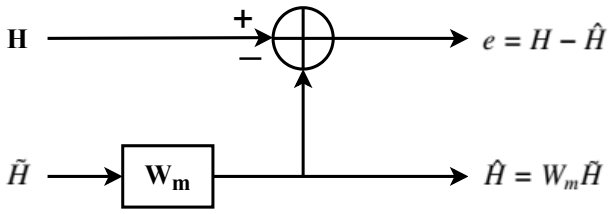

Figure 3.5: MMSE channel estimation.

where W is the weight matrix that corresponds to the MMSE estimate. The MSE of the estimate is represented as

$$E\left\{\left\|e^2\right\|\right\} = E\left\{\left\|H - \hat{H}\right\|^2\right\} \tag{3.15}$$

Then, the MMSE technique determines a better estimate by minimizing the MSE in eq(3.15) in terms of W_m.

The multipath fading channel and the AWGN channel are independent to each other. Hence, the channel estimate of MMSE is given as

$$\hat{H}^{MMSE} = R_{HY} R_{YY}^{-1} Y \tag{3.16}$$

where, R_{YY} is the auto covariance of output Y , R_{HH} is the auto covariance of true channel parameter H, R_{HY} is cross covariance of H and Y.

$$\begin{aligned} R_{HY} &= E\left\{HY^H\right\} \\ &= E\left\{H\left(XH + W_m\right)^H\right\} \\ &= E\left\{HH^H X^H + HW_m^H\right\} \\ &= E\left\{HH^H\right\} X^H + 0 \\ &= R_{HH} X^H \end{aligned} \tag{3.17}$$

$$\begin{aligned} R_{YY} &= E\left\{YY^H\right\} \\ R_{YY} &= E\left\{\left(HX + W_m\right)\left(HX + W_m\right)^H\right\} \\ &= E\left\{HXH^H X^H + HXW_m + W_m H^H X^H + W_m W_m^H\right\} \end{aligned}$$

$$= E\left\{HH^H\right\} XX^H + 0 + 0 + E\left\{W_m W_m^H\right\}$$

$$= XR_{HH}X^H + \sigma_N^2 I_N \tag{3.18}$$

If the auto covariance of H (i.e., R_{HH}) and σ_N^2 are known, then the CIR of the channel can be estimated by the MMSE scheme that is given below

$$\hat{H}^{MMSE} = R_{HY}R_{YY}^{-1}Y$$

$$= R_{HH}X^H\left(XR_{HH}X^H + \sigma_N^2 I_N\right)^{-1} XH^{LS}$$

$$\hat{H}^{MMSE} = R_{HH}\left(R_{HH} + \sigma^2\left(XX^H\right)^{-1}\right)^{-1}\hat{H}^{LS} \tag{3.19}$$

The MMSE estimator proffers enhanced performance gains than LS estimator, particularly at lower signal to noise ratios.

3.4 Interpolation techniques

Interpolation technique is one of the essential operations in channel estimation. In comb-type arrangement, the LS estimated CSI at the pilot positions must be interpolated in the frequency direction in order to get the CSI at data positions. The interpolators, such as linear, second-order, and cubic spline are generally employed for estimation. In linear interpolation (LI), the CSI at the data positions are obtained by estimating CSI between the two adjacent pilot positions that can be calculated simply by assuming a straight line between the two known positions. The linear interpolation can be expressed as

$$\hat{H}_K = \hat{H}\left(mN_f + d\right) = \left(\hat{H}_q(m+1) - \hat{H}_q(m)\right)\frac{1}{N_f} + \hat{H}_q(m) \quad m = 0, 1, ..., N_q - 1 \tag{3.20}$$

It can be seen from eq(3.20) that only two pilot symbols are employed in LI to estimate the CSI at data symbols. Therefore, the computational complexity of LI is low, but the performance of LI is not satisfactory. Second order interpolation that assumes second order curves to estimate the CSI between the two known positions and offers better accuracy than LI. It can be mathematically represented as

$$\hat{H}_K = \hat{H}\left(mN_f + d\right) = v_1\hat{H}_q(m-1) + v_0\hat{H}_q(m) + v_{-1}\hat{H}_q(m+1) \quad m = 0, 1, ..., N_q - 1 \tag{3.21}$$

The coefficients are described as

$$v_1 = \frac{\alpha_b(\alpha_b-1)}{2}$$

$$v_0 = -(\alpha_b - 1)(\alpha_b + 1), \quad \alpha_b = \frac{d}{N_f}$$

$$v_{-1} = \frac{\alpha_b(\alpha_b + 1)}{2} \tag{3.22}$$

The higher order interpolation schemes offer better estimation accuracy when compared to first order interpolation. But the computational complexity increases as the order of polynomial increases. The cubic spline interpolation provides a better smooth and continuous polynomial fitted to the given points and mathematically denoted as

$$\hat{H}_K = \hat{H}\left(mN_f + d\right) = j_1\hat{H}_q(m+1) + j_0\hat{H}_q(m) + N_f j_1\hat{H}_q^{'}(m+1) - N_f j_0\hat{H}_q^{'}(m) \tag{3.23}$$

where m = 0,1,....,N_q-1, $\hat{H}_q^{'}(m)$ is the first order derivative of $\hat{H}_q(m)$, and

$$j_1 = \frac{3\left(N_f-d\right)^2}{N_f^2} - \frac{2\left(N_f-d\right)^3}{N_f^3}$$

$$j_0 = \frac{3d^2}{N_f^2} - \frac{2d^3}{N_f^3} \tag{3.24}$$

The cubic spline interpolation provides better estimation accuracy when compared to first and second order interpolation schemes.

3.5 Performance evaluation

The performance of UFMC system that is shown in Fig. 3.3 is analyzed in terms of BER and MSE. The sub-bands considered for computer simulations are M = 8, the number of subcarriers in each sub-band is considered as 16, size of the FFT is N = 512, the number of pilots in each sub-band are 2, so total pilots employed in the system are 16, and the filter length is considered as 43. Quadrature amplitude modulation (QAM) and Phase shift keying (PSK) are employed as modulation schemes for UFMC system.

Fig. 3.6 presents the BER performance of UFMC system for different orders of M-ary PSK over AWGN channel. It can be observed from Fig. 3.6 that the BER performance deteriorates as

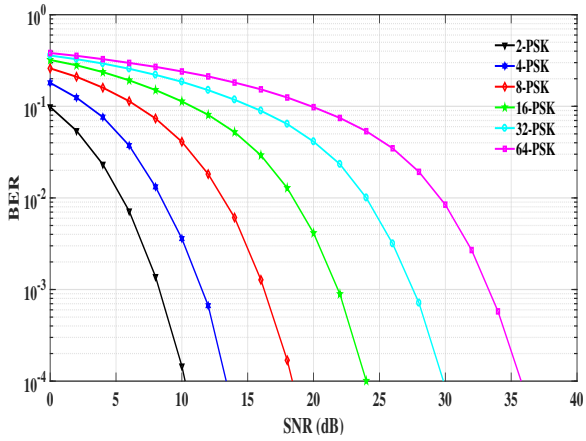

Figure 3.6: Comparison of BER performance of UFMC system for different orders of M-ary PSK over AWGN channel.

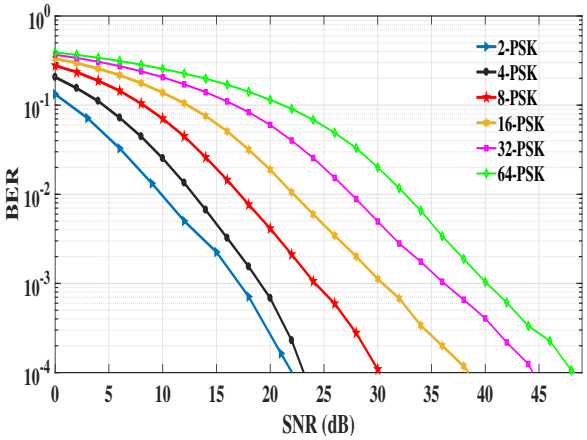

Figure 3.7: Comparison of BER performance of UFMC system for different orders of M-ary PSK over Rician channel.

the order of PSK increases. From Fig. 3.6, the BER of UFMC system for 4-PSK is 0.667×10^{-3} at SNR of 12 dB. While for 16-PSK, the BER is 8.07×10^{-2} at SNR of 12 dB.

Fig. 3.7 shows the BER performance of UFMC system for different orders of M-ary PSK over Rician channel. It can be observed from Fig. 3.7 that the BER performance deteriorates as the order of PSK increases. From Fig. 3.7, the BER of UFMC system for 4-PSK is 0.684×10^{-3} at SNR of 20 dB. Hence, the BER performance of AWGN channel is better when compared to the rician channel.

Fig. 3.8 illustrates the BER performance of UFMC system for different orders of M-ary QAM over AWGN channel. It can be observed from Fig. 3.8 that the BER performance deteriorates as the order of QAM increases. From Fig. 3.8, the BER of UFMC system for 4-QAM is 0.543×10^{-3} at SNR of 12 dB. While for 16-QAM, the BER is 4.24×10^{-2} at SNR

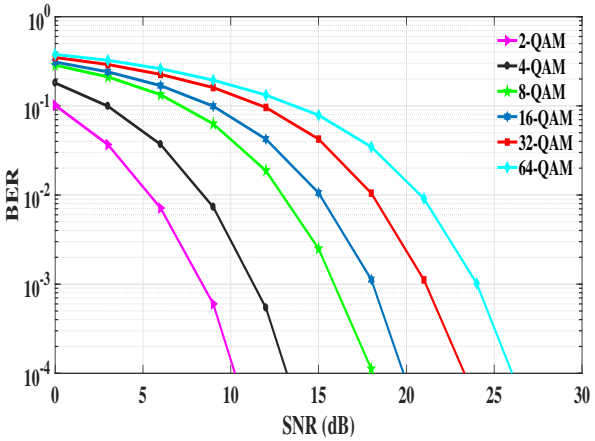

Figure 3.8: Comparison of BER performance of UFMC system for different orders of M-ary QAM over AWGN channel.

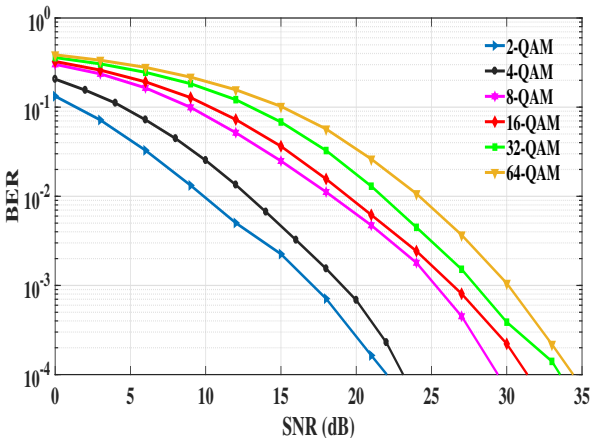

Figure 3.9: Comparison of BER performance of UFMC system for different orders of M-ary QAM over Rician channel.

of 12 dB. It is evident from Figs. 3.6 and 3.8, that the BER performance of 16-QAM is better than that of 16-QPSK.

Fig. 3.9 presents the BER performance of UFMC system for different orders of M-ary QAM over Rician channel. It can be observed from Fig. 3.9 that the BER performance deteriorates as the order of QAM increases. From Fig. 3.9, the BER of UFMC system for 4-QAM is 0.684×10^{-3} at SNR of 20 dB. Hence, the BER performance of AWGN channel is better when compared to the rician channel.

Fig. 3.10 and Fig. 3.11 illustrate the comparision of MSE performance of UFMC system for LS and MMSE techniques over AWGN channel and Rician channel, respectively. It can be concluded Fig. 3.10 and Fig. 3.11 that MMSE scheme provides better MSE performance than LS scheme.

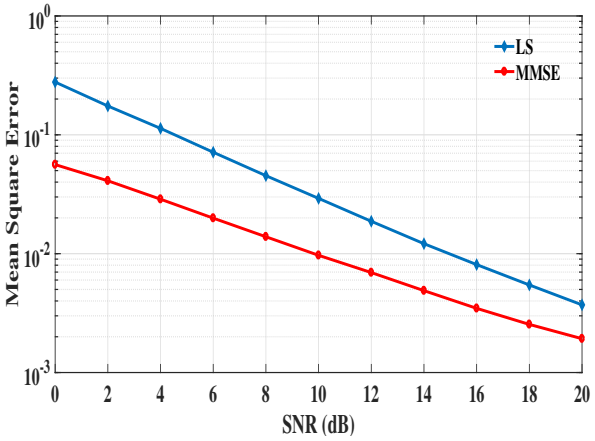

Figure 3.10: Comparison of MSE performance of UFMC system for LS and MMSE techniques over AWGN channel.

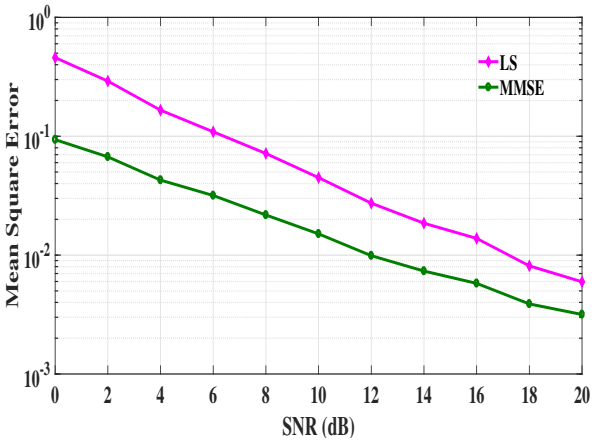

Figure 3.11: Comparison of MSE performance of UFMC system for LS and MMSE techniques over Rician channel.

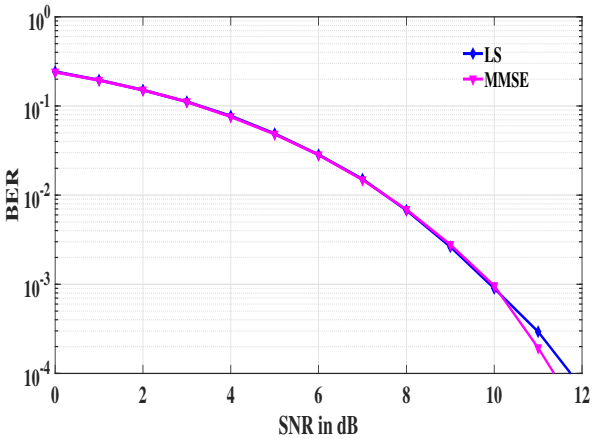

Figure 3.12: Comparison of BER performance of UFMC system for LS and MMSE techniques over AWGN channel.

Fig. 3.12 shows the comparision of BER performance of UFMC system for LS and MMSE techniques over AWGN channel. The MMSE provides better BER characteristics when compared to LS scheme. It can be observed from Fig. 3.12 that the BER of UFMC system with proposed MMSE technique is 0.962×10^{-3} at SNR of 10 dB. Hence, it is confirmed from Fig. 3.8 and Fig. 3.12 that the proposed UFMC system with channel estimation offers better BER performance when compared to UFMC system without channel estimation.

3.6 Conclusion

In this contribution, a comb type pilot structure has been employed to estimate and compensate the channel for UFMC system. The performance of UFMC system has been analyzed using different orders of PSK and QAM techniques over AWGN and multipath fading channels. Besides, LS and MMSE estimation techniques have been employed to measure the channel estimates at the receiver structure. The interpolation techniques, such as linear and spline have been applied to estimate the channel at data subcarriers. The estimation accuracy of LS technique is poor as MSE is inversely proportional to SNR. Whereas MMSE provides better accuracy when compared to LS technique. However, the computational complexity of MMSE is high due to the requirement of knowledge of channel statistics (KCS) parameters. Since LS method is simple, it is widely used for CE. Finally, it is concluded that the proposed UFMC system with channel estimation offers better BER performance when compared to UFMC system without channel estimation.

Chapter 4

Performance Analysis of Various Companding Transforms

4.1 Introduction

PAPR, which severely affects the performance of power amplifier [49], is one of the serious drawbacks of multi-carrier systems. Also, as high PAPR demands the large input backoff and decreases the efficiency of the transmit power amplifier considerably, linear amplification of the input signal must be ensured. Besides, high PAPR needs a high-resolution quantizer to reduce quantization error and also introduces more complexity at the receiver front end. The PAPR problem is more important in the uplink since efficiency of a power amplifier is critical due to limited battery power in a mobile terminal. Hence, high PAPR increases energy consumption, which should be minimum in 5G networks as energy efficiency is one of the essential requirements of 5G. Therefore, there is a need to reduce PAPR in 5G UFMC systems.

To the best of authors' knowledge, there has not been any significant work on the design of non-linear companding transforms to reduce PAPR in UFMC systems. In order to maintain a trade-off between the performances of PAPR and BER, companding transforms, which is one of the most challenging task need to be developed.

4.2 Nonlinear companding transform

Nonlinear companding is an efficient and simple technique to offer a low PAPR with no need of side information. It decreases the PAPR by suppressing large signals and enlarging small signals. Nevertheless, these schemes are characterized as distorting methods, which affect the BER performance. Consequently, the design of companding techniques is a challenging task as a trade-off between the PAPR and BER must be maintained.

The μ-law is the most popular nonlinear companding technique, and it is used to reduce the PAPR of the proposed system. In this scheme, the small amplitude values of the real signal are enlarged to decrease the variation between large amplitude values and small amplitude values of the transmitted signal. The μ-law companding diminishes PAPR effectively. However, this technique raises the average power level of companded signal. Therefore the improvement in performance metrics might be of an enhanced average power level of the UFMC signal after performing μ-law but not of companding function itself. Hence, new companding schemes are required for UFMC system to reduce PAPR and keep the average power level as constant.

In this contribution, an exponential companding technique is employed for UFMC signals. This EC scheme can successfully transform the rayleigh-distributed UFMC signals into uniform-distributed signals based on an optimum companding parameter d. Unlike μ-law companding technique, which mainly concentrates on enlarging small amplitude signals and raises the average power level, exponential companding technique alters both the small and large amplitude signals without bias and also maintains the constant average power level. Therefore, EC scheme improves the PAPR reduction with a slight deterioration in the bit error rate for UFMC system when compared to μ-law scheme.

To further improve the performance of UFMC system, we propose an optimal non-linear companding transform called "modified exponential companding". The proposed scheme employs two companding levels in which the first level of companding is attained for the magnitude of UFMC signal, which are below the threshold and the signals above the threshold are companded with the second level. Simulation outcomes confirm that the proposed MEC method offers enhanced PAPR and BER performance compared to the conventional EC scheme. A hybrid PAPR reduction scheme in which clipping function is performed on MEC signal based on a suitable clipping ratio is also proposed. An enhanced UFMC system performance is achieved in terms of net gain by adopting the proposed MEC and hybrid schemes.

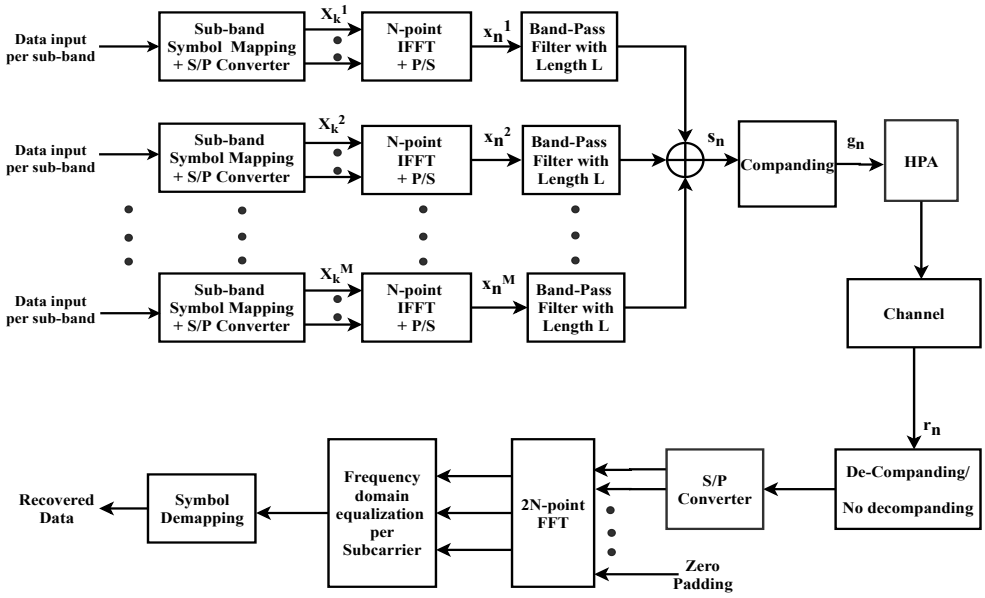

Figure 4.1: UFMC system model with companding

This contribution is organized as follows. Section 4.3 presents the UFMC system model and PAPR of UFMC system. Section 4.4 discusses about the proposed companding schemes to reduce PAPR in UFMC system. Section 4.5 illustrates the proposed MEC and hybrid schemes, selection of optimum companding parameters, performance evaluation of the proposed EC, MEC, and hybrid schemes, and demonstrates the experimental results of the proposed scheme. Section 4.6 exemplifies the proposed nonlinear companding transform based on error function, hybrid schemes, and performance analysis of proposed schemes for UFMC system and Section 4.7 describes the conclusions of this chapter.

4.3 UFMC system model with companding

A total of N subcarriers are present in the UFMC system as the UFMC system consists of M sub-bands in which each sub-band contains consecutive sub-carriers is shown in Fig. 4.1. The sub-bands are modulated by employing QAM. The QAM modulated signal is transformed to time domain signal by performing IFFT operation on every sub-band of the UFMC system. The mathematical modelling of UFMC system model is described as follows.

For an arbitrary p^{th} sub-band B^p, where $p\ \varepsilon(1:M)$, the frequency domain signal X_k^p is transformed to the time domain signal x_n^p by the IFFT operation, and the expression is

$$x_n^p = \frac{1}{N}\sum_{k\epsilon B^p} X_k^p \exp^{j\frac{2\pi}{N}nk} \qquad 0 \le n \le N-1 \tag{4.1}$$

Then the time domain signal x_n^p is passed through a Dolph-chebyshev band pass filter with filter length L. The filtering operation in UFMC system eliminate OOB emissions effectively. Now the UFMC signal is obtained by applying linear convolution between the time domain signal x_n^p and filter impulse response f_l. Therefore the length of UFMC symbol becomes $N + L - 1$. Then the transmitted UFMC signal at the transmitter can be denoted as

$$s_n = \sum_{p=1}^{M} b_n^p \qquad 0 \leq n \leq N + L - 1 \tag{4.2}$$

where M is total number of sub-bands and b_n^p is the p^{th} sub-band signal which can be given as

$$b_n^p = \sum_{l=0}^{L-1} x_{n-l}^p f_l^p \qquad 0 \leq n \leq N - 1 \tag{4.3}$$

where x_n^p is the time domain N-IFFT signal given in eq(4.1) and f_l^p is the l^{th} filter coefficient can be written as

$$f_l^p = f_l \exp^{\frac{j2\pi l C^p}{N}} \qquad 0 \leq l \leq L - 1 \tag{4.4}$$

where N indicates IFFT size, f_l is l^{th} reference filter coefficient and C^p denotes center sub-carrier index of p^{th} sub-band.

Finally, the UFMC signal at the transmitter end is obtained by incorporating eq(4.3) and eq(4.1) in eq(4.2) is

$$s_n = \frac{1}{N} \sum_{p=1}^{B} \sum_{l=0}^{L-1} \sum_{k=B^p} X_k^p f_l^p \exp^{\frac{j2\pi(n-l)k}{N}} \qquad 0 \leq n \leq N + L - 1 \tag{4.5}$$

4.3.1 PAPR of UFMC system

The discrete-time UFMC signal at the transmitter end s_n is sum of all independent random subcarriers. Therefore, the UFMC signal can have high peak values, which results high PAPR in UFMC system. The PAPR can be defined as

$$PAPR = \frac{\max_{n\epsilon[0,1,2.....N+L-1]} \left\{ |s_n|^2 \right\}}{E\left[|s_n|^2 \right]} \tag{4.6}$$

where $E\left[|s_n|^2 \right]$ is the average power of s_n.

The input data symbols are assumed to be statistically independent and identically distributed (i.i.d). By the central limit theorem, the real and imaginary parts of the complex time domain UFMC signal denoted by $Re\{s_n\}$ and $Im\{s_n\}$ are asymptotically Gaussian random variables for large values of N. The amplitude of UFMC signal can be represented as

$$|s_n| = \sqrt{Re^2\{s_n\} + Im^2\{s_n\}} \tag{4.7}$$

The amplitude of UFMC signals follows a Rayleigh distribution like OFDM signals. Then the probability density function can be written as

$$f_{|s_n|}(x) = \frac{x}{\sigma^2} \exp^{\frac{-x^2}{2\sigma^2}} \qquad 0 \leq n \leq N + L - 1 \tag{4.8}$$

The cumulative distribution function (CDF) can be obtained by integrating eq(4.8)

$$\begin{aligned} F_{|s_n|}(x) &= P(|s_n| \leq x) \\ &= \int_0^x \frac{x}{\sigma^2} \exp^{\frac{-x^2}{2\sigma^2}} dx \end{aligned} \tag{4.9}$$

On solving eq(4.9), The CDF is given by

$$F_{|s_n|}(x) = 1 - \exp\left(\frac{-x^2}{2\sigma^2}\right) \tag{4.10}$$

As PAPR is random, there is a need to estimate the statistical behaviour of PAPR. The CCDF characterizes the statistical behaviour of PAPR. The CCDF is given by [26]

$$\begin{aligned} F_{|s_n|}(x) &= P(|s_n| > x) \\ &= 1 - P(|s_n| \leq x) \\ &= 1 - F_{|s_n|}(x) \\ &= 1 - \left(1 - \exp\left(\frac{-x^2}{2\sigma^2}\right)\right) \end{aligned} \tag{4.11}$$

High PAPR is one of the most harmful aspects of any multicarrier system. Now, we have to implement PAPR reduction techniques for UFMC system. To reduce PAPR of UFMC system, the time domain UFMC signal has been transmitted through a companding block and then

amplified by the high power amplifier. The companding function can be represented as

$$g_n = t(s_n) \tag{4.12}$$

Now the companded signal has been transmitted through a wireless channel. Then the received signal r_n can be expressed as

$$r_n = g_n + w_n$$

$$r_n = t(s_n) + w_n \tag{4.13}$$

where w_n is the channel noise with mean zero and variance one. Now the decompanding operation can be performed to the received signal r_n is $t^{-1}(r_n)$. The decompanded signal is transmitted through $2N$-point FFT block to convert the time domain signal into the frequency domain. Then MMSE equalization is employed for each subcarrier to eradicate ISI. Finally, de-mapping is performed on equalized output to retrieve the data bits.

4.4 PAPR reduction in UFMC system using companding techniques

4.4.1 μ-law companding

The μ-law is a popular non-linear logarithmic based technique to reduce PAPR of multi-carrier systems. The mathematical formulation of μ-law companding is represented as [18]

$$t(x) = \frac{V}{\log(1+\mu)} \log\left(1 + \mu \frac{|x|}{V}\right) sgn(x) \tag{4.14}$$

where $V = max(x)$ is the maximum amplitude of the UFMC Signal, μ is the companding level, and sign(.) is the signum function. Then, at the receiver, decompanding is employed, which can be given as

$$t^{-1}(r) = \frac{V}{\mu}\left[\exp\frac{|r|\log(1+\mu)}{V} - 1\right] sgn(r) \tag{4.15}$$

4.4.2 A-law companding

The A-law companding is a standard nonlinear companding scheme that can be employed for PAPR reduction in multicarrier systems. In A-law scheme, when companding parameter A is greater than one (i.e., $A > 1$), the characteristic curve becomes nonlinear. The A-law companding is mathematically represented as

$$t(x) = \begin{cases} \frac{A|x|}{1+lnA}\ sgn(x), & 0 < |x| \leq \frac{V}{A} \\ V\frac{1+ln\left(A\frac{|x|}{V}\right)}{1+lnA}\ sgn(x), & \frac{V}{A} < |x| \leq V \end{cases} \tag{4.16}$$

where V, which is equal to $max\,(x)$, denotes the peak amplitude of s_n and $sign(.)$ is the signum function.

4.4.3 Hyberbolic tangent companding

In HT scheme, the transfer curve of the companding is expressed by a hyperbolic tangent function. The PAPR is effectively reduced by altering the small and large amplitudes of the transmitted signal based on the companding parameters. Additionally, HT scheme offers constant average power like EC scheme. The HT function is mathematically formulated as

$$t\,(x) = sgn(x)\ K\sigma\left[\tanh\left(\frac{|x|}{\sigma} - a\right) + b\right] \tag{4.17}$$

where tanh(.) is the hyperbolic tangent function, the terms a, b, and K are the companding parameters that can be used to get the optimum performance. The parameter K can be denoted as

$$K = \frac{1}{\sqrt{E\left\{\left|\tanh\left[\frac{|x|}{\sigma} - a\right] + b\right|^2\right\}}} \tag{4.18}$$

4.4.4 Advanced rooting companding technique

The ARCT scheme, which is also a nonlinear companding scheme, is the modified form of the square rooting companding technique. It is mathematically defined as

$$t\,(x) = |x|^R\ sgn\,(x) \tag{4.19}$$

where R denotes the companding parameter, which is nothing but the rate of change of amplitude of UFMC signal s_n. The value of the companding parameter R decides the optimum performance and lies between 0.1 and 0.9.

4.4.5 Proposed exponential companding

Exponential companding is also a nonlinear companding technique, which can efficiently reduce the PAPR of UFMC signals. In EC technique, the statistical distribution of amplitude of the UFMC signals is transformed into uniform distribution and maintains a constant average power level. The EC technique also provides some relaxation on the linearity requirements of HPA.

Let the d^{th} power of the amplitude of companded UFMC signal have uniform distribution in $[0, \rho_a]$, where the term d is degree of an exponential companding. The PAPR will be reduced for this scheme as all the amplitude values exhibit an equal probability. The d^{th} power of companded signal g_n have a CDF which can be written as

$$F_{|g_n|}d(x) = \frac{x}{\rho_a} \qquad 0 \leq x \leq \rho_a \tag{4.20}$$

The probability distribution of amplitude of the companded signal $|g_n|$ can be written as

$$\begin{aligned} F_{|g_n|}(x) &= P\{|g_n| \leq x\} \\ &= P\left\{|g_n|^d \leq x^d\right\} \\ &= \frac{x^d}{\rho_a} \qquad 0 \leq x \leq \sqrt[d]{\rho_a} \end{aligned} \tag{4.21}$$

The inverse function of $F_{|g_n|}(x)$ is given by

$$F^{-1}_{|g_n|}(x) = \sqrt[d]{\rho_a x} \qquad 0 \leq x \leq 1 \tag{4.22}$$

The companding function $t(x)$ is a strictly monotonic increasing function, which can be denoted as

$$F_{|g_n|}(x) = Pr\{|s_n| \leq x\}$$

$$= Pr\{t(|s_n|) \leq t(x)\}$$

$$= F_{|g_n|}(t(x)) \qquad 0 \leq x \leq t^{-1}(\sqrt[d]{\rho_a}) \tag{4.23}$$

Consider the phase of input signals, the companding function $t(x)$, which cannot affect the phase given by

$$t(x) = sgn(x) F^{-1}_{|g_n|}(F_{|s_n|}(x))$$

$$= sgn(x) \sqrt[d]{\rho_a \left[1 - exp\left(\frac{-x^2}{\sigma^2}\right)\right]} \tag{4.24}$$

The positive constant ρ_a decides the average power level of companded signal g_n. To retain the companded signal g_n average power level is same as that of s_n, we can described as

$$E\left[\left|s_n^2\right|\right] = E\left[\left|g_n^2\right|\right]$$

$$= E\left[\left[\rho_a\left(1 - \exp\left(\frac{-|s_n|^2}{\sigma^2}\right)\right)\right]^{\frac{2}{d}}\right] \tag{4.25}$$

Now ρ_a is given by

$$\rho_a = \left(\frac{E\left[\left|s_n^2\right|\right]}{E\left[\left[1 - \exp\left(\frac{-|s_n|^2}{\sigma^2}\right)\right]^{\frac{2}{d}}\right]}\right)^{\frac{d}{2}} \tag{4.26}$$

The companded signal g_n is passed through the channel. At the receiver section first, we have employed inverse operation of companding known as decompanding, on the received signal r_n, which can be mathematically represented as

$$t^{-1}(r) = sgn(r) \sqrt{-\sigma^2 \log_e\left(1 - \frac{r^d}{\rho_a}\right)} \tag{4.27}$$

The exponential companding scheme can change both the large and small amplitude values and also keep a similar average power by suitably choosing transform parameters. This technique can reduce the PAPR of UFMC signal effectively than μ-law companding scheme. However, there is a slight degradation in the BER performance compared to μ-law.

4.5 Proposed modified exponential companding

In proposed MEC transform, a threshold parameter α is a pioneer in the companding operation. Therefore, the UFMC signal is companded with d_1 value below the parameter α whereas d_2 can be applied to the rest. With these modifications, the proposed MEC technique provides optimum performance of both PAPR and BER with an appropriate selection of d_1, d_2 and the threshold α values based on the system requirements. Therefore, there is higher liberty than the conventional EC scheme.

The mathematical modelling of the modified exponential companding transform can be represented as

$$\begin{cases} t_1(x, d_1) = sgn(x) \sqrt[d_1]{\rho_a \left(1 - \exp\left(\frac{-x^2}{\sigma^2}\right)\right)} & |x| \leq \alpha \\ t_2(x, d_2) = sgn(x) \sqrt[d_2]{\rho_a \left(1 - \exp\left(\frac{-x^2}{\sigma^2}\right)\right)} & |x| > \alpha \end{cases} \tag{4.28}$$

At the receiver section, the inverse companding transform is performed on the received signal r_n. Now we have considered two possibilities, the first case is to perform decompanding transform on the received signal r_n and the other case is no decompanding at the receiver. The decompanding transforms of $t^{-1}(r, d_1)$ and $t^{-1}(r, d_2)$ can be expressed as

$$\begin{cases} t^{-1}(r, d_1) = sgn(r) \sqrt{-\sigma^2 \log_e \left(1 - \frac{r^{d_1}}{\rho_a}\right)} & |r| \leq \alpha \\ t^{-1}(r, d_2) = sgn(r) \sqrt{-\sigma^2 \log_e \left(1 - \frac{r^{d_2}}{\rho_a}\right)} & |r| > \alpha \end{cases} \tag{4.29}$$

4.5.1 No decompanding (NDC)

Here, we have considered the case without decompanding transform at the receiver section. The UFMC signal after companding transform g_n, can be represented as a combination of the attenuated UFMC signal and the noise component q_n due to companding transform, as expressed by

$$g_n = \psi s_n + q_n \tag{4.30}$$

where ψ is an attenuation factor,which is given by [110]

$$\psi = \frac{E\{g_n s_n^*\}}{E\{s_n s_n^*\}} = \frac{1}{\sigma^2} \int_0^\infty xt(x) f_{|s_n|} dx \tag{4.31}$$

The companded signal g_n average power can be expressed as

$$P_{g_n} = P_{\psi s_n} + P_{q_n} = \psi^2 P_{s_n} + P_{q_n} \tag{4.32}$$

consider that the average power levels of companded signal g_n and s_n are same in companding operation

$$P_{g_n} = P_{s_n} \tag{4.33}$$

$$\psi^2 P_{s_n} + P_{q_n} = P_{s_n} \tag{4.34}$$

$$P_{q_n} = P_{s_n}(1 - \psi^2) \tag{4.35}$$

From eq(4.35) we can decide that $\psi < 1$ and ψ closer to 1, the average power of companding noise q_n will be smaller. Then the received signal r_n with channel noise w_n written as

$$r_n = g_n + w_n \tag{4.36}$$

The recovered signal $s_n^{'}$ after decompanding at the receiver side is

$$s_n^{'} = \upsilon r_n + q_n^{'} \tag{4.37}$$

where $\upsilon = \frac{1}{\psi}$ and $q_n^{'} = -\frac{q_n}{\psi}$, then

$$s_n^{'} = \frac{1}{\psi}(g_n + w_n) + q_n^{'} = s_n^{'} = \frac{g_n + w_n}{\psi} - \frac{q_n}{\psi} = s_n + \frac{w_n}{\psi} \tag{4.38}$$

eq(4.38) depicts that decompanding operation at the receiver amplifies channel noise w_n to $\frac{w_n}{\psi}$. No decompanding results that the equivalent noise is combination of companding noise q_n and the channel noise w_n. Therefore, the equivalent noise with and without de-companding in the proposed scheme can be written as $\frac{w_n}{\psi}$ and $w_n + q_n$ respectively.

Let ψ is an attenuation factor and it was calculated as $\psi = 0.99$ (is close to 1). From eq(4.38), we can say that the proposed NDC technique results in little companding noise. Hence, we can conclude that the proposed MEC transform with no decompanding offers improved BER performance.

4.5.2 Proposed modified exponential companding transform with clipping scheme for UFMC system

A hybrid companding and clipping scheme is employed for UFMC system to reduce PAPR further. The schematic structure of UFMC transmitter with a hybrid scheme is shown in Fig. 4.2. The clipping operation can be applied at the transmitter section only. From Fig. 4.2,

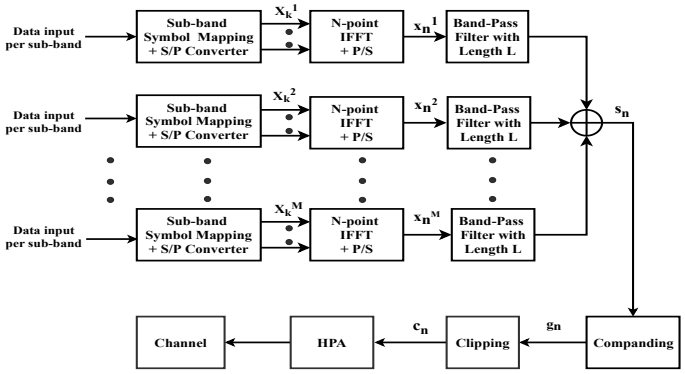

Figure 4.2: UFMC transmitter with the proposed hybrid scheme.

clipping operation is employed based on an appropriate threshold level on the MEC at the transmitter section whereas the receiver section remains unaltered.

The companded signal g_n of UFMC sytstem is clipped using a soft limiter based on a predefined threshold as

$$c_n = \begin{cases} g_n & |g_n| \leq \gamma \\ \gamma \exp^{j\phi_n} & |g_n| > \gamma \end{cases} \tag{4.39}$$

where c_n is the clipped signal, $\phi_n = arg\,[g_n]$, and γ is the threshold level at which clipping is applied on the companded signal. The clipping ratio (CR) is known as

$$CR = \frac{\gamma}{\sqrt{P_{avg}}} \tag{4.40}$$

Where the term P_{avg} is characterized as average power of UFMC signal. The PAPR performance has been improved further if companding scheme followed by clipping in hybrid technique. In [111], the hybrid scheme is presented, which employs first clipping operation on the transmitted signal and then companding scheme on the clipped signal. The data will be lost due to the transmitted signal is clipped to an appropriate threshold level of γ in the first step. On the other hand, our proposed hybrid model first employs the companding transform on the transmitted signal and then clipping operation on the companded signal. The majority of signal peaks will be compressed as companding is performed in the first step. Therefore, clipping operation at the second step will not cause much amount of data loss.

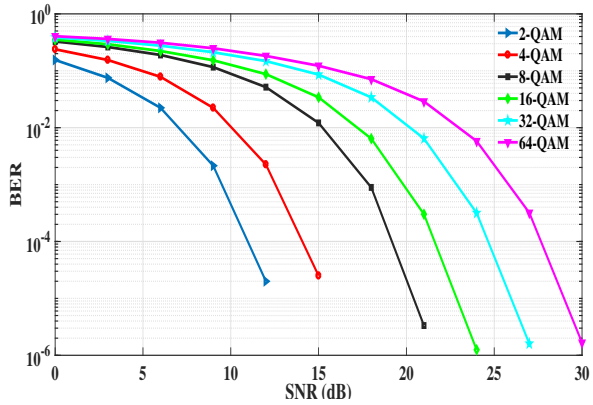

Figure 4.3: Comparison of BER performance of UFMC system for different orders of M-ary QAM over AWGN channel.

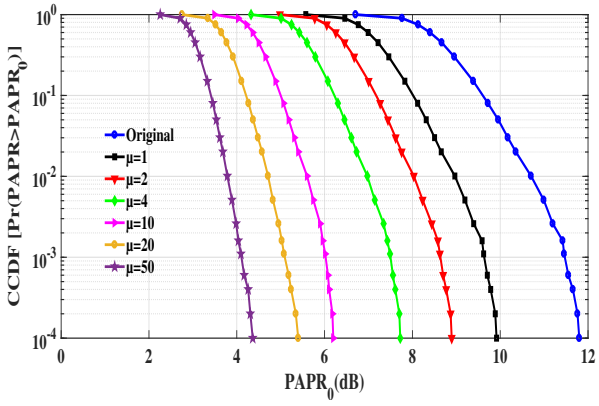

Figure 4.4: Comparison of CCDF curves for μ-law companding technique on different values of μ.

4.5.3 Selection of optimum companding parameters for PAPR and BER

To evaluate the UFMC system performance in terms of BER, power spectrum, and PAPR reduction of various companding techniques, we considered UFMC system, which is shown in Fig. 4.1. The sub-bands considered for computer simulations are $M = 10$, the number of subcarriers in each sub-band is considered as 20, size of the FFT is $N = 1024$, and the filter length is considered as 40. QAM is employed as a modulation scheme for UFMC system.

Fig. 4.3 illustrates the BER performance of UFMC system for different orders of M-ary QAM over AWGN channel. It is shown that as the order of QAM increases the BER performance deteriorates. Fig. 4.4 shows the PAPR performance in terms of complementary cumulative distribution function curves for different values of μ. The PAPR of original UFMC signal is 11.9 dB at CCDF of 10^{-4}, whereas μ-law provides PAPR values as 9.9 dB, 8.9 dB, 7.7

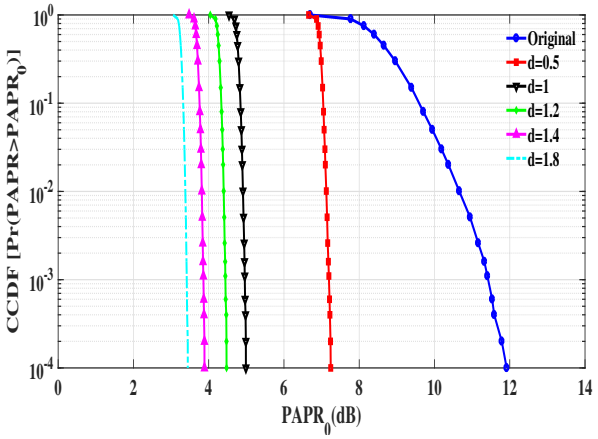

Figure 4.5: CCDF curves of exponential companding technique for different values of d.

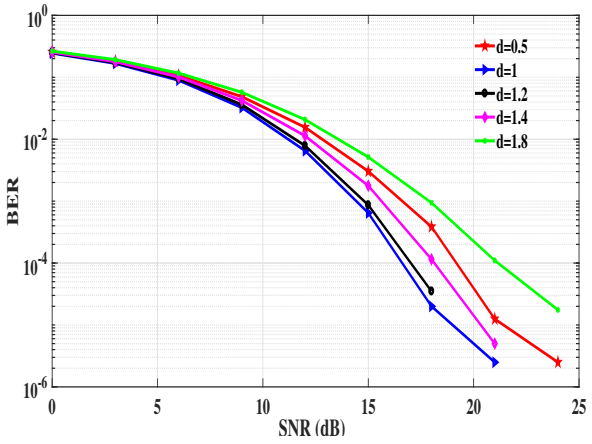

Figure 4.6: Variation of BER on SNR of exponential companding scheme with decompanding for different d values.

dB, 6.2 dB, 5.4 dB, and 4.4 dB at different companding levels of μ as 1, 2, 4, 10, 20, and 50 respectively. Therefore, PAPR can be reduced with increasing values of μ.

Fig. 4.5 shows the CCDF performance of exponential companding with different values of d. As the degree of d increases, the PAPR performance of EC technique also increases like μ-law technique. The PAPR values for proposed EC scheme are 7.24 dB, 4.99 dB, 4.47 dB, 3.89 dB, and 3.44 dB at different companding levels of d as 0.5, 1, 1.2, 1.4, and 1.8 respectively at CCDF of 10^{-4}.

In comparison with Fig. 4.4 and Fig. 4.5, the PAPR is reduced as increasing the values of μ and d. It finds that the proposed EC scheme provides better PAPR performance at the values of d 1, 1.2, 1.4, and 1.8 when compared to $\mu = 10$ in μ-law. However, for $d \geq 1.4$, there is a slight improvement in PAPR reduction. Hence we need to determine the optimum choice of d, which can achieve better BER performance.

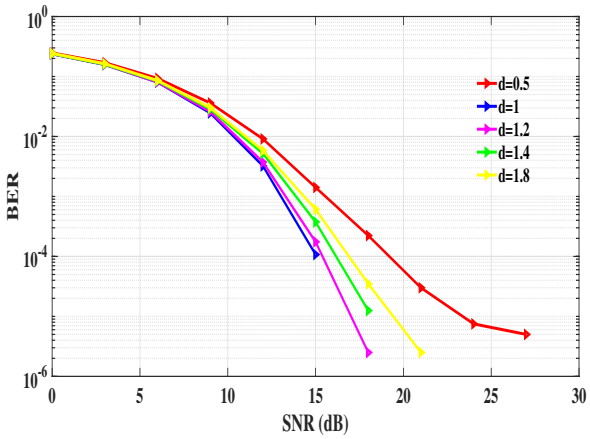

Figure 4.7: Variation of BER on SNR of exponential companding scheme with no decompanding for different d values.

Fig. 4.6 presents the BER vs SNR curves of exponential companding scheme with decompanding for various d values. It depicts that the BER is minimum at $d = 1$. Therefore, the optimum choice of the companding parameter d is 1 to get better BER performance.

Fig. 4.7 exemplifies the BER vs SNR curves of EC scheme with NDC at the receiver for various d values. Again it also depicts that the BER is minimum at $d = 1$. Hence, the optimum choice of the companding parameter d is 1 to get better BER performance.

Similarly, to determine the optimum μ value, which can achieves minmum BER, Fig. 4.8, presents the BER vs SNR curves of μ-law transform for various μ values. It clearly depicts that BER is minimum for $\mu = 4$. Hence, for μ-law scheme, the optimum value of μ is 4.

To determine the optimum companding parameters of the proposed MEC technique, Fig. 4.9 and Fig. 4.10, presents the PAPR and BER scatter plots for various values of d_1, d_2, and α respectively. It clearly shows that PAPR is high at low values of BER and BER is high at low values of PAPR. From scatter plots, we can realize that the optimum companding factors of MEC scheme for better PAPR and BER are $d_1 = 1.9$, $d_2 = 1$, and $\alpha = 0.3$.

4.5.4 Performance evaluation

In this section, we have compared the performances of the proposed modified exponential companding scheme and hybrid schemes with exponential companding and well-known μ-law schemes.

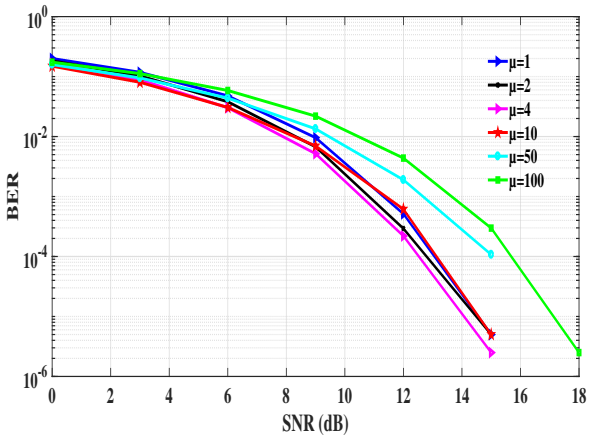

Figure 4.8: Variation of BER on SNR of μ-law scheme for various μ values.

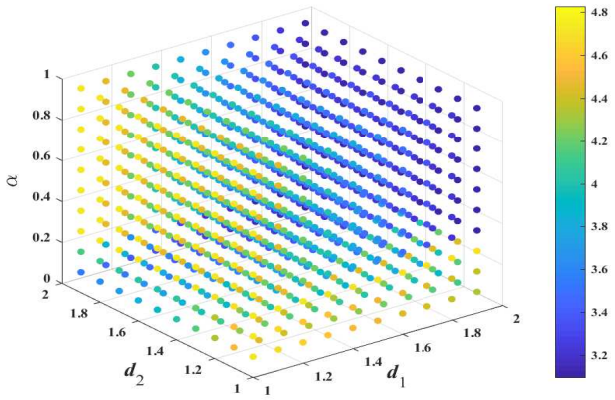

Figure 4.9: Variation of PAPR for proposed MEC technique on different values of d_1, d_2, and α.

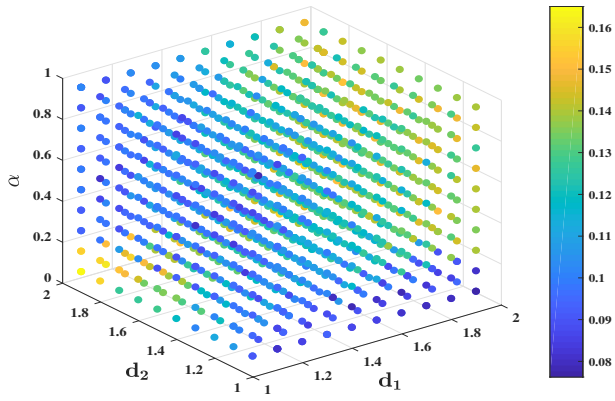

Figure 4.10: Variation of BER for proposed MEC technique on different values of d_1, d_2, and α.

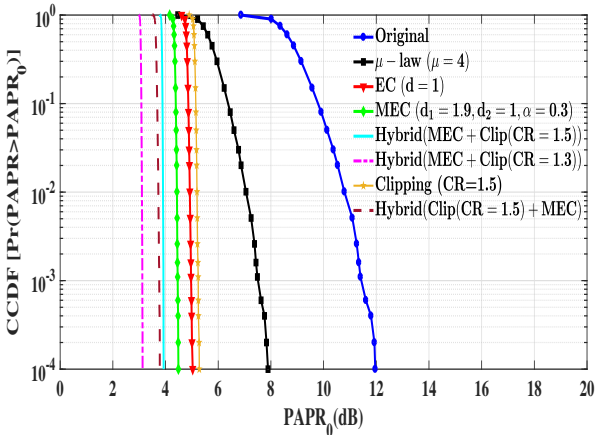

Figure 4.11: Comparison of CCDF curves for original, clipping and various companding techniques.

Fig. 4.11 depicts the performance of PAPR in terms of CCDF curves for various companding techniques such as μ-law, EC, proposed MEC with and without decompanding, hybrid scheme (MEC+clipping) with two clipping ratios, hybrid (clipping+MEC), original UFMC signal, and clipping scheme with clipping ratio of 1.5. It shows that the performance of PAPR is better for proposed EC scheme when it is compared with μ-law. In addition to this, the proposed MEC scheme proffers enhanced PAPR reduction than EC and μ-law techniques. Furthermore, the proposed hybrid scheme provides enhanced PAPR reduction than MEC, EC, μ-law, and clipping schemes. Moreover, the hybrid scheme (MEC+clipping) with the clipping ratio of 1.3 offers improved PAPR reduction when compared with the clipping ratio of 1.5, and hybrid (clipping+MEC) scheme. Therefore, the proposed hybrid scheme with a clipping ratio of 1.3 can be employed in power-efficient applications.

Table 4.1 provides PAPR values for original UFMC signal and different companding schemes at CCDF of 10^{-4}. It clearly exhibits that the PAPR of original UFMC system is 11.9 dB, μ-law offers 7.89 dB while proposed EC, MEC, and the proposed hybrid schemes offer 4.98 dB, 4.48 dB, 3.973 dB with CR = 1.5, and 3.15 dB with CR = 1.3, respectively.

Table 4.2 illustrates the improvement of PAPR reduction for various companding techniques with original UFMC signals at CCDF of 10^{-4}. In comparison with original UFMC signal, the well-known μ-law scheme provides an improvement in PAPR reduction about 4.09 dB, whereas EC transform provides about 7.02 dB, and the proposed MEC companding transform provides about 7.52 dB. Further, the optimal hybrid technique offers an improvement of 8.03 dB and 8.85 dB when clipping ratios are to be 1.5 and 1.3, respectively.

Table 4.1: PAPR values of original UFMC signal and several companding schemes

	Original signal	μ-Law (μ=4)	Proposed EC (d=1)	Proposed MEC $d_1 = 1.9, d_2 = 1$ $\alpha = 0.3$	Proposed hybrid scheme (CR=1.5)	Proposed hybrid scheme (CR=1.3)
PAPR in dB at CCDF=10^{-4}	11.9	7.89	4.98	4.48	3.973	3.15

Table 4.2: Improvement of PAPR reduction of several companding transforms with original UFMC signal

	μ-law	EC	MEC	Proposed Hybrid scheme (CR=1.5)	Proposed Hybrid scheme (CR=1.3)
PAPR in dB at CCDF=10^{-4}	4.09	7.02	7.52	8.02	8.85

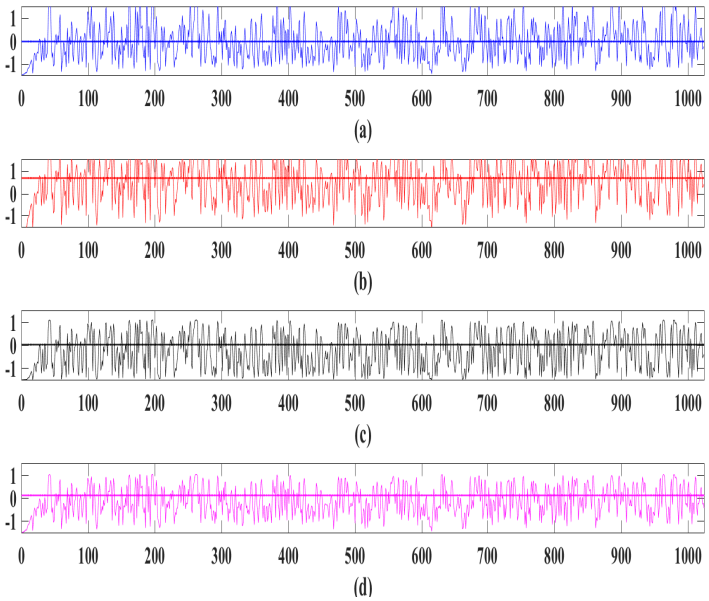

Figure 4.12: Comparison of original UFMC signal waveform and various companded signal waveforms (a) UFMC signal without companding (b) signal companded by μ-law with $\mu = 4$ (c) exponential companded signal with $d = 1$ (d) signal companded by MEC scheme with $d_1 = 1.9$, $d_2 = 1$, and $\alpha = 0.3$.

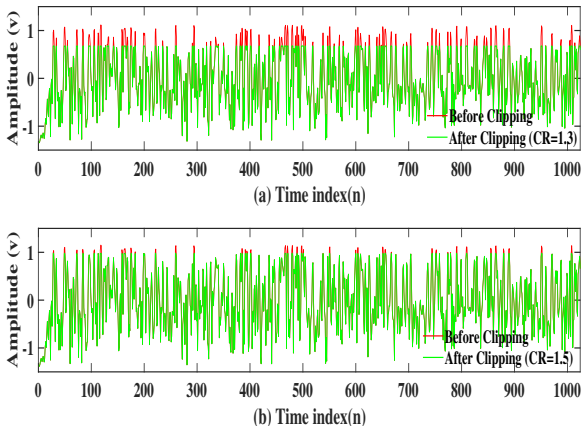

Figure 4.13: Comparison of MEC companded signal waveform and the proposed hybrid signal waveform for different clipping ratios (a) CR = 1.3 (b) CR = 1.5.

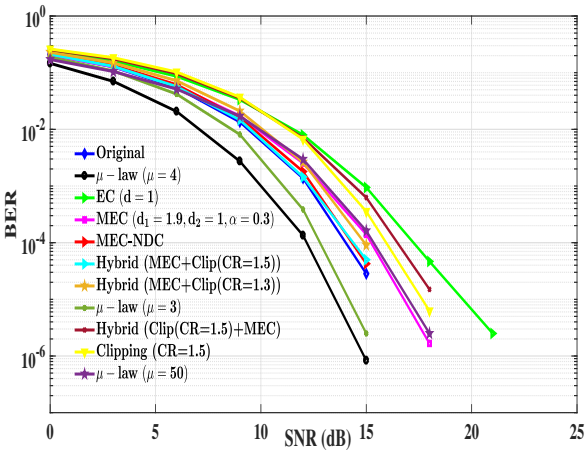

Figure 4.14: Comparison of BER curves of the UFMC signal, clipping and various companding techniques for 4-QAM under AWGN channel.

Fig. 4.12 shows the comparison of original UFMC signal waveform and various companded signal waveforms such as μ-law, proposed EC and MEC techniques. The μ-law scheme raises the average power level of a signal while proposed EC and MEC schemes maintain the constant average power level. Fig. 4.13, shows the comparison of MEC companded signal waveform and hybrid signal waveform. It shows that much amount of data is lost when the clipping ratio is 1.3. Therefore BER performance was degraded for CR = 1.3. While for the clipping ratio of 1.5, the data lost is minimum. So the performance of BER does not get affected significantly.

Fig. 4.14 describes the performance of BER of the original UFMC signal, various companding techniques such as μ-law, EC, proposed MEC with and without decompanding, hybrid schemes, and clipping scheme for 4-QAM over AWGN channel. It can be seen that the performance of proposed MEC scheme has improved when compared to EC technique, but it has

Table 4.3: SNR values required for original and various companding schemes at BER=10^{-4}

	Original UFMC signal	μ-law (μ=4)	Proposed EC (d=1)	Proposed MEC-NDC (d_1 = 1.9, d_2 = 1, α = 0.3)	Proposed MEC with decompanding (d_1 = 1.9, d_2 = 1, α = 0.3)	Proposed hybrid scheme (CR=1.5)	Proposed hybrid scheme (CR=1.3)
SNR in dB at BER=10^{-4}	14	12.2	17.2	14.3	15.2	14.3	14.9

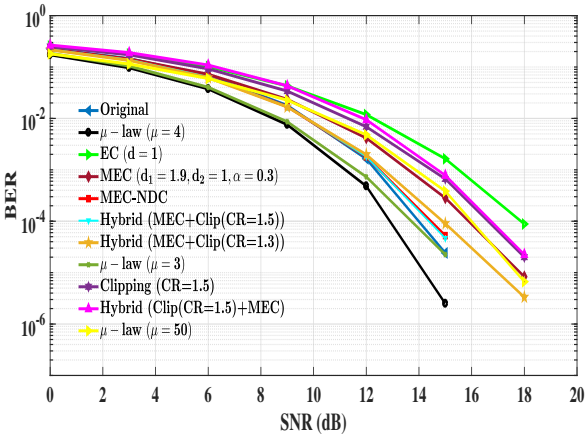

Figure 4.15: Comparison of BER curves for original, clipping and various companding techniques with SSPA under AWGN channel.

slightly degraded while compared with original UFMC system. Further, the proposed MEC scheme with no decompanding function provides enhanced BER performance than proposed MEC with decompanding function. The proposed hybrid scheme (MEC+clipping) affords almost similar BER performance with proposed MEC no decompanding when the clipping ratio is to be 1.5 but it is slightly degraded when the clipping ratio is to be 1.3. Moreover, the proposed hybrid schemes (MEC+clipping) offer superior performance when compared to hybrid scheme (clipping+MEC) and clipping alone. Table 4.3 describes the required SNR values of different companding schemes at BER of 10^{-4}.

Fig. 4.15, illustrates the performance of BER for original UFMC signal,various companding schemes, and clipping scheme with considering the effect of solid-state power amplifier over AWGN channel. Most of the radio systems frequently employ HPAs in the transmitter side to acquire sufficient transmit power. The SSPA is one of the well-known models of HPA. It can be recognized that the performance of BER is almost similar even in the existence of SSPA.

Fig. 4.16, presents the performance of BER of the original UFMC signal and various companding techniques for 16-QAM over AWGN channel. It depicts that proposed MEC with

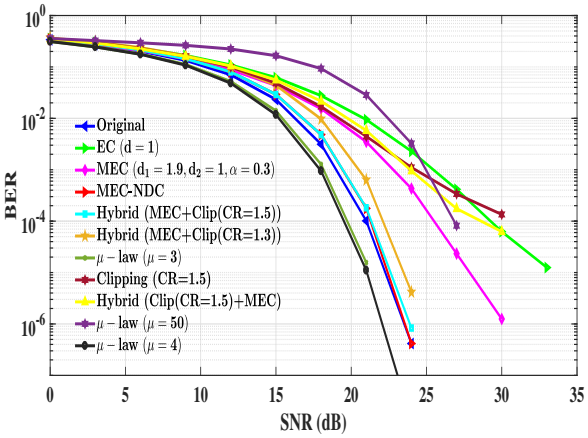

Figure 4.16: Comparison of BER curves of the UFMC signal, clipping and various companding techniques for 16-QAM under AWGN channel.

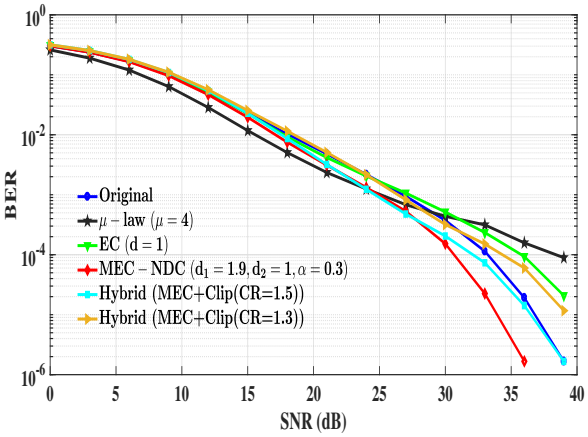

Figure 4.17: Comparison of BER curves for original and various companding techniques under Rician channel.

NDC and the proposed hybrid scheme with CR of 1.5 affords almost similar performance as that of the UFMC signal.

Fig. 4.17, describes the performance of BER for original UFMC signal and various companding techniques over multipath rician channel. It can be shown that the performance of BER for the proposed MEC with NDC scheme is better when compared to all other schemes. Hence, MEC with NDC scheme is robust in multipath fading channel. Fig. 4.18, illustrates the performance of BER for original UFMC signal and various companding techniques over multipath rician channel with considering the effect of a SSPA. It can be recognized that the proposed MEC with NDC and hybrid scheme with CR=1.5 exhibits better performance than all other techniques.

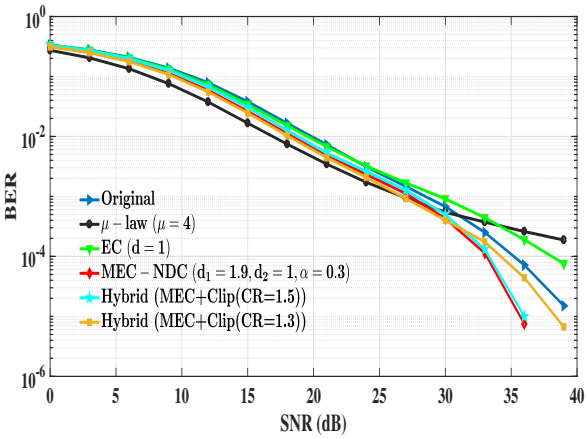

Figure 4.18: Comparison of BER curves for original and various companding techniques with SSPA under Rician channel.

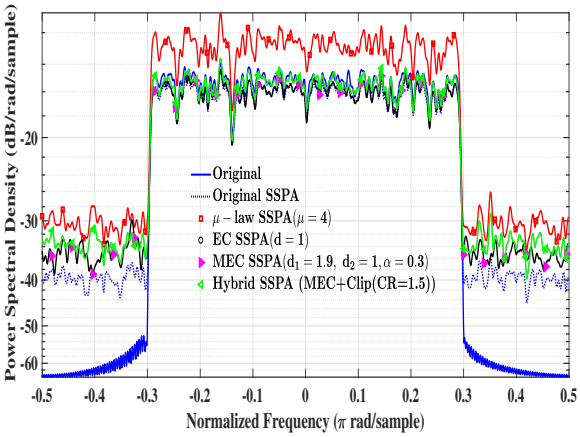

Figure 4.19: Comparison of power spectral density curves for original and various companding techniques with SSPA.

Fig. 4.19 describes the PSD curves of various companding schemes and original UFMC signal. Here we have considered the parameter p_a of a solid-state power amplifier is 2 and another parameter IBO is 5 dB [112]. To estimate power spectral density in MATLAB, we have considered welch's method with 50% overlap and windowing function is Hamming. It shows that the μ-law technique produces both in-band and OOB distortions, whereas the proposed MEC scheme produces only OOB distortion. The hybrid scheme also commences OOB distortion due to the clipping function. The proposed MEC with NDC and hybrid scheme with CR of 1.5 affords enhanced PAPR performance, better BER performance, and fewer side-lobe levels.

Table 4.4 depicts the comparison of performance analysis of the UFMC system for various companding transforms. The proposed MEC-NDC and hybrid scheme with CR = 1.5 offers improved performance with net gains of 7.22 dB and 7.72 dB, respectively when compared to conventional μ-law and EC schemes. Whereas, the proposed hybrid scheme with CR = 1.3 of-

Table 4.4: Comparison of performance analysis of the UFMC system for various companding transforms for 4-QAM

Companding scheme	Reduction of PAPR at CCDF=10^{-4}	Required Additional SNR values at BER=10^{-4}	net gain (Reduction of PAPR-Additional SNR)
μ-law (μ=4)	4.09	-1.8	5.89
EC (d=1)	7.02	3.2	3.82
MEC-NDC (d_1=1.9, d_2=1, α=0.3)	7.52	0.3	7.22
Proposed hybrid (CR=1.5)	8.02	0.3	7.72
Proposed hybrid (CR=1.3)	8.85	0.9	7.95

Table 4.5: Performance Comparision of the proposed optimal transforms with existing companding schemes in the literature for 16-QAM.

Companding Transform	Improved PAPR reduction at CCDF=10^{-3}	Required Additional SNR Values at BER=10^{-3}	net gain (Reduction of PAPR-Additional SNR)
μ-law (μ=4)	4	-1.5	5.5
EC (d=1)	6.52	6.5	0.02
Proposed MEC-NDC scheme	7.02	3.8	3.22
Proposed hybrid transform (CR=1.3)	8.4	1.5	6.9
Proposed hybrid transform (CR=1.5)	7.6	0.5	7.1
hybrid (clipping+MEC) (CR=1.5)	7.7	5.5	2.2
DFT-ARCT (R=0.4) [79]	7.3	3	4.3
DFT-μ-law (μ=50) [79]	8.3	5.5	2.8
ICF-ENC (γ=1.5) [113]	7.2	1.5	5.8
ENC (v=0.72) [113]	7.3	3.5	3.8
μ-law (μ=2) [114]	3.6	2.3	1.3

fers superior performance with a net gain of 7.95 dB when compared to all existing companding schemes.

The proposed optimal hybrid transforms are compared with various companding schemes in the literature, such as DFT-ARCT and DFT-μ-law [79] of UFMC system, ICF-ENC (Iterative clipping and filtering-enhanced nonlinear companding) and ENC [113] of OFDM system, and μ-law [114] of OFDM system, as illustrated in Table 4.5. It is evident that from Table 4.5, The proposed hybrid scheme with CR = 1.3 offers improved PAPR reduction of 8.4 dB at CCDF = 10^{-3} when compared to other companding schemes. Moreover, the required additional SNR value of the proposed hybrid scheme with CR = 1.5 is 0.5 dB at BER = 10^{-3}, which is minimum when compared to other companding schemes. Hence, the proposed hybrid scheme with CR = 1.5 offers enhanced system net gain of 7.1 dB when compared to various companding schemes.

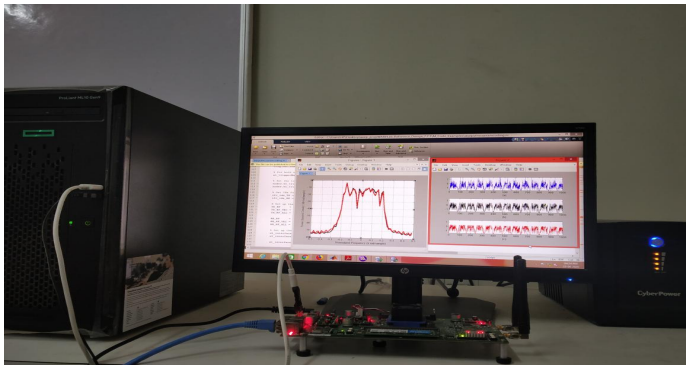

Figure 4.20: Experimental arrangement using WARP V3 kit.

4.5.5 Experimental results

The wireless open-access research platform (WARP) V3 hardware is used to conduct the real time experiments. The physical layer algorithms are modeled in WARPLab framework [115] with the combination of MATLAB and the features of WARP V3 board. The WARP node contains 2 identical RF interfaces, which are named as RF A and RF B. In this experiment, the interfaces RF A and RF B are used as transmitting and receiving antennas, respectively. Each RF interface that is used in the kit possesses a 2.4/5 GHz transceiver and the RF bandwidth of 40 MHz.

The Ethernet switch is used to connect WARP node to a host PC. The WARPLab framework provides the software that is used to upload the MATLAB simulation programs to FPGA buffers. To broadcast the samples from transmitting antenna (RF A) to the receiving antenna (RF B), the host PC activates the hardware WARP node by transmitting a trigger signal. The baseband samples are converted to RF signal by the up-conversion at the transmitter and the received RF signal is converted to baseband samples by the down-conversion at the receiver. Finally, the received baseband samples are loaded to the MATLAB and operated in MATLAB workspace on host PC.

The experimental arrangement of the proposed UFMC system using WARP V3 kit is illustrated in Fig. 4.20. The transmitted UFMC signal without PAPR reduction, MEC, and the proposed hybrid signals are depicted in Fig. 4.21. It can be observed from Fig. 4.21 (a), a few samples possess high amplitude, which can raise the PAPR of the UFMC system. Also, these high peaks drive the PA into saturation region that degrades the system performance. Hence, the PAPR of the UFMC system has to be reduced by applying optimal companding schemes. From Fig. 4.21 (b) and (c), the time domain MEC and hybrid (MEC+clipping) waveforms describe that the significant PAPR reduction is attained over real time channel. The results validate that

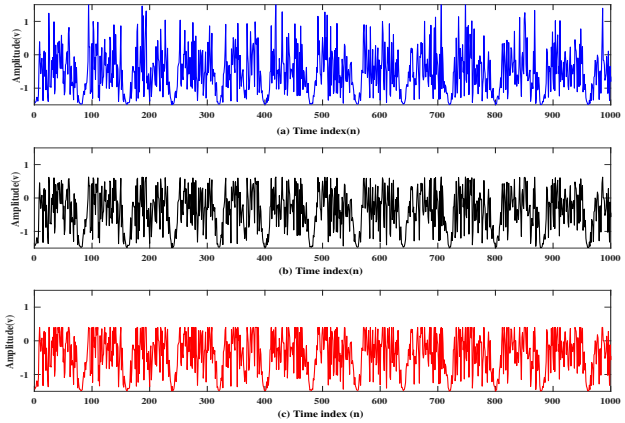

Figure 4.21: Real time transmitted UFMC signal, MEC, and hybrid signal with CR=1.5 (a) Transmitted UFMC signal without companding (b) MEC signal (c) Proposed hybrid signal.

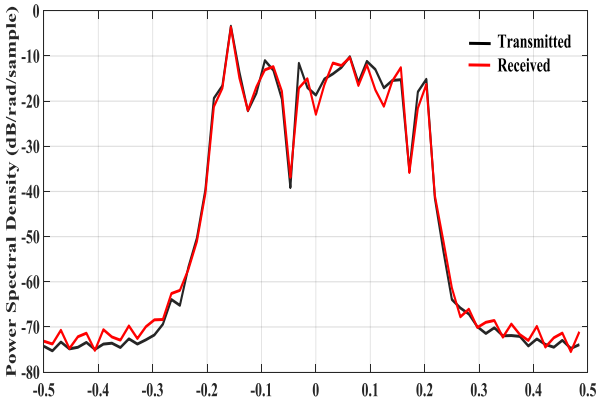

Figure 4.22: Transmitted and received power spectrum by using hardware.

the proposed hybrid scheme offers better PAPR reduction when compared to MEC scheme and the transmitted UFMC signal. The power spectrum of the transmitted and received signals is illustrated in Fig. 4.22. It can be clearly noticed from Fig. 4.22 that there is no remarkable distortion between transmitted and received spectrum.

4.6 Proposed nonlinear companding transform based on error function for UFMC system

In the proposed companidng scheme, the nonlinear companding transform is employed to reduce the PAPR of the UFMC system. The NCT scheme transforms the UFMC amplitude signals from statistical distribution to quasi-uniform distribution. The companding function is

mathematically given below.

$$t(x) = \beta_1 . erf(\beta_2 x) \tag{4.41}$$

Here, $erf(x) = \left(\frac{2}{\sqrt{\pi}}\right) \int_0^x e^{-t^2} dt$ denotes the error function. β_1 and β_2 are the companding parameters, which play a key role in the transformation of UFMC signals. The companding parameters can be properly chosen to get an optimum performance. Hence, this companding scheme is flexible and the signal power cannot change after performing companding transform.

4.6.1 Proposed hybrid technique (NCT + clipping)

The combination of NCT and clipping in UFMC system reduces PAPR furthermore. The block diagram of the proposed hybrid scheme is shown in Fig. 4.2. The clipping is applied on the proposed companded signal by using an appropriate CR. The companded signal is clipped based on a clipping threshold as given below.

$$c_n = \begin{cases} g_n, & |g_n| \leq \delta \\ \gamma \exp^{j\phi_n}, & |g_n| > \gamma \end{cases} \tag{4.42}$$

Here, c_n denotes clipped signal, γ is the clipping threshold, and $\phi_n = arg[g_n]$. The CR is mathematically calculated as

$$CR = \frac{\gamma}{\sqrt{P_{avg}}} \tag{4.43}$$

where P_{avg} is average power of UFMC signal.

The hybrid model presented in [111] employs companding scheme on the clipped signal. Hence, clipping of the transmitted signal by using proper clipping threshold at first stage itself results in data loss. Whereas the proposed hybrid transform employs clipping on the companded signal. Therefore, the signal peaks of the transmitted UFMC signal are compressed due to companding at the first stage. Hence, the data loss is minimum as clipping is performed at second stage.

4.6.2 Choosing optimum parameters for the proposed hybrid scheme

In this section, the optimum parameters of the UFMC system with the proposed hybrid scheme are determined. The sub-bands, sub-carriers in every sub-band, filter length, and the FFT length are considered as 9, 16, 40, and 512, respectively, in simulations.

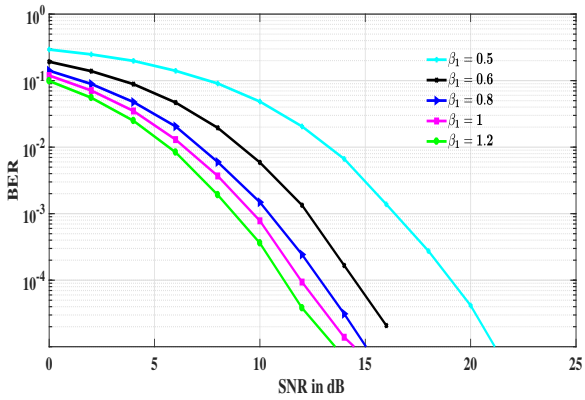

Figure 4.23: BER curves of the proposed companding scheme on various values of β_1.

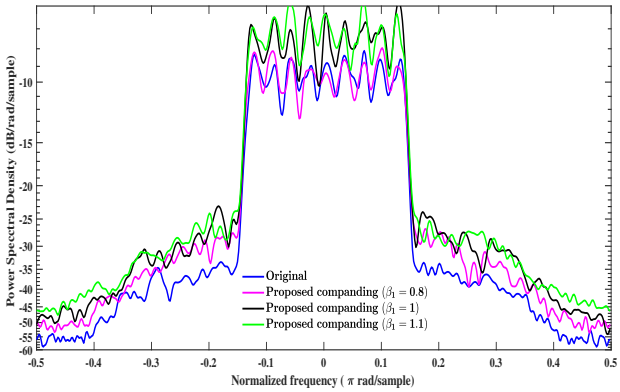

Figure 4.24: PSD curves of the proposed companding scheme on various values of β_1.

Fig. 4.23 shows the BER curves of the proposed companding scheme for various values of β_1. As the companding parameter β_1 increases, the BER performance increases. Fig. 4.24 depicts the PSD curves of the proposed companding scheme for various values of β_1. It is observed from Fig. 4.24 that the PSD performance is better at lower values of β_1. As β_1 increases, the companding scheme produces in-band and OOB distortions. Therefore, it can be concluded from Fig. 4.23 and Fig. 4.24 that the optimum value of β_1 is 0.8.

Fig. 4.25 depicts the CCDF curves of the proposed companding scheme for various values of β_2. At CCDF of 10^{-4}, the proposed companding offers PAPR of 10.2 dB, 8.1 dB, 6.8 dB, 5.8 dB, and 4.9 dB at various companding levels of β_2 of 0.5, 0.8, 1, 1.2, and 1.4, respectively. Hence, the performance of PAPR can be improved by increasing β_2.

Fig. 4.26 shows the BER characteristics of the proposed companding scheme for various values of β_2. It is obvious from Fig. 4.26 that the BER performance of the proposed scheme with no decompanding can be improved at $\beta_2 = 1.4$. Therefore, from Fig. 4.25 and Fig. 4.26, both PAPR and BER performances become better as the companding parameter β_2 increases.

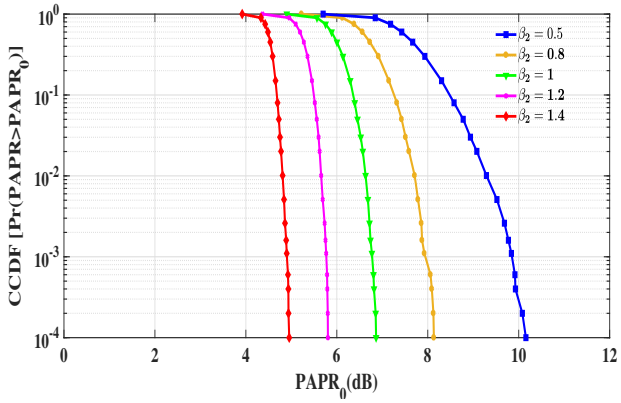

Figure 4.25: CCDF curves of the proposed companding scheme on various values of β_2.

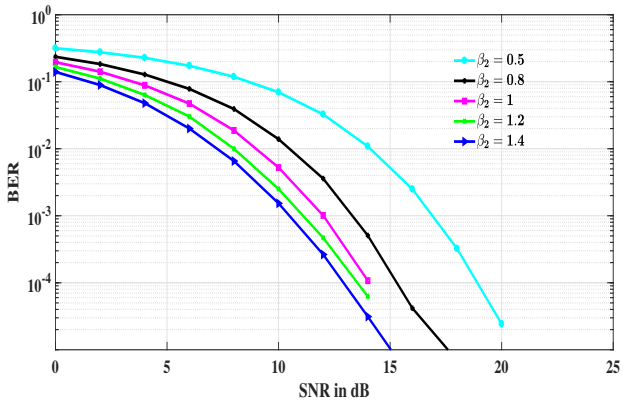

Figure 4.26: BER curves of the proposed companding scheme with no decompanding on various values of β_2.

Since it is difficult to find out the optimum parameter from PAPR and BER performance, the optimum value of β_2 is obtained from the PSD performance.

Fig. 4.27 depicts the PSD curves of the proposed companding scheme for various values of β_2. It is observed from Fig. 4.27 that the PSD performance is better at lower values of β_2. As β_2 increases, the companding scheme exhibits both in-band and OOB distortions. Also, it can be concluded from Fig. 4.27 that the average power of the proposed companded signal is same as that of the original UFMC signal at $\beta_2 = 1.4$, whereas the average power of the proposed companded signal increases and is more than the average power of the UFMC signal when β_2 is greater than 1.4 (i.e., $\beta_2 > 1.4$). Hence, the optimum value of β_2 is 1.4. Finally, it is concluded that the optimum values of β_1 and β_2 of the proposed companding scheme are 0.8 and 1.4, respectively.

Fig. 4.28 illustrates the CCDF curves of the proposed hybrid scheme for several values of CRs. It is obvious from Fig. 4.28 that the PAPR reduction of the hybrid scheme becomes

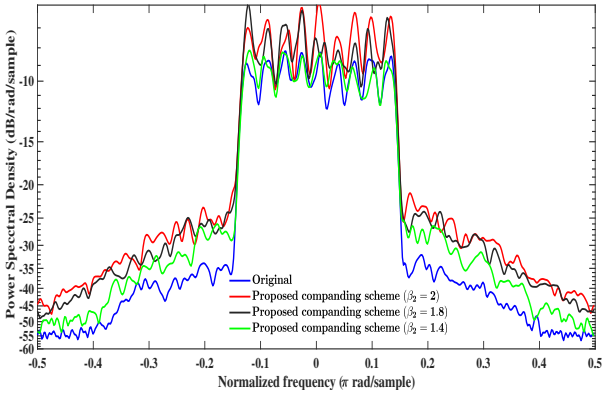

Figure 4.27: PSD curves of the proposed companding scheme on various values of β_2.

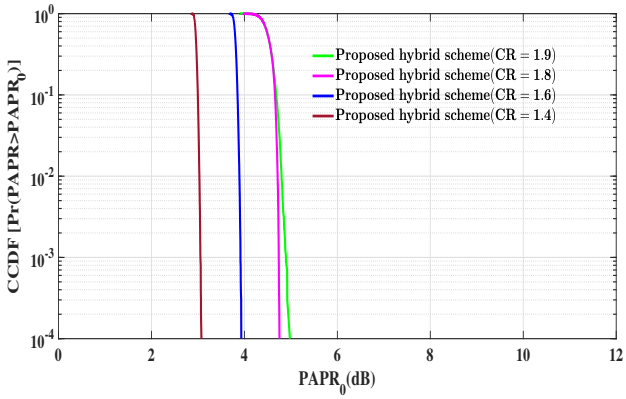

Figure 4.28: Variation of CCDF for several values of CRs of the proposed hybrid scheme.

better as the CR decreases. Fig. 4.29 exemplifies the BER characteristics of the proposed hybrid scheme for several values of CRs. It is confirmed from Fig. 4.29 that the least BER is obtained at a CR of 2. However, highest PAPR is obtained at a CR of 2. Hence, an optimum value of CR of the proposed hybrid scheme is chosen as 1.6 since better BER characteristics and PAPR reduction can be achieved at a CR of 1.6.

4.6.3 Performance evaluation

In this section, the PAPR, BER, and PSD characteristics of the proposed hybrid scheme and the performance comparison of various companding schemes are illustrated.

Fig. 4.30 describes the CCDF performance of the proposed hybrid scheme, original UFMC signal, and several companding schemes, such as ARCT, LNST, *A*-law, μ-law, HT, EC, and the proposed compadning scheme. It shows that the PAPR performance is better with EC and HT schemes when compared to LNST, ARCT, μ-law, and *A*-law schemes. Moreover,

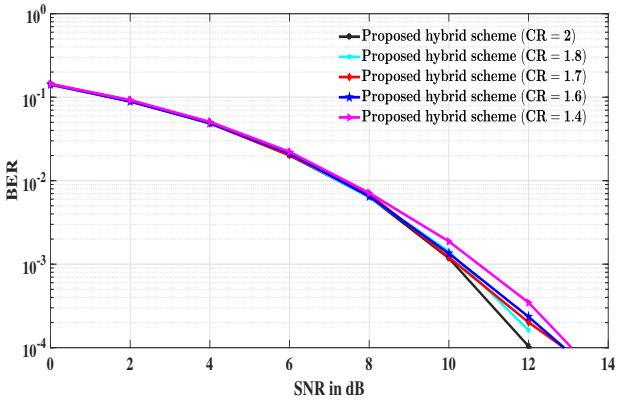

Figure 4.29: Variation of BER for several values of CRs of the proposed hybrid scheme.

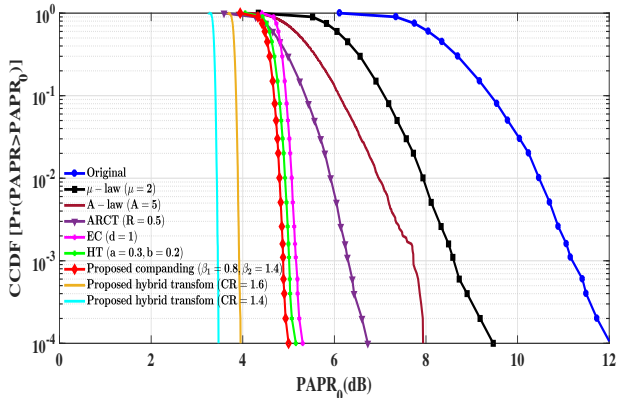

Figure 4.30: CCDF curves of the proposed hybrid scheme, original signal, and several companding schemes.

the proposed companding scheme provides better PAPR reduction than HT and EC transforms. Besides, the proposed hybrid scheme with CR of 1.4 provides better PAPR reduction than the proposed hybrid scheme with CR of 1.6. Hence, the proposed hybrid transform with CR of 1.4 can be used in energy-efficient applications.

Table 4.6 gives the PAPR of the proposed hybrid scheme, original UFMC signal, and several companding transforms at a CCDF of 10^{-4}. The PAPR of UFMC system without companding, EC, HT, μ-law, and the proposed companding are 12 dB, 5.3 dB, 5.2 dB, 9.5 dB, and 5 dB, respectively. The PAPR of the proposed hybrid transforms with clipping ratios of 1.6 and 1.4 are 3.9 dB and 3.5 dB, respectively, as shown in Table 4.6.

The betterment of PAPR reduction of the proposed hybrid scheme with original UFMC signal is illustrated in Table 4.7. Also, it is compared with several companding schemes, as shown in Table 4.7. The increase in PAPR reduction of the logarithmic μ-law, EC, HT, and the proposed companding are 2.5 dB, 6.7 dB, 6.8 dB, and 7 dB, respectively. The increase in

Table 4.6: PAPR values of the proposed hybrid schemes, UFMC signal and various companding schemes

	Original signal	EC (u= 0.8)	HT (a= 0.3, b= 0.2)	μ-law (μ= 2)	Proposed companding (β_1= 0.8, β_2= 1.4)	Proposed hybrid transform (CR= 1.6)	Proposed hybrid transform (CR= 1.4)
PAPR in dB at CCDF= 10^{-4}	12	5.3	5.2	9.5	5	3.9	3.5

Table 4.7: PAPR reduction improvement of several companding schemes with the UFMC signal without companding at CCDF of 10^{-4}

	μ-law (μ= 2)	EC (d= 1)	HT (a= 0.3, b= 0.2)	Proposed companding (β_1= 0.8, β_2= 1.4)	Proposed hybrid transform (CR= 1.6)	Proposed hybrid transform (CR= 1.4)
PAPR in dB	2.5	5.7	5.8	7	8.1	8.5

PAPR reduction of the proposed hybrid schemes with CRs of 1.6 and 1.4 are 8.1 dB and 8.5 dB, respectively, as shown in Table 4.7.

Fig. 4.31 exemplifies the comparison of waveforms of the proposed hybrid scheme for different clipping ratios. It shows that the proposed hybrid scheme with clipping ratio of 1.4 losses more amount of data. Hence, the BER performance of the hybrid scheme with CR of 1.4 deteriorates. Whereas the proposed hybrid scheme with CR of 1.6 losses little amount of data, which is insignificant. Therefore, this scheme does not show significant effect on the BER performance.

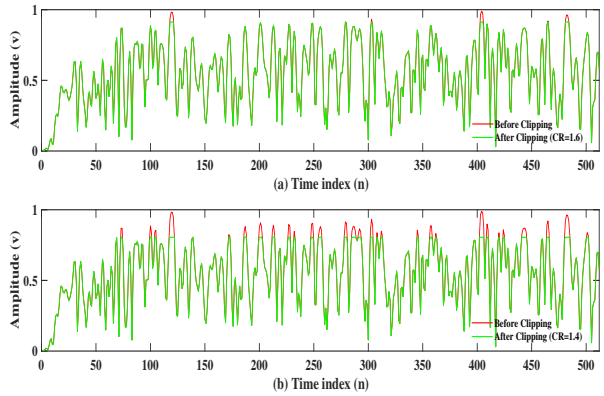

Figure 4.31: Comparison of waveforms of the proposed hybrid scheme and the companded signal without clipping (a) CR = 1.6 (b) CR = 1.4.

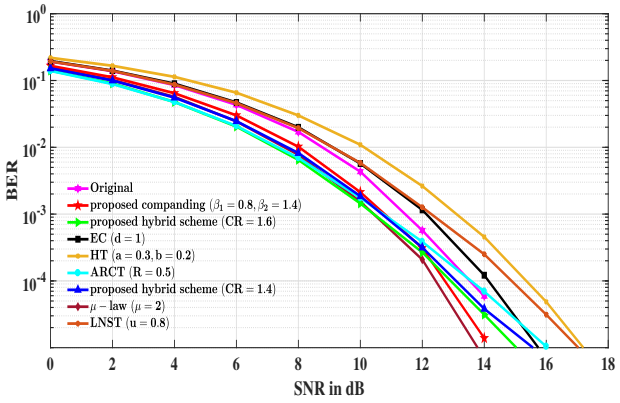

Figure 4.32: Performance comparison of the BER characteristics of the proposed hybrid schemes, several companding techniques, and original UFMC signal over AWGN channel.

Table 4.8: SNR values of the proposed hybrid schemes, UFMC signal and various companding schemes

	Original signal	EC (u= 0.8)	HT (a= 0.3, b= 0.2)	μ-law (μ= 2)	Proposed companding (β_1= 0.8, β_2= 1.4)	Proposed hybrid transform (CR= 1.6)	Proposed hybrid transform (CR= 1.4)
SNR in dB at BER= 10^{-4}	13.5	14.1	15.3	12.4	12.7	12.8	13.1

Fig. 4.32 depicts the performance comparison of the BER characteristics of the proposed hybrid schemes, several companding schemes, and original UFMC signal over AWGN channel. It can be seen from Fig. 4.32 that the BER performance of the proposed hybrid transform with CR of 1.4 is better than original signal and other companding schemes. Whereas the BER performance of EC and HT schemes deteriorate when compared to the original signal. The additional SNR values required at BER of 10^{-4} of various companding schemes are provided in Table 4.8.

Fig. 4.33 depicts the performance comparison of the BER characteristics of the proposed hybrid scheme, several companding transforms, and original UFMC signal with SSPA over AWGN channel. It illustrates that the BER performance of the hybrid transform is better than EC, HT, ARCT, and original signal.

Fig. 4.34 provides the performance comparison of the BER characteristics of the proposed hybrid scheme, several companding transforms, and original UFMC signal over rician fading channel. It can be seen from Fig. 4.34 that the proposed hybrid method with CR of 1.6 provides

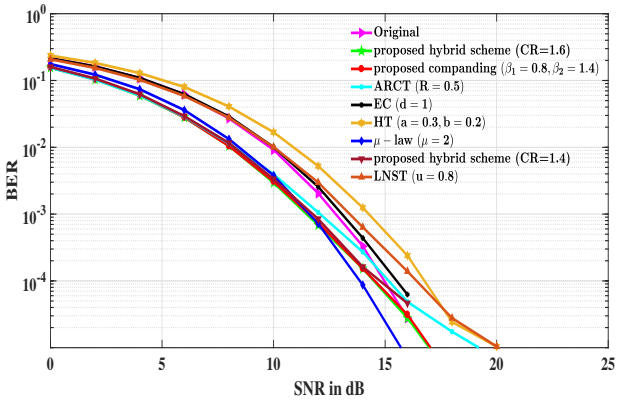

Figure 4.33: Comparison of BER curves for original and various companding techniques with SSPA.

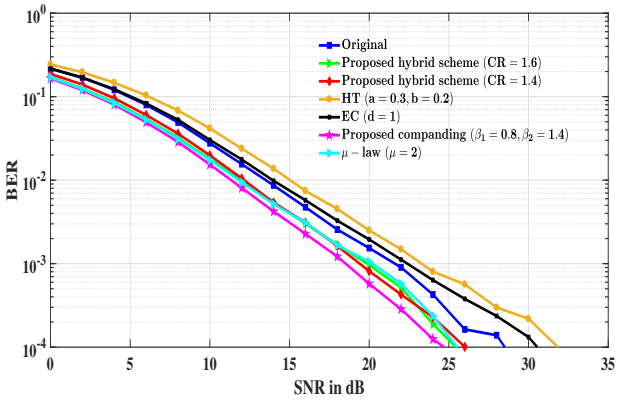

Figure 4.34: Comparison of the BER characteristics of the proposed hybrid scheme, several companding transforms, and original UFMC signal over rician fading channel.

better BER characteristics when compared to other companding schemes and original UFMC signal. Therefore, the hybrid transform is robust against multipath rician channel.

Fig. 4.35 describes the performance comparison of the BER characteristics of the proposed hybrid scheme, several companding transforms, and original UFMC signal over multipath fading channel with SSPA. It can be seen from Fig. 4.35 that the proposed hybrid method with CR of 1.6 provides better BER characteristics when compared to other companding schemes and original UFMC signal.

Fig. 4.36 shows the power spectrum performances of the proposed hybrid scheme with CR of 1.6, original UFMC signal, and several companding schemes. The power spectrum performance is estimated in MATLAB by considering the hamming window function and Welch's method with an overlap of 50%. It is clear from Fig. 4.36 that the proposed hybrid scheme provides better PSD performance than EC scheme. The proposed hybrid transform with CR of 1.6 provides superior PAPR reduction, better BER characteristics, and less OOB radiation.

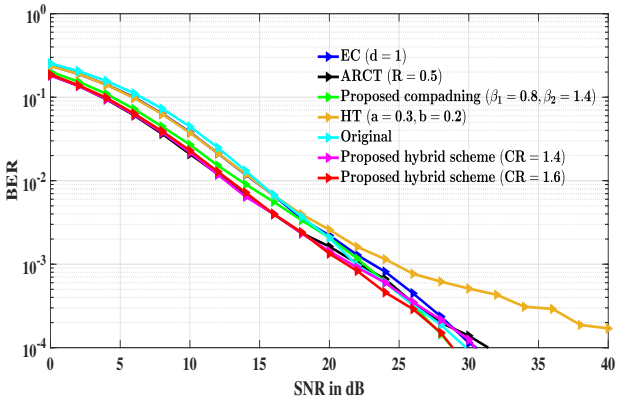

Figure 4.35: Comparison of BER curves for original and various companding techniques with SSPA under Rician channel.

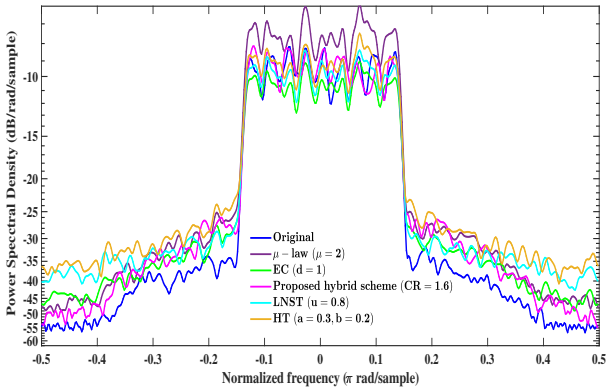

Figure 4.36: Comparison of PSD curves of the proposed hybrid scheme and several companding schemes.

The performance comparison of the UFMC system with the proposed hybrid scheme and several companding schemes is depicted in Table 4.9. The proposed hybrid transform with CR of 1.6 provides enhanced performance with a net-gain of 7.22 dB when compared to other companding schemes.

The proposed hybrid schemes are also compared with several state of art companding transforms, such as DFT-ARCT and DFT-μ-law [79] of UFMC system, companding scheme [116] and amplitude-limiting companding (ALC) of OFDM system, and companding function [117] of OFDM system , as illustrated in Table 4.10. It is evident that from Table 4.10, the proposed hybrid scheme with CR of 1.4 offers betterment of PAPR reduction of 7.8 dB at CCDF of 10^{-3} when compared to other companding transforms. Besides, the required additional SNR value of the proposed hybrid scheme with CR of 1.4 is -0.8 dB at BER = 10^{-3}, which is minimum when compared to other companding schemes. Hence, the proposed hybrid scheme with

Table 4.9: Performance comparison of the proposed hybrid scheme and various companding schemes of the UFMC system

Companding scheme	Improved PAPR reduction at CCDF= 10^{-4}	Additional SNR values required at BER= 10^{-4}	net gain (Improved PAPR reduction-Additional SNR)
EC (d= 1)	5.7	0.6	5.1
μ-law (μ= 2)	2.5	-1.1	3.6
HT (a= 0.3, b= 0.2)	5.8	1.8	4
Proposed companding (β_1= 0.8, β_2= 1.4)	7	-0.8	7.8
Proposed hybrid (CR= 1.6)	8.1	-0.7	8.8
Proposed hybrid (CR= 1.4)	8.5	-0.4	8.9

Table 4.10: Comparison of performance analysis of the proposed hybrid transforms with the literature.

Companding Scheme	Improved PAPR reduction at CCDF= 10^{-3}	Required Additional SNR Values at BER= 10^{-3}	net gain (Reduction of PAPR-Additional SNR)
Proposed companding (β_1= 0.8, β_2= 1.4)	6.3	-0.7	7
Proposed hybrid transform (CR= 1.6)	7.3	-1	8.3
Proposed hybrid transform (CR= 1.4)	7.8	-0.8	8.6
DFT-ARCT (R= 0.4) [79]	7.2	3	4.2
DFT-μ-law (μ= 50) [79]	8.2	4	4.2
ALC (M= 1, s= 1.2, v= 1.8) [116]	4.7	1.7	3
Scheme of [116] (c= 0.5218)	4.6	0.1	4.5
Scheme of [117] (c= 0, A= 1.414)	7.3	2.2	5.1

CR of 1.4 offers enhanced system net gain of 8.6 dB when compared to various companding schemes.

4.6.4 Experimental results

The proposed hybrid scheme is validated in real time by using WARP V3 kit. The experimental setup of the UFMC system with the proposed hybrid transform using WARP V3 board is displayed in Fig. 4.37. The UFMC signal without companding scheme, the proposed hybrid scheme signals, and μ-law signal are depicted in Fig. 4-38. It is observed from Fig. 4.38 (a) that high peak amplitudes increases the PAPR, so the SSPA is driven into saturation region, thus degrading the system efficiency. Therefore, PAPR reduction in UFMC system by employing optimal hybrid schemes is necessary to enhance the system performance.

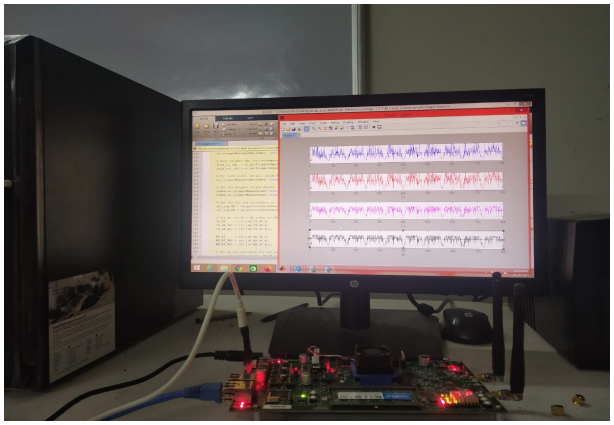

Figure 4.37: Experimental arrangement using WARP V3 kit.

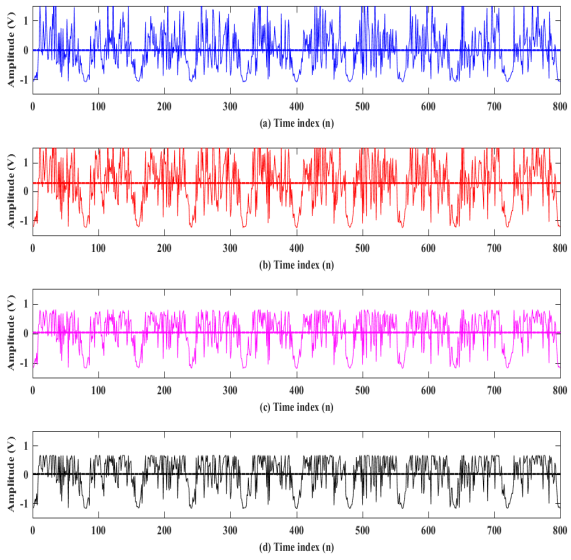

Figure 4.38: Real time UFMC signal, μ-law, proposed companding signal and the proposed hybrid signal with CR=1.4 (a) Transmitted UFMC signal (b) μ-law signal (c) Proposed companding signal (d) Proposed hybrid signal.

The conventional μ-law waveform reduces the PAPR significantly; however, it raises the average power level, as depicted in Fig. 4.38 (b). The proposed companding and the proposed time domain hybrid waveforms are depicted in Fig. 4.38 (c) and Fig. 4.38(d), respectively. It is confirmed from Fig. 4.38 (d) that significant PAPR diminution is achieved over real time environment. Also, the proposed hybrid transform possesses constant average power level. The hardware outcomes confirm that the proposed hybrid transform provides enhanced PAPR reduction with constant average power when compared to μ-law scheme. Power spectrums of transmitted and received signals are depicted in Fig. 4.39. It is obvious that remarkable distortion is not observed between transmitted spectrum and received spectrum, as shown in Fig. 4.39.

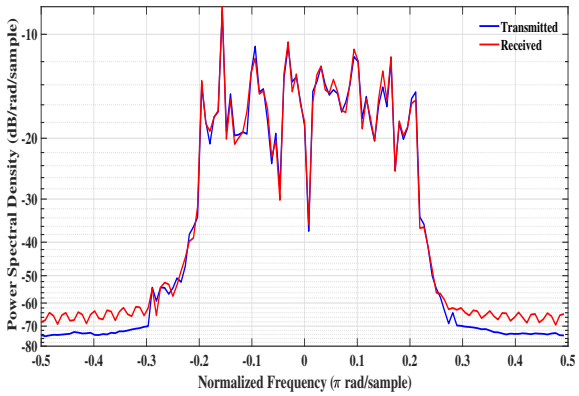

Figure 4.39: Power spectrum's of transmitted and received signals by using WARP V3

4.7 Conclusion

An exponential companding scheme, which transforms Rayleigh distributed UFMC signals into uniform distribution, has been presented for UFMC system. Simulation results have illustrated that EC technique provides better PAPR reduction with degradation in BER when compared to original UFMC signal and μ-law scheme. Further, we have proposed a new nonlinear companding scheme called "modified exponential companding", which alters the large and small amplitudes of UFMC signals depending on two companding levels based on a threshold parameter. Simulation results have proven that MEC-NDC scheme provides improved BER of 9.1×10^{-4} at SNR of 15 dB than EC technique. Moreover, by properly choosing companding factors d_1, d_2, and α, the system becomes more flexible and can be used in various applications. The theoretical analysis has proven that the proposed MEC scheme with no decompanding operation offers an enhanced BER performance than with decompanding at the receiver. Furthermore, by properly choosing the clipping ratio of 1.5, an optimal hybrid scheme provides enhanced PAPR reduction of 8.02 dB and the net gain of 7.72 dB. In addition to this, the BER performance of various companding techniques has been analyzed over a multipath fading channel. Moreover, the experimental results show that a significant PAPR reduction has been attained by using the proposed hybrid scheme. Finally, it has been concluded that the proposed hybrid schemes improve the efficiency of the UFMC system performance.

Chapter 5

Joint Time Domain Channel Estimation with Hybrid PAPR Reduction in UFMC Systems

5.1 Introduction

The energy efficiency of UFMC is limited by high PAPR. The PAPR problem is compensated at the transmitter by employing either a costly HPA or adopting PAPR reduction schemes. Since high PAPR may drive the transmit PA into saturation region, the PA needs large input back-off to ensure the linear amplification. As IBO increases, the PA requires high power consumption, thus resulting in degradation of performance of power amplifier.

The clipping scheme is well suitable for low modulation orders, but it degrades the system performance for higher orders. Hence, companding schemes are more appropriate for achieving high data rates. In this chapter, a low-complexity linear companding (LC) scheme is presented for UFMC system to offer improved performance, but this scheme requires SI to decompand the signal at the receiver.

The requirement of SI for decompanding results in reducing the SE and data reliability of the UFMC system. Hence, the pilots are used to transmit the SI and estimate the channel characteristics. In [89], the joint estimation of channel sate information and PAPR reduction is proposed for OFDM. The estimation of CIR has a great impact on the system performance, so the frequency domain channel estimation methods are inappropriate at high noise regimes

and also reduce the spectral efficiency. Hence, time domain CE methods, which are discussed in [46]-[48], are attractive for OFDM systems. The estimation of channel in time domain outperforms the frequency domain estimation. To our knowledge, the time domain CE has not been addressed for UFMC system. Moreover, the design of joint time domain CE with PAPR reduction has not been employed for UFMC system.

In this contribution, a hybrid PAPR reduction scheme that improves PAPR performance by employing clipping scheme on the linear companded signal is proposed. The optimum companding parameters (i.e., ρ_1, ρ_2, and ρ_3) and clipping ratio (CR), which provide better performance metrics such as PAPR, BER, and power spectrum, are obtained for the proposed system. Moreover, they enable the proposed hybrid scheme to provide more flexibility and have freedom to get optimum performance.

A joint time domain CE with hybrid PAPR reduction of UFMC system is proposed. Unlike in traditional companding schemes, the pilots are inserted in time domain to perform time domain channel estimation and are also used to transmit the SI that is required for decompanding at the receiver. Moreover, the proposed time domain channel estimation does not require the symbol interval to be much longer than the maximum channel delay spread. As a result, UFMC systems could use less number of subcarriers or shorter symbol interval than those systems that use frequency domain methods. Therefore, the proposed time domain CE method has less computational complexity and greater capability of adapting to fast channel variations. Moreover, the performance of proposed system is analyzed in the presence of SSPA and is validated in real time using WARP V3 kit.

This contribution is ordered as follows. The proposed UFMC system model and the proposed time domain CE model with PAPR reduction schemes for UFMC system are discussed in section 5.2. The nonlinear HPA model is described in section 5.3. The simulation results of joint time domain CE with linear companding scheme and hybrid schemes are illustrated in section 5.4. The experimental verification of the results and conclusions are discussed in section 5.5 and section 5.6, respectively.

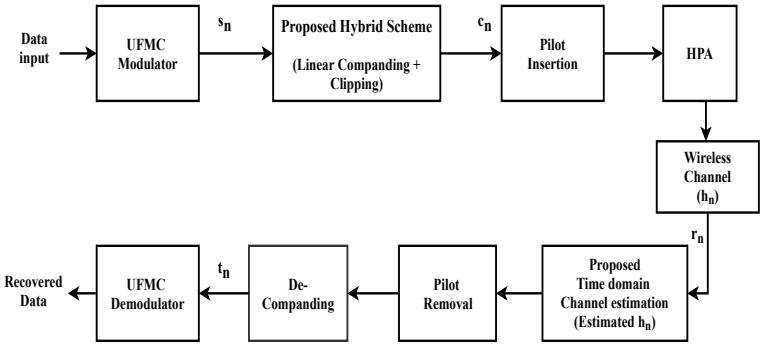

Figure 5.1: Proposed joint time domain CE with hybrid scheme.

5.2 Proposed joint time domain CE with PAPR reduction

The overview of the proposed joint time domain CE with the hybrid scheme structure is shown in Fig. 5.1. The UFMC signal is mathematically represented as

$$s_n = \frac{1}{N} \sum_{p=1}^{B} \sum_{l=0}^{L-1} \sum_{k=B^p} X_k^p f_l^p \exp^{\frac{j2\pi(n-l)k}{N}} \qquad 0 \leq n \leq N+L-1 \tag{5.1}$$

The PAPR of the UFMC system is reduced by employing companding transforms on the transmitted signal s_n. The companding function is represented as shown below.

$$g_n = t(s_n) \tag{5.2}$$

5.2.1 Proposed linear companding scheme

Companding schemes are simple and efficient in reducing the PAPR of UFMC system. But the companding schemes affect the system performance in terms of PAPR reduction, spectral regrowth, and BER. Hence, an effective trade-off among these performance metrics is the most challenging task in the design of companding schemes.

In the proposed LC scheme, a most precise case is taken into consideration to attain better performance gains. The UFMC signal consists of three types of amplitude values, i.e., large values, average values, and small values. In the proposed scheme, the three amplitude ranges of UFMC signal can be treated separately with a different scale. This can be accomplished by employing two inflexion thresholds (i.e., δ_1 and δ_2), which can be obtained from the UFMC

signal. The mathematical representation of the proposed companding function is given below.

$$g_n = \begin{cases} \rho_1.s_n & |s_n| \leq \delta_1 \\ \rho_2.s_n & \delta_1 < |s_n| \leq \delta_2 \\ \rho_3.s_n & |s_n| > \delta_2 \end{cases} \tag{5.3}$$

The PAPR of the proposed LC scheme is reduced by enlarging the small values of the UFMC signal with the aid of companding parameter ρ_1, so ρ_1 must be greater than one (i.e., $\rho_1 > 1$). Moreover, the large amplitude values are compressed by ρ_3; therefore, ρ_3 must be less than one (i.e., $\rho_3 < 1$), and the average values are maintained at the same level, (i.e., $\rho_2 = 1$). Also, by employing $\rho_2 = 1$, there is no need of inverse scaling for the average amplitudes at the receiver. With these arrangements, the LC scheme provides performance enhancement by proper choice of companding parameters. However, the inflexion points are required in order to perform decompanding at the receiver. The inflexion points that are considered in the proposed LC scheme are δ_1 and δ_2, which are 30% of V and 60% of V, respectively, where V denotes the maximum of absolute of the transmitted signal s_n (i.e., $V = max|s_n|$). The required SI is transmitted through the pilots that can be obtained from the CE block, which is discussed in section 5.2.3. The decompanding at the receiver is mathematically expressed as shown below.

$$z_n = \begin{cases} \frac{1}{\rho_1}.r_n & n \,\epsilon\, \varphi_1\,(\delta_1) \\ \frac{1}{\rho_2}.r_n & n \,\epsilon\, \varphi_2\,(\delta_{1,2}) \\ \frac{1}{\rho_3}.r_n & n \,\epsilon\, \varphi_3\,(\delta_2) \end{cases} \tag{5.4}$$

5.2.2 Proposed hybrid scheme (LC+clipping)

The PAPR performance of the UFMC system is further improved by employing clipping on the linearly companded signal. The clipping is performed by using an appropriate clipping threshold value on the LC signal at the transmitter side, while there is no need of reverse operation at the receiver. The equation for the clipping operation is given mathematically as

$$c_n = \begin{cases} g_n & |g_n| \leq \gamma \\ \gamma \exp^{j\phi_n} & |g_n| > \gamma \end{cases} \tag{5.5}$$

where c_n is the clipped signal, $\phi_n = arg[g_n]$ and γ is the threshold level at which clipping is applied on the companded signal. The clipping ratio (CR) is known as

$$CR = \frac{\gamma}{\sqrt{P_{avg}}} \tag{5.6}$$

where P_{avg} denotes the average power of the companded signal. In [111], the clipping is performed on the OFDM signal followed by companding. The information is lost at the first stage due to the clipping. Whereas our proposed LC+clipping scheme employs companding initially followed by clipping. The signal peaks are compressed as LC companding is employed in the first stage. Hence, the clipping scheme in the second stage does not cause significant amount of data loss.

5.2.3 Proposed time domain channel estimation

To perform time domain CE, the pilot symbols are inserted in hybrid UFMC signal c_n. Two pilots (i.e., δ_1 and δ_2) are appended at the end of the data carriers of the transmitted signal. These pilots can be used both for channel estimation and decompanidng. Now, the pilot added signal c_n is distorted by the wireless multipath fading channel. The resultant received signal is written as

$$r_n = c_n * h_n + w_n \tag{5.7}$$

where w_n denotes the noise samples of channel and h_n is the channel impulse response (CIR). At receiver, the CE has a significant impact on the performance of the system. The CSI can be obtained by employing either frequency-domain CE or time-domain CE. The time domain CE is better when compared to frequency-domain CE as time domain CE has two advantages. For time domain CE, there is no need to have the length of UFMC symbol to be larger than the maximum delay spread of the channel. As a result, channel estimation tolerance of the multipath fading effect is improved. Also, as CSI is generally present in time-domain model, it can be used to enhance the performance of the channel estimation. The key idea in the proposed model is to employ time domain pilots to determine the time domain CIR as well as the required SI that is necessary to perform decompanding. The time domain CIR is attained by employing the linear minimum mean square error channel estimation technique.

Linear Minimum Mean Square Error (LMMSE) Channel Estimation:

The LMMSE channel estimator for the time domain model is determined based on the priori knowledge of the channel. The covariance of the channel is used as a priori knowledge. The covariance matrix of the channel is represented as shown below.

$$R_{h_n h_n} = E\left[h_n h_n^H\right] \tag{5.8}$$

The joint distribution of the received signal vector r_n and the channel vector h_n can be represented as

$$P(r_n; h_n) = \frac{1}{\sqrt{2\pi\sigma^2}} \exp \frac{-(r_n - c_n h_n)^2}{2\sigma^2} \tag{5.9}$$

The LMMSE offers optimal CE performance by reducing the estimation error, which can be expressed as

$$e = h_n - \hat{h_n} \tag{5.10}$$

where h_n is the true CIR and $\hat{h_n}$ is the estimated CIR. Then the mean squared error is given as

$$E\left\{|e|^2\right\} = E\left\{\left|h_n - \hat{h_n}\right|^2\right\} \tag{5.11}$$

Finally, the LMMSE estimator is obtained as

$$\hat{h}_n^{LMMSE} = R_{h_n h_n}\left(R_{h_n h_n} + \sigma^2\left(c_n c_n^H\right)^{-1}\right)^{-1} \hat{h}_n^{LS} \tag{5.12}$$

where $\hat{h}_n^{LS}$ is expressed as shown below.

$$\hat{h}_n^{LS} = \left(c_n^H c_n\right)^{-1} c_n^H r_n \tag{5.13}$$

Initially, the CIR is obtained at the pilot locations from eq(5.13). Later, the CIR at data locations is obtained by employing interpolation techniques. Here, spline interpolation is employed to obtain CIR at data sub-carriers as the spline interpolation provides a continuous polynomial fitting and better smooth to the data sub-carriers. In MATLAB, the spline interpolation is attained by using spline function. Finally, the LMMSE channel impulse response is estimated by using eq(5.12). The estimated CIR is used in the data recovery process to improve the data efficiency of the system. After estimating the channel, the pilots are removed from the received signal.

Then decompanding is performed on the received signal by using eq(5.4). In this way, the inserted pilots can be employed in both CE and PAPR reduction of UFMC system. Now,

the time domain decompanded signal is converted to frequency domain by employing $2N$-FFT. Then, equalization is performed to combat the ISI. Finally, demodulation is employed on the equalized output to recover the original data.

5.3 Nonlinear power amplifier

The BER characteristics and power spectrum performance of the proposed hybrid schemes are analyzed by including a SSPA over AWGN channel. Most of the radio systems have employed HPAs in the transmitter to achieve required transmit power. The SSPA is one of the widely accepted models of HPAs and is advantageous due to the utilization of Gallium Arsenide (GaAs) device technology. The GaAs based devices employed in SSPA offer high power handling capability than Silicon based devices due to the large energy band gap of GaAs material. According to the model [55], the complex envelope of the SSPA input signal can be expressed as

$$c_n(t) = |c_n(t)| e^{j\theta_n(t)} \tag{5.14}$$

and the output signal is given as

$$c_{no}(t) = \frac{a|c_n(t)|}{\left[1 + \left(\frac{|c_n(t)|}{A_{sat}}\right)^{2p_a}\right]^{\frac{1}{2p_a}}} e^{j\theta_n(t)} \tag{5.15}$$

where, A_{sat} denotes the saturation level, a represents the amplifier gain, and p_a is a random positive integer that controls the nonlinearity of the amplifier. The SSPA produces only the AM/AM conversion and no phase distortion ($\theta_n(t)$=0). So, substituting $\theta_n(t)$=0 in eq(5.15) gives eq(5.16)

$$c_{no}(t) = \frac{a|c_n(t)|}{\left[1 + \left(\frac{|c_n(t)|}{A_{sat}}\right)^{2p_a}\right]^{\frac{1}{2p_a}}} \tag{5.16}$$

The input back off, which reduces nonlinear distortions in the transmitted signal can be denoted as

$$IBO = \frac{A_{sat}^2}{P_{in}} \tag{5.17}$$

Where $P_{in} = E\left[|c_n(t)|^2\right]$ is the average power of the input signal. On the other hand, the higher IBO lowers the SSPA efficiency. Hence, the IBO must be chosen carefully to achieve better BER performance without degrading power amplifier efficiency since there is a trade-off between low distortion and high SSPA efficiency.

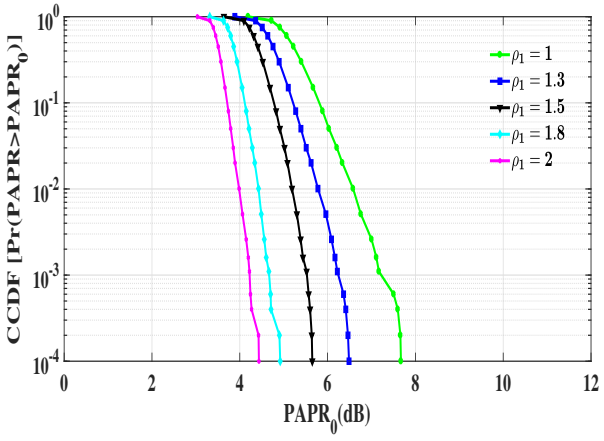

Figure 5.2: CCDF performance of the proposed LC scheme for various values of ρ_1 with constant ρ_2 and ρ_3.

5.4 Performance evaluation

The performance of the proposed joint time domain CE with hybrid PAPR reduction scheme of the UFMC system has been evaluated in terms of system BER, PAPR reduction, and power spectrum. For simulation, the number of sub-bands, the sub-carriers in each sub-band, and the filter length are considered as 8, 20, and 40, respectively. The sub-bands are modulated by employing QAM as a modulation scheme.

Initially, the selection of optimum parametres of LC scheme to attain better performance gains is done. Fig. 5.2 illustrates the CCDF performance of the proposed LC scheme for various values of ρ_1 while keeping the other companding parameters (i.e., ρ_2 and ρ_3) constant. It depicts that the PAPR reduction increases as the companding parameter ρ_1 increases.

Fig. 5.3 shows the CCDF performance of the proposed LC scheme for various values of ρ_3 while keeping the other parameters (i.e., ρ_1 and ρ_2) constant. As the companding parameter ρ_3 increases, the PAPR reduction increases up to a ρ_3 of 0.5 (i.e., $\rho_3 \leq 0.5$), but the PAPR reduction of the proposed LC scheme decreases when ρ_3 is greater than 0.5 (i.e., $\rho_3 > 0.5$), as illustrated in Fig. 5.3. It is evident from Fig. 5.3 that the PAPRs of 5.8 dB and 7.7 dB are obtained at ρ_3 of 0.5 and 0.7, respectively. Since there is a trade-off between PAPR and BER, the BER performance on the variation of ρ_1 and ρ_3 of the proposed LC scheme to determine the optimum values of ρ_1 and ρ_3 is described in Fig. 5.4 and Fig. 5.5, respectively.

As seen in Fig. 5.2 and Fig. 5.4, the performance of PAPR and BER is better at $\rho_1 = 1.5$. Hence, the optimum value of ρ_1 is 1.5. Similarly, as depicted in Fig. 5.3 and Fig. 5.5, the performance of PAPR and BER is better at $\rho_3 = 0.5$. Hence, the optimum value of ρ_3

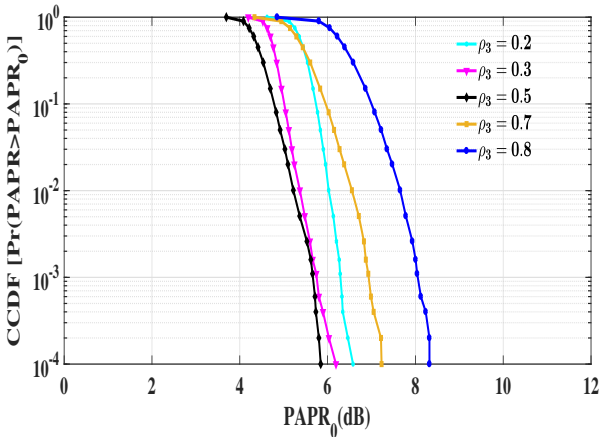

Figure 5.3: CCDF performance of the proposed LC scheme for various values of ρ_3 with constant ρ_1 and ρ_2.

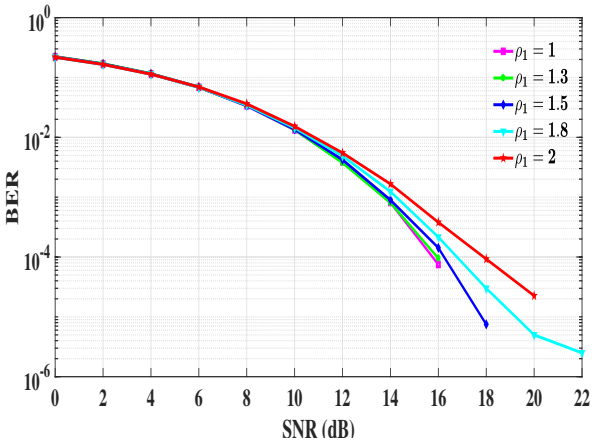

Figure 5.4: BER performance of the proposed LC scheme on the variation of ρ_1 with constant ρ_2 and ρ_3.

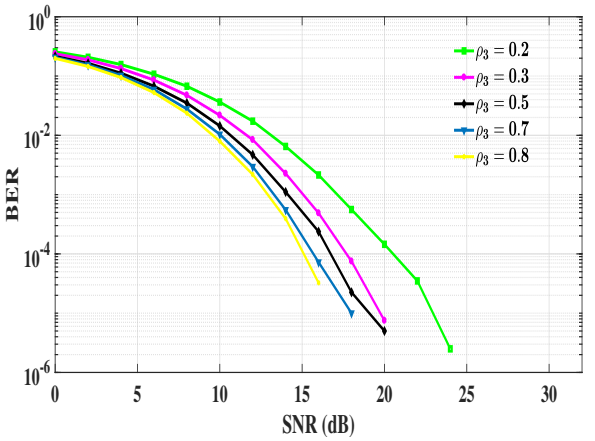

Figure 5.5: BER performance of the proposed LC scheme on the variation of ρ_3 with constant ρ_1 and ρ_2.

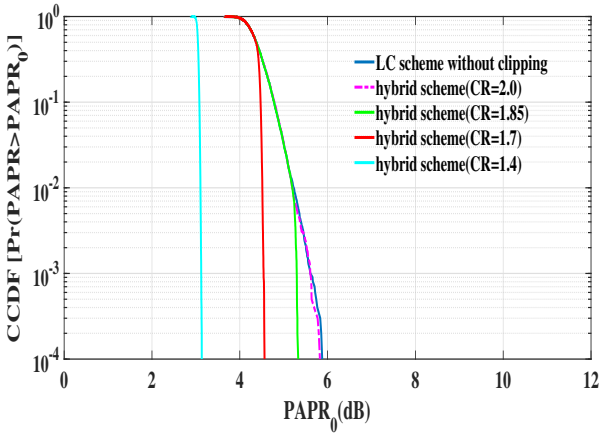

Figure 5.6: CCDF performance of the proposed hybrid scheme for various values of clipping ratio.

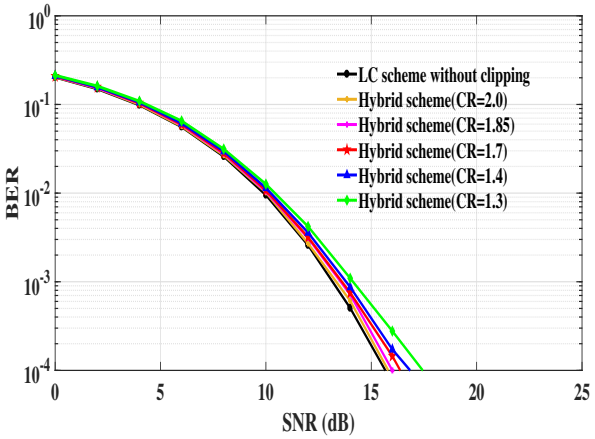

Figure 5.7: BER curves of the proposed hybrid scheme for various values of clipping ratio.

is 0.5. The optimum value of ρ_2 is chosen as 1 since inverse scaling is not needed for the average amplitudes at the receiver when $\rho_2 = 1$. It can be concluded that the optimum choice of companding parameters of the proposed LC scheme are $\rho_1 = 1.5$, $\rho_2 = 1$, and $\rho_3 = 0.5$.

In the proposed hybrid scheme, clipping is performed with suitable clipping ratio on the LC companded signal to reduce PAPR of the UFMC system. Fig. 5.6 illustrates the CCDF curves of the proposed hybrid scheme for different clipping ratios and LC scheme without clipping. The proposed hybrid scheme with CR of 1.4 offers better PAPR reduction than other schemes.

Fig. 5.7 demonstrates the BER curves of the proposed hybrid scheme for different clipping ratios and LC scheme without clipping. The hybrid scheme with CR of 2 offers better BER performance, but there is no significant improvement of PAPR reduction compared to LC scheme, as seen in Fig. 5.6. It is observed from Fig. 5.6 and Fig. 5.7 that the proposed hybrid

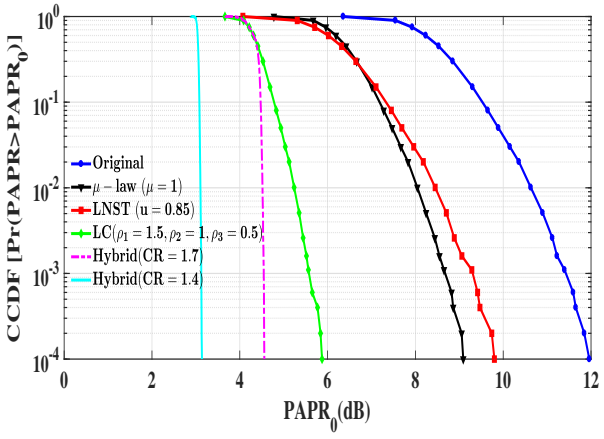

Figure 5.8: Comparison of the PAPR performance of various companding schemes and original signal.

Table 5.1: Comparison of PAPR values for several companding schemes and original signal

	Original	μ-law (μ=1)	LNST (u=0.85)	Proposed LC scheme (ρ_1=1.5, ρ_2=1, ρ_3=0.5)	Proposed hybrid scheme (CR=1.7)	Proposed hybrid scheme (CR=1.4)
PAPR (dB) at CCDF=10^{-4}	12.0	9.1	9.8	5.8	4.6	3.2

scheme with a suitable clipping ratio of 1.4 offers enhanced PAPR reduction with degradation in BER. Hence, the proposed hybrid scheme with a CR of 1.7 is chosen to achieve better PAPR performance without much degradation in BER.

Fig. 5.8 demonstrates the PAPR performance of the UFMC signal without companding, μ-law, LNST companding, proposed LC scheme, and hybrid techniques with clipping ratios of 1.7 and 1.4. The proposed LC scheme offers better PAPR reduction than μ-law, LNST scheme, and original signal. Besides, the proposed hybrid schemes provide enhanced PAPR reduction when compared to μ-law, LNST, and original signal. Moreover, the proposed LC+clipping with a clipping ratio of 1.4 offers better PAPR reduction than LC+clipping with a clipping ratio of 1.7. Table 5.1 shows the PAPR values of several companding schemes at a CCDF of 10^{-4}. The PAPR values of UFMC signal, μ-law, LNST, LC scheme, the proposed LC+clipping with a CR of 1.7, and the proposed LC+clipping with a CR of 1.4 are 12.0 dB, 9.8 dB, 9.1 dB, 5.8 dB, 4.6 dB, and 3.2 dB, respectively. When compared to the original UFMC signal at CCDF of 10^{-4}, the decrease in PAPR of the μ-law, LNST, the proposed LC, the proposed LC+clipping with a CR of 1.7, and the proposed LC+clipping with a CR of 1.4 are 2.2 dB, 2.9 dB, 6.2 dB, 7.4 dB, and 8.8 dB, respectively, as shown in Table 5.2.

Table 5.2: Improvement of PAPR reduction of several companding transforms with original UFMC signal

	μ-law (μ=1)	LNST (u=0.85)	Proposed LC scheme (ρ_1=1.5, ρ_2=1, ρ_3=0.5)	Proposed hybrid scheme (CR=1.7)	Proposed hybrid scheme (CR=1.4)
PAPR (dB) at CCDF=10^{-4}	2.9	2.2	6.2	7.4	8.8

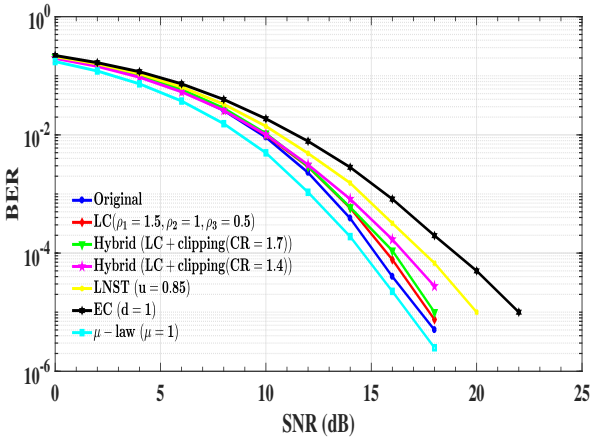

Figure 5.9: BER characteristics of the UFMC signal without companding and several companding schemes over AWGN channel.

Fig. 5.9 shows the BER characteristics of the UFMC signal without companding, μ-law, LNST companding, EC, proposed LC scheme, and hybrid techniques with CRs of 1.7 and 1.4 over AWGN channel. The μ-law offers better BER characteristics, but it increases the average power of the signal. It is evident that the proposed LC scheme offers better performance than EC and LNST scheme. Also, the proposed hybrid scheme with a CR of 1.7 offers better BER performance than with a CR of 1.4. Table 5.3 provides the BER analysis at a SNR of 10^{-4} for the UFMC signal, μ-law, LNST companding, proposed LC scheme, and hybrid schemes.

Table 5.3: Comparison of BER performance of the several companding transforms and original UFMC signal

	Original	μ-law (μ=1)	LNST (u=0.85)	Proposed LC scheme (ρ_1=1.5, ρ_2=1, ρ_3=0.5)	Proposed hybrid scheme (CR=1.7)	Proposed hybrid scheme (CR=1.4)
SNR (dB) at BER=10^{-4}	15.2	14.7	17.3	15.8	16.1	16.7

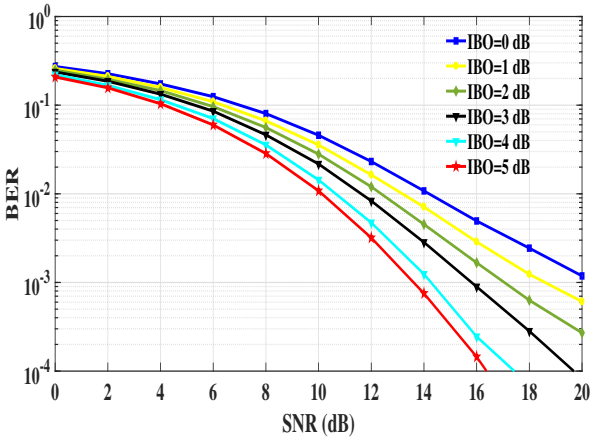

Figure 5.10: BER performance of the proposed hybrid scheme with a CR of 1.7 for different values of IBO.

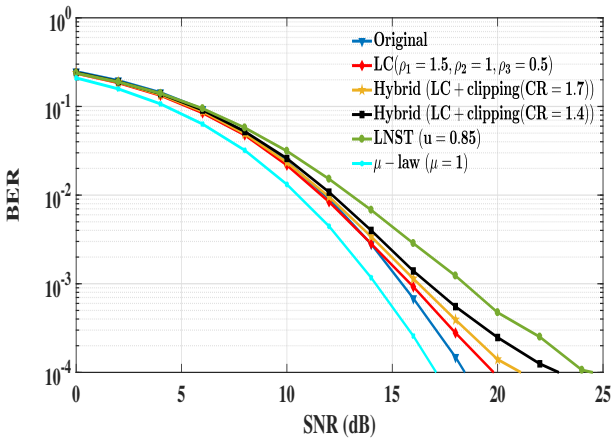

Figure 5.11: BER characteristics of the UFMC signal without companding and several companding schemes with SSPA (p_a = 2, IBO = 3 dB) over AWGN channel.

Fig. 5.10 illustrates the BER performance of the proposed hybrid scheme with a CR of 1.7 for different values of IBO. As IBO increases, the distortion decreases and BER performance becomes better. Since better BER performance is achieved when IBO is 5 dB, so the SSPA has been employed with the parameter p_a of 2 and the input back-off of 5 dB. Fig. 5-11 shows the BER characteristics of the UFMC signal without companding, μ-law, LNST companding, proposed LC scheme, and hybrid techniques with CRs of 1.7 and 1.4 with SSPA (p_a = 2, IBO = 3 dB) over AWGN channel. It is confirmed from Fig. 5.11 that the performance is degraded in the presence of SSPA with an IBO of 3 dB.

Fig. 5.12 shows the BER characteristics of the UFMC signal without companding, μ-law, LNST companding, proposed LC scheme, and hybrid techniques with CRs of 1.7 and 1.4 with SSPA (p_a = 2, IBO = 5 dB) over AWGN channel. It is confirmed from Fig. 5.12 that the performance is nearly similar even in the presence of SSPA.

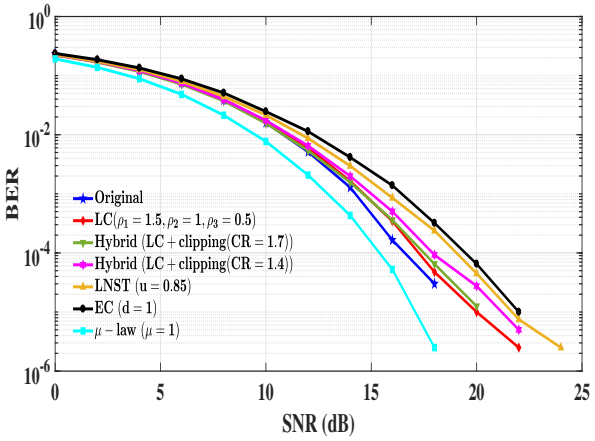

Figure 5.12: BER characteristics of the UFMC signal without companding and several companding schemes with SSPA (p_a = 2, IBO = 5 dB) over AWGN channel.

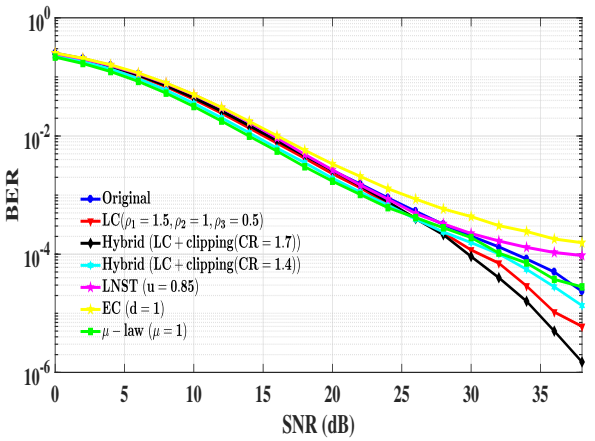

Figure 5.13: BER characteristics of the UFMC signal without companding and several companding schemes over rician channel.

Fig. 5.13 shows the BER characteristics of the UFMC signal without companding, μ-law, LNST companding, proposed LC scheme, and hybrid techniques with CRs of 1.7 and 1.4 over multipath rician channel. The proposed LC scheme offers better performance than LNST, μ-law, and original signal. Also, the proposed hybrid scheme with a CR of 1.7 offers better BER performance than with a CR of 1.4.

Fig. 5.14 illustrates the power spectrum performance of the proposed hybrid scheme with a CR of 1.7, μ-law, and LNST scheme. The SSPA is employed with the parameter p_a of 2 and the input back-off of 5 dB. The proposed hybrid scheme with a clipping ratio of 1.7 offers better PSD performance than LNST and μ-law companding. The proposed hybrid scheme and LNST produce only OOB emissions, while the μ-law produces OOB radiations along with in-band distortion. The average and peak values of the ratio of the in-band power to the out of band

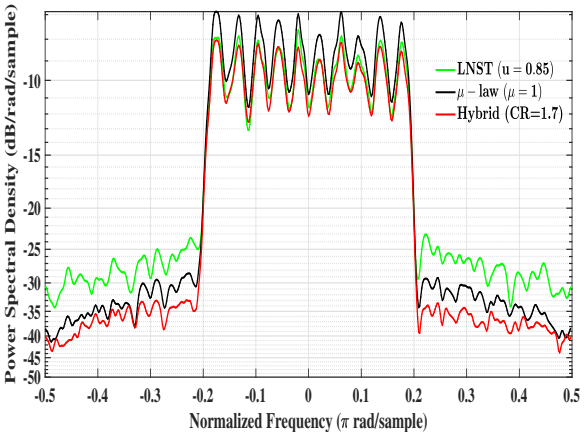

Figure 5.14: Power spectrum performance of the proposed hybrid scheme with a CR of 1.7, μ-law, and LNST scheme.

Table 5.4: Analysis of the UFMC system performance for various companding schemes at CCDF and BER of 10^{-4}

Companding Scheme	Improvement of PAPR reduction (dB)	Additional SNR values (dB)	Net gain
μ-law (μ=1)	2.9	-0.5	3.4
LNST (u=0.85)	2.2	2.1	0.1
Proposed LC (ρ_1=1.5, ρ_2=1, ρ_3=0.5)	6.2	0.6	5.6
Proposed hybrid scheme (CR=1.7)	7.4	0.9	6.5
Proposed hybrid scheme (CR=1.4)	8.8	1.5	7.3

power of the proposed hybrid transform is greater than μ-law with SSPA and LNST with SSPA.

Table 5.4 shows the performance analysis in terms of net gain for several companding schemes. The net gain of the companding scheme is obtained by subtracting the required additional SNR values from the improved PAPR reduction. It is observed from Table 5.4 that the proposed hybrid schemes with CRs of 1.7 and 1.4 provide enhanced performance with net gains of 6.5 dB and 7.3 dB, respectively. Hence, the proposed hybrid schemes provide enhanced performance in terms of net gain when compared to LC, μ-law, and LNST schemes.

The performance analysis of the proposed hybrid schemes has been compared with the other works in the literature, as shown in Table 5.5. The proposed hybrid schemes are compared with the techniques EC, amplitude-limiting companding (ALC), and companding scheme based on piecewise nonlinear companding [116] of OFDM system, hybrid DFT-ARCT [79] of UFMC system, hybrid Iterative clipping and filtering-enhanced nonlinear companding (ICF-ENC) [113] of OFDM system, and low complexity companding function [117] of OFDM sys-

Table 5.5: Comparison of performance analysis of the proposed hybrid schemes with the state-of-art schemes

Companding Scheme	Improvement of PAPR reduction (dB) at CCDF=10^{-3}	Additional SNR values (dB) at BER=10^{-3}	Net gain
Proposed hybrid scheme (CR=1.7)	7.1	0.4	6.9
Proposed hybrid scheme (CR=1.4)	8.3	0.7	7.6
μ-law (μ=1)	2.5	-1	3.5
LNST (u=0.85)	2	1.5	0.5
EC (d=0.7) [116]	4.8	1.9	2.9
ALC (M=1, s=1.2, v=1.8) [116]	4.7	1.7	3
Scheme of [116] (c=0.5218)	4.6	0.1	4.5
DFT-ARCT (R=0.4) [79]	7.3	3.0	4.3
ICF-ENC (γ=1.5) [113]	7.2	1.5	5.7
Scheme of [117] (c=0, A=1.414)	7.3	2.2	5.1

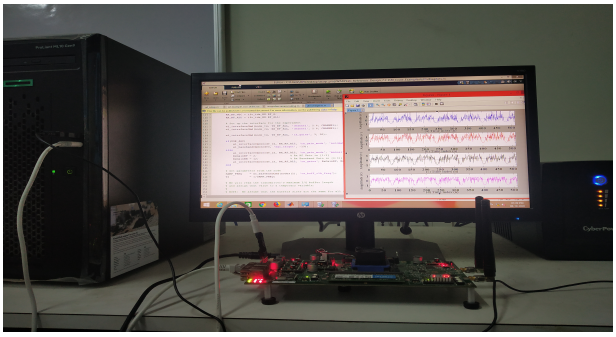

Figure 5.15: Experimental arrangement of the proposed model using WARP V3 kit.

tem. At a CCDF of 10^{-3}, the proposed LC+clipping with a CR of 1.4 provides enhanced PAPR reduction of 8.3 dB when compared to proposed LC+clipping with a CR of 1.7 and various companding techniques in the literature. Moreover, the net gain of the UFMC system of the proposed LC+clipping with CR of 1.4 is 7.6 dB, which is higher than the other schemes available in the literature.

The computational complexity of the proposed hybrid scheme is measured by the number of floating-point operations (flops). In particular, the flop count does not comprise signal amplitude calculation that is quite normal in all the companding schemes. The linear companding techniques are less complex than the nonlinear companding techniques. In case of the proposed hybrid method, only 1 flop/sample is required at both the transmitter and the receiver. In linear companding scheme, $0.45N$ companded samples $\left(\because N\int_{\beta_1}^{\infty} f_{|s_n|}(x)\,dx = 0.45N\right)$ are required. Where $f_{|s_n|}(x)$ denotes the probability density function. Therefore, the total number of flops required for the hybrid scheme are $0.45N{\times}2{=}0.9N$.

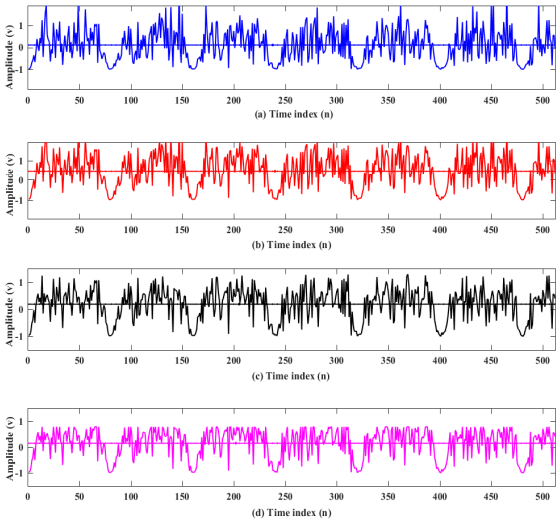

Figure 5.16: Real time waveforms of UFMC signal and various companding schemes (a) Original signal (b) μ-law signal (c) LC signal (d) LC+clipping signal with a CR of 1.7.

5.5 Experimental results

The proposed UFMC system is experimentally verified in real time by employing WARP V3 board. With the combination of MATLAB and the features of WARP kit, the physical layer algorithms are implemented in WARPLab framework. The two RF interfaces, i.e., RF A and RF B in WARP node can be employed as transmitting antenna and receiving antenna, respectively. Each interface has a 2.4/5 GHz transceiver with RF bandwidth of 40 MHz.

In WARPLab setup, a WARP node is attached to a host PC through an Ethernet switch. The software in the WARPLab is employed to upload the baseband samples that are created in the MATLAB to FPGA buffers. To send the baseband samples from RF A to RF B, the host PC drives the WARP node by sending a trigger signal. The radio board processes the baseband samples by employing up-conversion to convert baseband samples to RF waveform and down-conversion to convert the received RF waveform to baseband samples at the transmitter side and the receiver side, respectively. Then the received samples are processed in the MATLAB workspace.

The proposed joint time domain CE with PAPR reduction of UFMC system is experimentally verified by using WARP V3 kit and it can be demonstrated in Fig. 5.15. The waveforms of the proposed hybrid scheme with CR of 1.7, LC scheme, μ-law, and UFMC signal without companding are illustrated in Fig. 5.16. It can be seen from Fig. 5.16 (a) that the UFMC signal possess low amplitudes, average amplitudes, and high amplitudes. The high peaks in the UFMC signal not only increases the PAPR but also drives the PA into nonlinear region, which

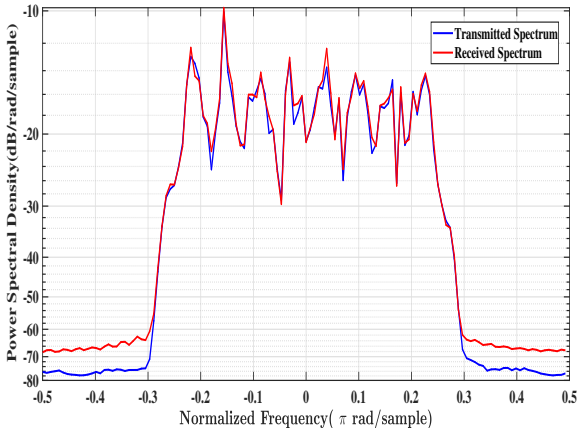

Figure 5.17: Power spectrum plots of the transmitted and received signals.

in turn reduces the system efficiency. So, PAPR reduction is essential in the proposed UFMC system by applying suitable schemes. It can be recognized from Fig. 5.16 (c) and (d) that a significant reduction of PAPR is obtained over real time channel by employing the proposed LC and LC+clipping with a CR of 1.7. The proposed hybrid technique provides better PAPR performance than LC scheme and μ-law. Besides, the average power of the proposed schemes is almost similar with the original signal, where as the μ-law increases the average power of the companded signal. Fig. 5.17 illustrates the power spectrum plots of the transmitted and received signals. Significant distortion is not observed between the transmitted and received spectrums in Fig. 5.17.

5.6 Conclusion

A joint pilot-based time domain CE with hybrid PAPR reduction scheme has been proposed for UFMC system. In the proposed time domain CE, the CSI, which has been employed to improve the performance of channel estimation, is obtained in advance. Moreover, the proposed CE does not need the length of UFMC symbol to be much larger than the maximum delay spread of the channel. Hence, the computational complexity of the proposed time domain CE is less and adaptable to rapid channel variations. Also, LC scheme that improves the PAPR performance with more design flexibility by using two inflexion points has been proposed. Simulation results show that the proposed LC scheme offers improved PAPR reduction of 6.2 dB at a CCDF of 10^{-4} and the BER is 0.3875×10^{-4} at a SNR of 14 dB. Moreover, a hybrid scheme with proper clipping ratio has been proposed. The proposed LC+clipping with a CR of 1.4 offers improved PAPR reduction of 8.8 dB and the net gain of 7.3 dB. Besides, the proposed hybrid transforms have been compared with the DFT-ARCT and ICF-ENC schemes. Addition-

ally, the proposed time domain CE with hybrid scheme has been validated and the experimental results have concluded that the PAPR performance has been improved by employing the proposed hybrid method. Eventually, it has been concluded that the proposed channel estimation along with PAPR reduction method enhances the performance of UFMC system.

Chapter 6

Performance analysis of UFMC based Massive MIMO downlink systems

6.1 Introduction

In order to provide better performance gains, the future wireless communication systems greatly depend on the utilization of multiple antennas. Hence, the combination of massive MIMO with UFMC is a promising technology to meet the requirements of next-generation wireless networks (5G and Beyond). Moreover, the robustness of the system can be increased against the multi path fading channels by combining the massive multi user MIMO with the multicarrier waveform techniques.

In massive MIMO downlink systems, precoding is necessary to reduce multi user interference. However, precoding results in the generation of time-domain signals that suffer from high PAPR. Additionally, PAPR problem becomes more in all multicarrier systems. Consequently, the high-power amplifier in the transmission section operates in non-linear region, thereby producing OOB radiation, in-band distortion, and adjacent channel interference. To alleviate these distortions, the HPA must be operated in linear-region with large IBO. However, the large IBO makes the system operates with low power levels, so the efficiency of the HPA decreases. Therefore, this is not a feasible solution for 5G communications as the energy efficiency is one of the essential requirements of 5G systems. So, the most desirable task to reduce PAPR is employing precoders, which generates time-domain signals with low PAPR.

The precoding that yields low PAPR is of great importance in UFMC based massive MIMO systems. The CE precoder switches the power amplifiers to operate in the nonlinear region; therefore, a power efficient analog circuitry at the BS is required. In [119], a precoder that generates a constant modulus signal constrained to only eight phase outputs for MU-MIMO systems was proposed. It needs the data converters called digital to analog converters (DACs) at the base station to produce eight phases.

In multiuser massive MIMO, the data converters are one of the main blocks that consume more power. The total number of ADCs can be increased as each receiving antenna needs a pair of ADCs. The power dissipation of DACs raises exponentially with the resolution and linearly with the bandwidth. Several hundreds of BS antennas in massive MIMO require more number of DACs, thereby leading to high power consumption. Therefore, the resolution of DACs must be restricted to maintain the power consumption within acceptable levels. Thus, recently, the low resolution DACs has grabbed the attention of researchers working in massive MU-MIMO downlink systems.

The distortion due to the low resolution DACs becomes negligible as the number of transmit antennas at the base station increase. Hence, the precoders with 1-bit DACs offer enhanced power efficiency for massive MIMO systems. The design of quantized low PAPR precoders is of great importance for massive MIMO systems.

To our knowledge, the combination of massive MIMO with UFMC modulation has not been developed so far. Additionally, the combination of quantized MU precoding and companding schemes to reduce the PAPR of the massive MU-MIMO-UFMC has not been presented.

In this contribution, the massive MU-MIMO-UFMC downlink transmission scheme is developed to achieve the benefits of both massive MIMO technology and the UFMC modulation scheme. The proposed combination provides high data rate, high SE, high EE, high robustness, and high throughput for multiuser networks. Moreover, a quantized precoding is employed for massive MU-MIMO-UFMC downlink systems over flat fading channels. For 1-bit DAC, a nonlinear phase-quantized precoder called SQUID-UFMC that addresses the high PAPR problem for massive MU-MIMO-UFMC downlink systems is proposed. The proposed SQUID-UFMC precoder produces constant modulus signals that reduce the PAPR of the massive MU-MIMO-UFMC system. Furthermore, a PLC scheme is proposed for the reduction of PAPR of the massive MU-MIMO-UFMC system. The proposed PLC scheme offers more freedom and design flexibility to achieve an optimum performance.

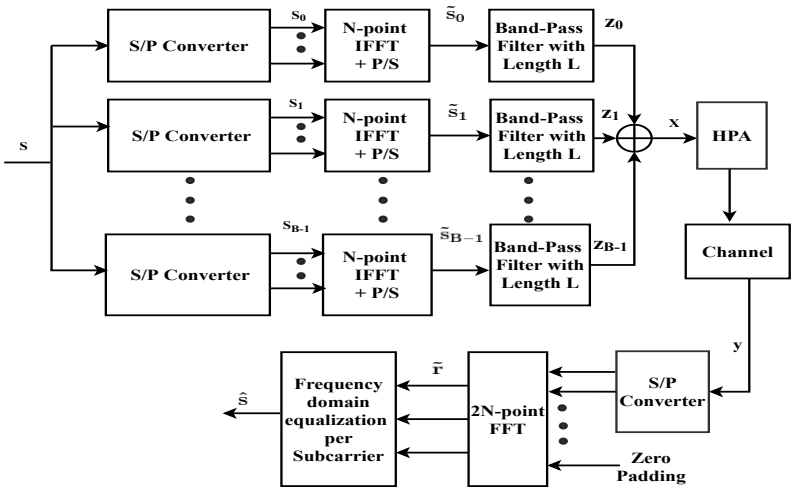

Figure 6.1: Single antenna UFMC system model.

This contribution is ordered as follows. The single antenna UFMC system model is presented in section 6.2. The proposed massive MU-MIMO-UFMC system model is described in section 6.3. The proposed quantized MU precoding and companding schemes for PAPR reduction of the proposed system is presented in section 6.4. The proposed piece wise linear companding scheme is described in section 6.5. Their performance evaluation and conclusions are illustrated in section 6.6 and section 6.7, respectively.

6.2 Single antenna UFMC system model

The block diagram of single antenna UFMC system is depicted in Fig. 6.1. In UFMC system, a total of N subcarriers are split into M sub-bands. Each sub-band consists of k subcarriers ($\therefore\ N = M \times k$). The single UFMC symbol consists of N subcarriers that are arranged in a N-dimensional vector s. The multiple symbols transmission by using multiple antennas will be discussed in section 6.3. Let s_i be the N-dimensional symbol vector. The n^{th} entry of $s_{i,(n)}$ is represented as shown below

$$s_{i,(n)} \triangleq \begin{cases} s_n & n = ik, ik+1, ...(i+1)k-1 \\ 0 & \text{otherwise} \end{cases} \tag{6.1}$$

where i ranges from 0 to M-1 and n ranges from 0 to N-1. The matrices are defined as follows.

$$P_i = \text{diag}\left([\underbrace{0...0}_{\text{ik}}\ \underbrace{1...1}_{\text{k}}\ \underbrace{0...0}_{\text{N-(i+1)k}}] \right), \qquad i = 0, 1....M-1,$$

Therefore, the N-dimensional vector s_i can be denoted as $s_i = P_i s$. Then the sub-band vectors s_i are transformed to time domain by employing IFFT transformation on each sub-band.

$$\tilde{s_i} = IFFT\,(s_i) = W_{N,IFFT} P_i s \tag{6.2}$$

where $W_{N,IFFT}$ denotes the $(N \times N)$-dimensional IFFT matrix. The $(m,n)^{th}$ entry of the IFFT matrix can be given as

$$W_{N,IFFT} = \frac{1}{\sqrt{N}} e^{j2\pi(m-1)(n-1)/N} \tag{6.3}$$

To improve the localization property, the vectors $\tilde{s_i}$ are passed through the Dolph chebyshev filter with finite impulse response f_l. The pass band filter employed in the system successfully reduces the OOB radiations with reference to the peak of the main lobe. The finite impulse response of the Dolph chebyshev prototype filter employed in i^{th} sub-band is denoted by $f_{i,l}$, which can be defined as

$$f_{i,l} = f_i e^{j2\pi \frac{C_i l}{N}}, \quad i = 0, 1....M-1, \quad l = 0, 1....L-1 \tag{6.4}$$

where C_i is the normalized frequency shift of the i^{th} sub-band and can be denoted as $C_i \triangleq \frac{k-1}{2} + ik$.

Let z_i be the filter output that can be obtained by employing discrete convolution between the f_i and the IFFT output $\tilde{s_i}$.

$$z_i = F_i \tilde{s_i} = F_i W_{N,IFFT} P_i s \tag{6.5}$$

The matrix F_i is the $[(N+L-1) \times N]$ dimensional toeplitz matrix of f_i. The UFMC signal is obtained by summing the vectors z_i and multiplied by the amplification factor $\sqrt{P_T}$. Therefore, the UFMC signal is formulated as

$$x = \sqrt{P_T} \left(\sum_{i=0}^{M-1} F_i W_{N,IFFT} P_i \right) s \tag{6.6}$$

Now, the UFMC signal is propagated through the wireless channel with channel vector h of length L_h. Then H is the toeplitz matrix of channel with dimensions $[(N+L+L_h-2) \times (N+L-1)]$. Now, the received vector is obtained by employing matrix multiplication between UFMC signal and the toeplitz matrix of channel. The received vector is expressed as

$$y = Hx + w = \sqrt{P_T} H \left(\sum_{i=0}^{M-1} F_i W_{N,IFFT} P_i \right) s + w \tag{6.7}$$

where w is the AWGN with zero mean. Assume that there is a perfect synchronization between transmitter and receiver and no phase distortion at the receiver. The received vector y is zero-

padded and $2N$-FFT is applied to get the frequency domain vector. The toeplitz matrix of $2N$-FFT is denoted as $W_{2N,FFT}$ and the $(m,n)^{th}$ entry of $W_{2N,FFT}$ vector can be represented as $\frac{1}{\sqrt{2N}}e^{-j2\pi(m-1)(n-1)/2N}$. Now the $2N$-dimensional vector is expressed as

$$r = W_{2N,FFT}y \tag{6.8}$$

The N-dimensional received vector $\bar{r}$ is attained by down-sampling the $2N$-dimensional vector r by a factor of 2. The $\tilde{h}_n$ and $\tilde{f}_{i,(n)}$ are the n^{th} co-efficient of the channel vector and the i^{th} sub-band of the FIR filter f_i, respectively. Then the q^{th} entry of the vector $\bar{r}$ is modeled as

$$\bar{r}_{(q)} \approx \frac{2N}{\sqrt{2}}\tilde{h}_{(2q-1)}\tilde{f}_{\lfloor q/k \rfloor,(2q-1)}s_{(q)} + \tilde{w}_{(2q-1)} \tag{6.9}$$

Finally, the soft estimate of the UFMC symbol s can be obtained by employing frequency domain equalization on the vector $\bar{r}$ and is modeled as given below.

$$\begin{aligned}\hat{s}_{(q)} &\approx \frac{\sqrt{2}}{2N}\frac{\bar{r}_{(q)}}{\tilde{h}_{(2q-1)}\tilde{f}_{\lfloor q/k \rfloor,(2q-1)}} \\ &= s_{(q)} + \frac{\sqrt{2}}{2N}\frac{\tilde{w}_{(2q-1)}}{\tilde{h}_{(2q-1)}\tilde{f}_{\lfloor q/k \rfloor,(2q-1)}}\end{aligned} \tag{6.10}$$

6.3 Proposed massive MU-MIMO-UFMC system model

The schematic of the proposed massive MU-MIMO-UFMC down link system is illustrated in Fig. 6.2. The mathematical analysis of the proposed model is done by using the analysis of single antenna UFMC system discussed in section 6.2. The system model consists of massive number of BSs with B antennas, where B antennas act as U single antenna UEs simultaneously in the same frequency band. Let $S = [s_0, s_1, ...s_{N-1}]$ be the $U \times N$ - dimensional symbol matrix that undergoes a QAM constellation. The symbol vector associated with the n^{th} subcarrier is described as $s_n = [s_{1,n}, ...s_{U,n}]^T$, where n ranges from 0 to N-1. The precoding is performed on each column of symbol matrix S. It is of two forms, which are linear and nonlinear. In linear case, the precoding matrix is simply multiplied by the symbol vector. Whereas in nonlinear case, the nonlinear precoding function produces the transmit signals depending on the symbol vector S. $Q_B(n)$ denotes the $B \times U$ - dimensional precoding matrix for the n^{th} column of symbol matrix. Therefore, the n^{th} column of the precoded output $X(:,n)$ can be given as

$$X(:,n) = Q_B(n)\,S(:,n) \tag{6.11}$$

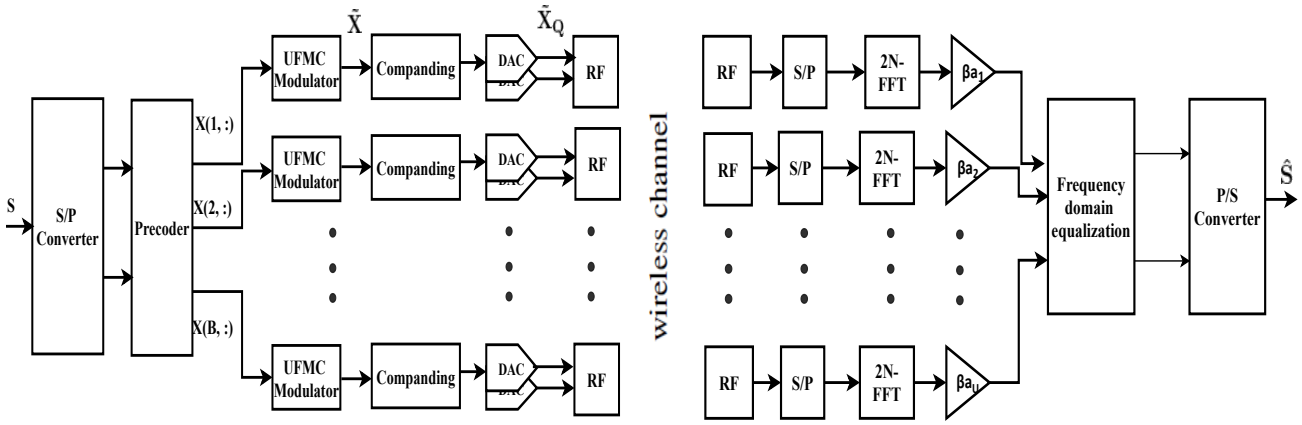

Figure 6.2: Proposed massive MU-MIMO-UFMC system model.

where X is the precoded output matrix of dimension $B \times N$ and satisfies the average power constraint, i.e., $E\left[||X||_2^2\right] \leq P$. After precoding, each row of the precoded output matrix X is transmitted through an UFMC modulator, as illustrated in Fig. 6.2. Then the quantization is performed on the UFMC symbol of length $N + L - 1$ by using very low-resolution DACs to reduce the power consumption and hardware complexity of the massive MIMO based UFMC system. The matrix $\tilde{X}_Q$ of dimension $[B \times (N + L - 1)]$ denotes the 1-bit quantized massive MU-MIMO-UFMC signal, which is obtained by grouping all the outputs of the parallel UFMC modulators. The j^{th} row of the matrix $\tilde{X}_Q$ is represented below.

$$\tilde{X}_Q(j,:)^T = \sum_{i=0}^{M-1} G_i W_{N,IFFT} P_i X(j,:)^T \tag{6.12}$$

The massive MU-MIMO-UFMC signal (i.e., $\tilde{X}_Q$) can be represented in matrix notation by using the eq(6.12) as

$$\tilde{X}_Q = X\left(\sum_{i=0}^{M-1} P_i^T W_{N,IFFT}^T G_i^T\right) \tag{6.13}$$

The massive MIMO-UFMC signal (i.e., $\tilde{X}_Q$) is passed through the channel with channel impulse response $H(l) \in \mathbb{C}^{U \times B}$, where $l = 0, 1...L_{ch} - 1$. Then the received matrix at the receiver is denoted by Y_Q of $[U \times (N + L + L_{ch} - 2)]$ dimension. The m^{th} column of the output matrix Y_Q is expressed as

$$Y_Q = \sum_{l=0}^{L_{ch}-1} \sqrt{\frac{P_T}{U}} H(l) \tilde{X}_Q(:, m - l) + w_m \tag{6.14}$$

where w_m is the AWGN with mean and noise variance of zero and one, respectively.

6.4 Non-linear constant-envelope precoding for 1-bit DACs

The design of optimal precoders in the downlink is the most challenging task since the precoders reduce the MUI while enhancing the array gain to the intended user equipment. This optimization problem is addressed by employing nonlinear precoders, which reduce the mean square error (MSE) between received and transmitted symbol vectors. Also, the usage of 1-bit DACs simplifies the hardware design of the proposed massive MIMO based UFMC system. Let $\left|x^2\right| = P_{ant} = \frac{S}{BN},\ x \in \tilde{X}_Q$, where P_{ant} represents the per antenna transmit power.

For $Q < \infty$, the d^{th} element $\left(d = 0, ..., 2^Q - 1\right)$ of the set $\tilde{X}_Q$ is expressed by $(P_{ant})^{\frac{1}{2}}\, e^{j(\pi+2\pi d)/2^Q}$, where 2^Q denotes the number of phases of the transmitted signal at each antenna. For $Q = \infty$, $\tilde{X}_\infty = \left\{x \in \mathbb{C} : |x|^2 = P_{ant}\right\}$. In 2-phase-bit case (i.e., $Q = 2$), the in-phase and quadrature components of the transmitted signal are produced independently by a pair of 1-bit-DAC as shown below

$$\varrho\,(z) = \sqrt{\frac{P_{ant}}{2}}\,(sgn\,(\Re\,\{z\}) + j sgn\,(\Im\,\{z\})) \tag{6.15}$$

where $\varrho\,(.)$ denotes the quantized mapping function.

The MSE of the u^{th} UE on the k^{th} sub-carrier is defined as the average of square of the error between received and transmitted symbol vectors and it is mathematically represented below.

$$MS\,E_{u,k} = E_{w_{u,k}}\left[\left|s_{u,k} - \beta_a \hat{y}_{u,k}\right|^2\right].$$

Here, β_a ($\beta_a \in \mathbb{R}^+$) is a constant and denotes the precoded factor. The vector $\hat{y}_{u,k}$ represents the u^{th} element of the estimated received signal vector of the k^{th} sub-carrier. The MSE over the U user equipments is obtained by summing the MSE of the each UE over all the subcarriers and is given by

$$\sum_{u=1}^{U}\sum_{k\in I_c} MS\,E_{u,k} = \sum_{k\in I_c} E_{\hat{w}_k}\left[\|s_k - \beta_a \hat{y}_k\|_2^2\right] \tag{6.16}$$

$$= \sum_{k\in I_c}\left[\left\|s_k - \beta_a \hat{H}_k \hat{x}_k\right\|_2^2\right] + \beta_a^2 US\,N_0 \tag{6.17}$$

The MSE of the U user equipments in optimal precoding problem (PP) is defined as follows

$$(PP)\begin{cases} \min\limits_{X\in X_Q^{B\times N}, \beta_a\in\mathbb{R}^+} & \sum\limits_{k\in I_c}\left[\left\|s_k - \beta_a \hat{H}_k \hat{x}_k\right\|_2^2\right] + \beta_a^2 US\,N_0 \\ \text{subject to} & X = \hat{X} F_H^N \end{cases} \tag{6.18}$$

where F_H^N is the $N \times N$ IFFT matrix that satisfies the condition, i.e., $FF_H^N = I_N$.

Since there is an average power constraint on the constant envelope signals, the condition (i.e., $\|\text{vec}(X)\|_\infty^2 = P_{ant}$) must be satisfied. Then the precoding problem (PP) in eq(6.18) can be modified by considering $\gamma_a = BUNN_0$ and it is given below.

$$\begin{aligned} \min_{X \in X_Q^{B\times N}, \beta_a \in \mathbb{R}^+} \quad & \sum_{k \in I_c} \left[\left\| s_k - \beta_a \hat{H}_k \hat{x}_k \right\|_2^2 \right] + \beta_a^2 \gamma_a \|\text{vec}(X)\|_\infty^2 \\ \text{subject to} \quad & X = \hat{X} F_H^N \end{aligned} \tag{6.19}$$

Also, the above problem is simplified by neglecting the non-convex constraints X ($X \in X_Q^{B\times N}$) and by assuming $\hat{B} = \beta_a \hat{X}$. Then the non-convex problem in eq(6.19) is converted to convex problem. Now, the convex problem is denoted by $\left(Pl_\infty^2\right)$ and can be mathematically represented as given in eq(6.20).

$$\left(Pl_\infty^2\right) \min_{\hat{B} \in \mathbb{C}^{B\times N}} \quad \sum_{k \in I_c} \left[\left\| s_k - \beta_a \hat{H}_k \hat{b}_k \right\|_2^2 \right] + \gamma_a \left\| \text{vec}\left(\hat{B} F_H^N \right) \right\|_\infty^2 \tag{6.20}$$

Here, the vector $\hat{b}_k$ is k^{th} column of the matrix $\hat{B}$. The matrices $\hat{B}^{Pl_\infty^2}$ and $\beta_a^{Pl_\infty^2}$ are the optimal solutions to the convex problem $\left(Pl_\infty^2\right)$. The desired matrix $X^{Pl_\infty^2}$ is obtained by converting the matrix $\hat{B}^{Pl_\infty^2}$ to time-domain and mapping the resultant matrix to the set $X_Q^{B\times N}$.

$$X^{Pl_\infty^2} = \varrho\left(\hat{B}^{Pl_\infty^2} F_N^H \right) \tag{6.21}$$

For 2-phase bit (i.e., $Q = 2$), the convex problem $\left(Pl_\infty^2\right)$ is simplified to hold the condition that is expressed as

$$\|\text{vec}(X)\|_\infty^2 = 2\|\text{vec}(X)\|_{\widetilde{\infty}}^2 \tag{6.22}$$

Then the convex optimization problem $\left(Pl_\infty^2\right)$ is given as below.

$$\left(Pl_{\widetilde{\infty}}^2\right) \min_{\hat{B} \in \mathbb{C}^{B\times N}} \quad \sum_{k \in I_c} \left[\left\| s_k - \beta_a \hat{H}_k \hat{b}_k \right\|_2^2 \right] + 2\gamma_a \left\| \text{vec}\left(\hat{B} F_H^N \right) \right\|_\infty^2 \tag{6.23}$$

6.4.1 Proposed SQUID-UFMC precoding

The convex optimization problems are solved efficiently by employing iterative Douglas-Rachford splitting (DRS) scheme. They are represented in the form of closed convex functions,

such as $f(.)$ and $g(.)$.

$$\min_{\hat{B}\in\mathbb{C}^{B\times N}} \quad f\left(\hat{B}\right)+g\left(\hat{B}\right) \tag{6.24}$$

The closed convex functions ($f(.)$ and $g(.)$) have proximal operators, which are denoted as follows:

$$\text{prox}_f(V)=\underset{\hat{B}\in\mathbb{C}^{B\times N}}{\arg\min} \quad f\left(\hat{B}\right)+\frac{1}{2}\left\|\hat{B}-V\right\|_F^2 \tag{6.25}$$

$$\text{prox}_g(V)=\underset{\hat{B}\in\mathbb{C}^{B\times N}}{\arg\min} \quad g\left(\hat{B}\right)+\frac{1}{2}\left\|\hat{B}-V\right\|_F^2 \tag{6.26}$$

The DRS is an iterative technique and can solve the convex optimization problems of the form represented in eq(6.24) by doing iterations for $t=1,2....,T_{max}$. Here, T_{max} represents the maximum number of iterations of the SQUID precoder and the procedure is described below.

$$\hat{A}^{(t)}=\text{prox}_f\left(2\hat{B}^{(t-1)}-\hat{C}^{(t-1)}\right) \tag{6.27}$$

$$\hat{B}^{(t)}=\text{prox}_g\left(\hat{A}^{(t)}+\hat{C}^{(t-1)}-\hat{B}^{(t-1)}\right) \tag{6.28}$$

$$\hat{C}^{(t)}=\hat{A}^{(t)}+\hat{C}^{(t-1)}-\hat{B}^{(t)} \tag{6.29}$$

Then, the SQUID-UFMC precoder is used to support UFMC waveform, arbitrary constant envelope alphabets, and oversampling DACs. The proposed SQUID-UFMC precoder solves the convex optimization problems $\left(Pl_\infty^2\right)$ and $\left(Pl_{\widetilde{\infty}}^2\right)$ by performing iterations. Let us assume the convex function $f\left(\hat{B}\right)$ as $f\left(\hat{B}\right)=\sum_{k\in I_c}\left\|s_k-\hat{H}_k\hat{b}_k\right\|_2^2$ for both optimization problems $\left(Pl_\infty^2\right)$ and $\left(Pl_{\widetilde{\infty}}^2\right)$, the convex function $g\left(\hat{B}\right)$ as $g\left(\hat{B}\right)=\gamma_a\left\|\text{vec}\left(\hat{B}F_N^H\right)\right\|_\infty^2$ for the optimization problem $\left(Pl_\infty^2\right)$, and $g\left(\hat{B}\right)$ as $g\left(\hat{B}\right)=\gamma_a\left\|\text{vec}\left(\hat{B}F_N^H\right)\right\|_{\widetilde{\infty}}^2$ for the optimization problem $\left(Pl_{\widetilde{\infty}}^2\right)$.

The proximal operator for convex function $f(.)$ in eq(6.25) is independent in the columns of the matrix $\hat{B}$. Therefore, the $\hat{A}^{(t)}$ in eq(6.27) is calculated for information subcarriers and guard subcarriers independently. The k^{th} column of $\hat{A}^{(t)}$ for guard subcarriers (i.e., $k\in G_c$) can be obtained as $a_k^{(t)}=2\hat{b}_k^{(t-1)}-\hat{c}_k^{(t-1)}$ and the k^{th} column of $\hat{A}^{(t)}$ for information subcarriers (i.e., $k\in I_c$) can be determined as

$$a_k^{(t)}=\left(\hat{H}_k^H+\frac{1}{2}I_B\right)^{-1}\left(\hat{H}_k^H s_k+\hat{b}_k^{(t-1)}-\frac{1}{2}\hat{c}_k^{(t-1)}\right) \tag{6.30}$$

The eq(6.30) can be written in a simplified form as

$$a_k^{(t)}=\left(I_B-J_k\hat{H}_k\right)\left(2\hat{b}_k^{(t-1)}-\hat{c}_k^{(t-1)}\right)+d_k \tag{6.31}$$

Algorithm 1: Determination of proximal operator (u) for the squared infinity norm (l_∞^2)

Inputs: $z \in \mathbb{R}^N$,$\lambda \in (0, \infty)$
$o \leftarrow \text{abs}(z)$
$e \leftarrow \text{sort}(o, \text{'descending'})$
For $k = 1, 2, ..., N$ do
$c_k \leftarrow \frac{1}{2\lambda+k} \sum_{i=1}^{k} e_i$
end for
$\delta_a \leftarrow max\{0, max_k\{c_k\}\}$
For $k = 1, 2, ..., N$ do
$u_k \leftarrow min\{o_k, \delta_a\}\, sgn(z_k)$
end for
return u

where the vector $a_k^{(t)}$ and the vector $c_k^{(t)}$ are the k^{th} columns of $\hat{A}^{(t)}$ and $\hat{C}^{(t)}$, respectively. The matrix J_k ($J_k \in \mathbb{C}^{B\times U}$) and the vector d_k ($d_k \in \mathbb{C}^B$) can be defined as given below.

$$J_k = \hat{H}_k^H \left(\hat{H}_k \hat{H}_k^H + \frac{1}{2} I_U\right)^{-1} \tag{6.32}$$

$$d_k = 2\left(\hat{H}_k^H s_k - J_k \hat{H}_k \hat{H}_k^H s_k\right) \tag{6.33}$$

Next, the proximal operator for convex function $g(.)$ in eq(6.26) can be determined by considering $\lambda > 0$ and modifying the proximal operator in eq(6.28) as

$$u = \text{prox}_{\lambda l_\infty^2}(z) = \underset{u\in\mathbb{R}^N}{\arg\min} \quad \lambda \|u\|_\infty^2 + \frac{1}{2}\|z - u\|_2^2 \tag{6.34}$$

The proximal operator u can be calculated by employing Algorithm 1. Later, the convex optimization problems $\left(Pl_\infty^2\right)$ and $\left(Pl_{\bar{\infty}}^2\right)$ are solved by employing the iterative scheme that is described in Algorithm 2.

Algorithm 2 (SQUID-UFMC): Determine J_k and d_k for information subcarriers (i.e., $k \in I_c$) from eq(6.32) and eq(6.33), respectively. Initialize the matrices $\hat{C}^{(0)} = 0_{B\times N}$ and $\hat{B}^{(0)} = 0_{B\times N}$. Subsequently, calculate the following quantities at each iteration $t = 1, 2, ...T$.

$$a_k^{(t)} = \begin{cases} R_k\left(2\hat{b}_k^{(t-1)} - \hat{c}_k^{(t-1)}\right) + d_k, & \text{if } k \in I_c. \\ 2\hat{b}_k^{(t-1)} - \hat{c}_k^{(t-1)}, & \text{if } k \in G_c \end{cases} \tag{6.35}$$

$$\hat{B}^{(t)} = \text{prox}_g\left(\hat{A}^{(t)} + \hat{C}^{(t-1)} - \hat{B}^{(t-1)}\right) F_N \tag{6.36}$$

$$\hat{C}^{(t)} = \hat{A}^{(t)} + \hat{C}^{(t-1)} - \hat{B}^{(t)} \tag{6.37}$$

Where $R_k = \left(I_B - J_k \hat{H}_k\right)$. The $\text{prox}_g(.)$ in eq(6.36) is determined using Algorithm 1. After the final iteration, $\hat{B}^{(T)} F_N^H$ is quantized to the constant envelope alphabet $X_Q^{B\times N}$ to get the massive MIMO-UFMC signal $X^{(T)}$ at the transmitter.

6.5 Proposed piecewise linear companding scheme

The massive MIMO-UFMC signal contains peak amplitudes, average amplitudes, and small amplitudes. The companding transform reduces the PAPR of the proposed system by employing PLC scheme.

In the proposed PLC scheme, the original signal is companded based on the peak amplitude. It linearly transforms the signals with amplitudes that are close to the peak amplitude and clips the signals with amplitudes that are over the peak amplitude. The small amplitudes (i.e., $\left|\tilde{X}\right| \leq \alpha_1$) are transmitted directly and the average amplitudes (i.e., $\alpha_1 < \left|\tilde{X}\right| \leq \alpha_2$) are transformed linearly by using the companding factor ρ, whereas the large amplitudes (i.e., $\left|\tilde{X}\right| > \alpha_2$) are clipped to reduce the peak power of the system.

The peak amplitude (i.e., α_2) can be expressed in terms of σ_x and $PAPR_{preset}$ (i.e., $\alpha_2 = \sigma_x 10^{PAPR_{preset}/20}$). Based on the value of α_2, the minimum amplitude α_1 is determined. The companding transform of the proposed PLC scheme is given below.

$$t(x) = \begin{cases} x, & \text{if } |x| \leqslant \alpha_1 \\ \rho x + (1-\rho)\,\alpha_2, & \text{if } \alpha_1 < |x| \leqslant \alpha_2, \\ sgn(x)\,\alpha_2 & \text{if } |x| > \alpha_2 \end{cases} \tag{6.38}$$

Here, the $sgn(x)$ denotes the signum function.

6.5.1 No decompanding (NDC)

The received signal with no decompanding offers better BER performance than the received signal with decompanding at the receiver. The companded signal t_n^c is the combination of distorted MU massive MIMO-UFMC signal and the companding noise component q_n and is described as

$$t_n^c = \psi \tilde{X} + q_n \tag{6.39}$$

where ψ denotes attenuation factor and is expressed as [31]

$$\psi = \frac{E\left\{t_n \tilde{X}^*\right\}}{E\left\{\tilde{X}\tilde{X}^*\right\}} = \frac{1}{\sigma^2}\int_0^\infty xt\,(x)\, f_{|\tilde{X}|}dx \tag{6.40}$$

The average power of the t_n^c signal is calculated as

$$P_{t_n^c} = P_{\psi\tilde{X}} + P_{q_n} = \psi^2 P_{\tilde{X}} + P_{q_n} \tag{6.41}$$

In companding operation, the average power of the t_n^c signal and the average power of the $\tilde{X}$ signal are kept at the same level.

$$P_{t_n^c} = P_{\tilde{X}} \tag{6.42}$$

$$\psi^2 P_{\tilde{X}} + P_{q_n} = P_{\tilde{X}} \tag{6.43}$$

$$P_{q_n} = P_{\tilde{X}}(1 - \psi^2) \tag{6.44}$$

It can be concluded from eq(6.44) that the average power of the noise component q_n will be small when $\psi < 1$. Then the received signal y_n at the receiver with channel noise w_n is given as

$$y_n = t_n^c + w_n \tag{6.45}$$

The recovered signal $\tilde{X}'$ after decompanding at the receiver side is

$$\tilde{X}' = \upsilon y_n + q_n^c \tag{6.46}$$

substituting $\upsilon = \frac{1}{\psi}$ and $q_n^c = -\frac{q_n}{\psi}$ in eq(6.46) gives $\tilde{X}'$

$$\tilde{X}' = \frac{1}{\psi}\left(t_n^c + w_n\right) + q_n^c = \frac{t_n^c + w_n}{\psi} - \frac{q_n}{\psi} = \tilde{X} + \frac{w_n}{\psi} \tag{6.47}$$

It is noticed that from eq(6.47), the received signal with decompanding amplifies channel noise as w_n changes from w_n to $\frac{w_n}{\psi}$. Whereas the equivalent noise without decompanding is represented as the combination of companding noise and the channel noise. Hence, the equivalent noise with and without decompanding can be given as $\frac{w_n}{\psi}$ and $w_n + q_n$, respectively.

The attenuation factor is found to be 0.99, which is close to one. Hence, we conclude from eq(6.47), that the proposed PLC scheme provides little companding noise, thus resulting in attaining better BER characteristics when decompanding is not applied at the receiver.

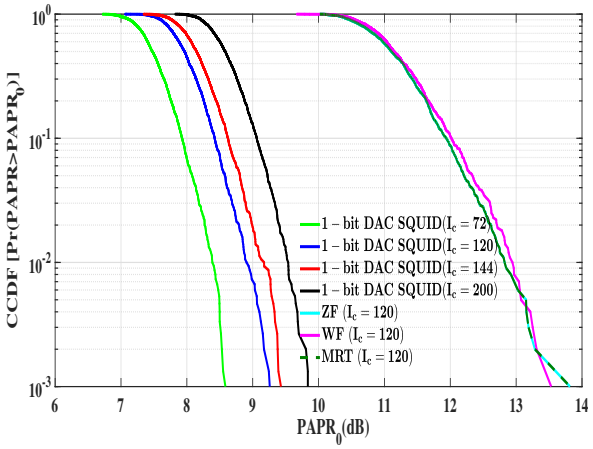

Figure 6.3: Comparison of PAPR performance of the proposed quantized MU massive MIMO-UFMC system with SQUID precoder for different number of subcarriers and various precoding schemes.

6.6 Performance evaluation

In this section, the performance of the proposed UFMC based MU massive MIMO is evaluated in terms PAPR and BER. Simulations are carried out by considering the 128 base station antennas (i.e., $B = 128$) at the BS and 8 user equipments (i.e., $U = 8$) at the receiver. Also, the UFMC parameters, such as number of sub-bands, number of sub-carriers in each sub-band, filter length, and the size of FFT are considered as 8, 15, 20, and 512, respectively. The PAPR performance of the proposed quantized UFMC based MU massive MIMO system for different subcarriers (i.e., 72, 120, 144, and 200) is illustrated in Fig. 6.3. The proposed quantized SQUID precoder offers better PAPR reduction when 72 subcarriers are incorporated. Moreover, Fig. 6.3 shows the PAPR performance of the ZF, MRT, and WF precoding schemes for I_c=120. It is observed from Fig. 6.3 that the PAPR values of the proposed system model with ZF, MRT, WF, and SQUID precoding at CCDF of 10^{-3} are 13.8 dB, 13.8 dB, 13.5 dB, and 9.2 dB, respectively. Since the PAPR of the proposed system model with SQUID precoding is least among all the schemes, the proposed SQUID precoding offers better PAPR reduction when compared to ZF, MRT, and WF precoding schemes.

The PAPR of the proposed system is further reduced by employing a PLC scheme. As there is a trade-off between PAPR and BER, optimum companding parameter (i.e., ρ) has to be chosen carefully in the design of companding schemes. The threshold parameters α_1 and α_2 are 20.2 mV and 67.2 mV, respectively. The CCDF performance of the PLC scheme for different values of ρ is depicted in Fig. 6.4. It is shown in Fig. 6.4 that the PAPR values of the proposed PLC scheme are 5.15 dB, 4.5 dB, 5.15 dB, 4.95 dB, and 4.5 dB at $\rho = 0.3$, $\rho =$

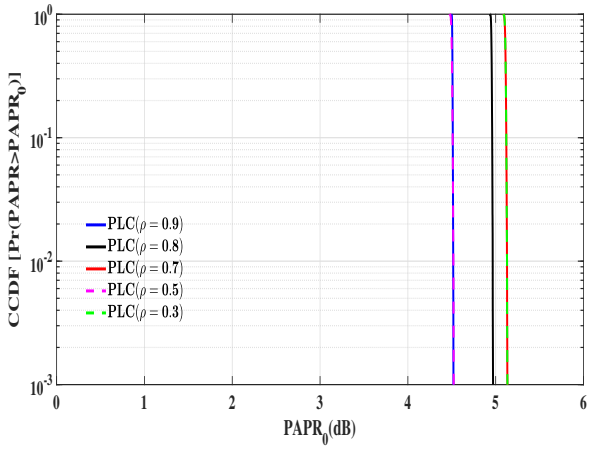

Figure 6.4: PAPR performance of the proposed quantized MU massive MIMO-UFMC system with SQUID precoder for the proposed PLC technique on various values of ρ.

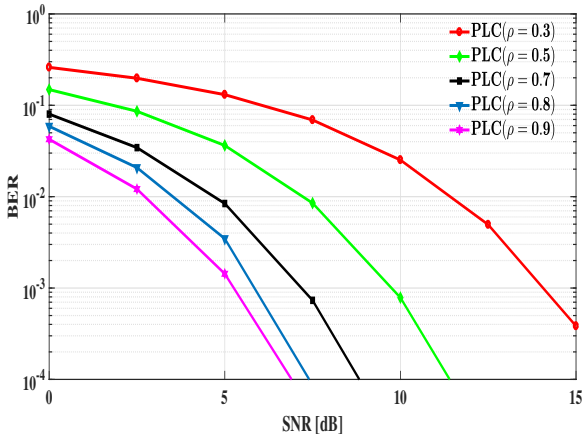

Figure 6.5: Variation of BER curves of the proposed quantized MU massive MIMO-UFMC system with SQUID precoder for the proposed PLC scheme with no decompanding on different values of ρ.

0.5, $\rho = 0.7$, $\rho = 0.8$, and $\rho = 0.9$, respectively. Hence, it is concluded that as ρ increases PAPR decreases. However, the proposed PLC offers better PAPR reduction when $\rho = 0.9$ and $\rho = 0.5$. Therefore, it is necessary to find the optimum value of ρ that can attain better BER performance. The BER characteristics of the quantized UFMC based massive MIMO with PLC scheme for different values of ρ are illustrated in Fig. 6.5. It shows that minimum BER is attained at $\rho = 0.9$. Furthermore, the PSD characteristics of the proposed model for different values of ρ are described in Fig. 6.6. It is obvious from Fig. 6.6 that as ρ increases, the PLC scheme reduces the OOB emissions. Finally, it is concluded from Fig. 6.4, Fig. 6.5, and Fig. 6.6 that the ρ of 0.9 offers better PAPR, BER, and PSD performance.

The CCDF performance of the proposed quantized massive MIMO-UFMC signal and various companding schemes, such as μ-law, LNST, LC, and the proposed PLC scheme at $BS = 64$

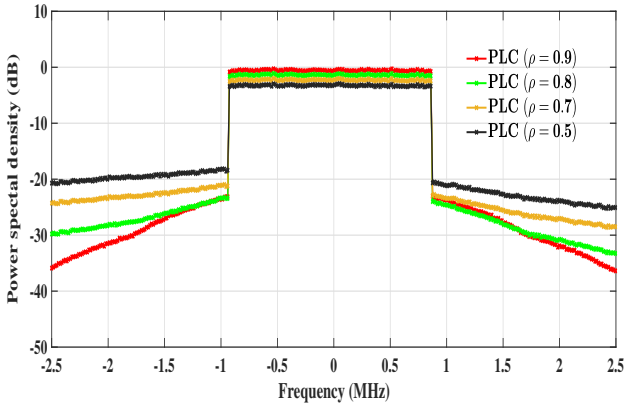

Figure 6.6: Variation of PSD curves of the proposed quantized MU massive MIMO-UFMC system with SQUID precoder for the proposed PLC scheme on various values of ρ.

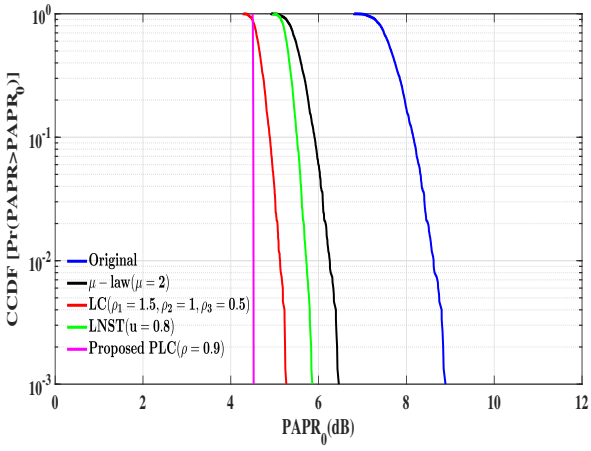

Figure 6.7: Performance comparison of PAPR curves of the proposed massive MIMO-UFMC signal, LNST, LC, and the proposed PLC schemes for QPSK by considering $BS = 64$ and $U = 8$.

and $U = 8$ are presented in Fig. 6.7. The proposed PLC scheme provides improved PAPR performance than other companding transforms and original massive MIMO-UFMC signal without companding.

The CCDF performance of the proposed quantized massive MIMO-UFMC signal and various companding schemes, such as μ-law, LNST, LC, and the proposed PLC scheme at $BS = 128$ and $U = 8$ are presented in Fig. 6.8. The μ-law, LNST, and LC schemes offer better PAPR reduction than the massive MIMO-UFMC signal. Moreover, the proposed PLC scheme provides improved PAPR performance than other companding transforms and original massive MIMO-UFMC signal without companding. Hence, the proposed 1-bit DAC quantized massive MIMO-UFMC signal with PLC scheme can be used in power-efficient applications.

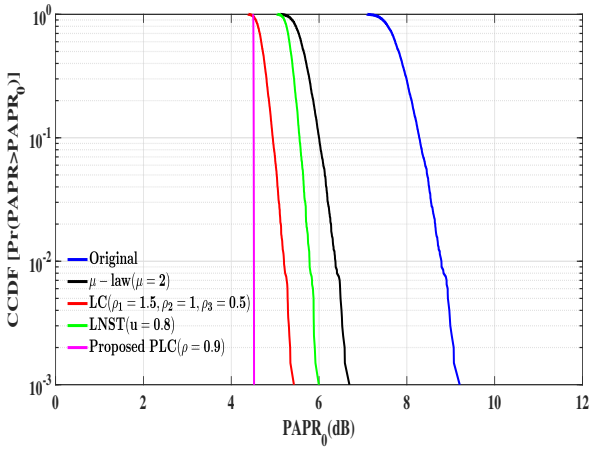

Figure 6.8: Comparison of PAPR performance of the proposed massive MIMO-UFMC signal, μ-law, LNST, LC, and the proposed PLC scheme for QPSK by considering $BS = 128$ and $U = 8$.

Table 6.1: PAPR values of quantized massive MIMO-UFMC signal and various companding transforms

	Quantized massive MIMO-UFMC signal without companding	μ-law ($\mu = 2$)	LNST ($u = 0.8$)	LC ($\rho_1 = 1.5$, $\rho_2 = 1$, $\rho_3 = 0.5$)	Proposed PLC ($\rho = 0.9$)
PAPR in dB at CCDF = 10^{-3}	9.2	6.69	6.0	5.42	4.5

Table 6.2: Improvement of PAPR reduction of various companding techniques with the quantized massive MIMO-UFMC

	μ-law ($\mu = 2$)	LNST ($u = 0.8$)	LC ($\rho_1 = 1.5$, $\rho_2 = 1$, $\rho_3 = 0.5$)	Proposed PLC ($\rho = 0.9$)
PAPR in dB at CCDF = 10^{-3}	2.51	3.2	3.7	4.7

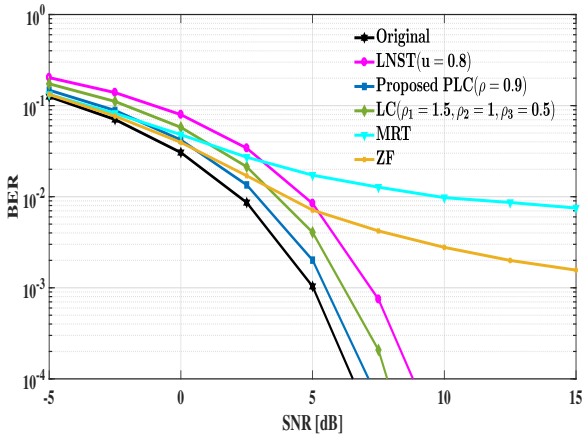

Figure 6.9: BER curves of the proposed nonlinear SQUID precoding 1-bit quantized massive MIMO-UFMC signal and various companding schemes for QPSK.

The PAPR values of the proposed 1-bit quantized DAC massive MIMO-UFMC and several companding transforms are depicted in Table 6.1. It is obvious from Table 6.1 that the 1-bit quantized DAC massive MIMO-UFMC, μ-law, LNST, LC, and the proposed PLC schemes provide 9.2 dB, 6.69 dB, 6.0 dB, 5.42 dB, and 4.5 dB, respectively.

The improvement of PAPR reduction of several companding transforms with reference to massive MIMO-UFMC without companding is illustrated in Table 6.2. In comparison with massive MIMO -UFMC signal, the μ-law, LNST, LC, and the proposed PLC schemes provide improvements of 2.51 dB, 3.2 dB, 3.7 dB, and 4.7 dB, respectively.

The BER curves of the massive MIMO-UFMC signal, LNST, LC, and the proposed PLC schemes for QPSK are illustrated in Fig. 6.9. It is confirmed from Fig. 6.9 that the proposed nonlinear 1-bit SQUID precoder provides better BER performance than linear quantized 1-bit ZF precoder. Moreover, the proposed PLC transform offers better BER characteristics than LC and LNST schemes. The proposed PLC without decompanding provides a slight degradation in BER when compared to the massive MIMO-UFMC signal without companding. Table 6.3 illustrates the BER analysis at SNR of 10^{-3} for the massive MIMO-UFMC signal, LNST, LC, and the proposed PLC scheme. Additionally, it provides the comparison of BER characteristics of the proposed quantized massive MIMO-UFMC SQUID precoded signal with the massive MIMO SQUID precoded signal and massive MIMO with symbol scaling approach [32]. It is concluded from Table 6.3 that the proposed model offers improved BER performance when compared to the state-of-art schemes.

The BER curves of the proposed massive MIMO-UFMC and the proposed massive MIMO-UFMC model with various companding schemes, such as LNST, LC, μ-law, and the

Table 6.3: Comparison of SNR values of the proposed model without companding, various companding schemes, and massive MIMO with SQUID and symbol scaling methods

	massive MIMO-UFMC SQUID without companding	LNST (u=0.8)	LC (ρ_1=1.5, ρ_2=1, ρ_3=0.5)	Proposed PLC (ρ=0.9)	Massive MIMO-SQUID precoding [32]	Massive MIMO-symbol scaling [32]
SNR in dB at BER=10^{-4}	6.5	8.8	7.8	7	7	8.5

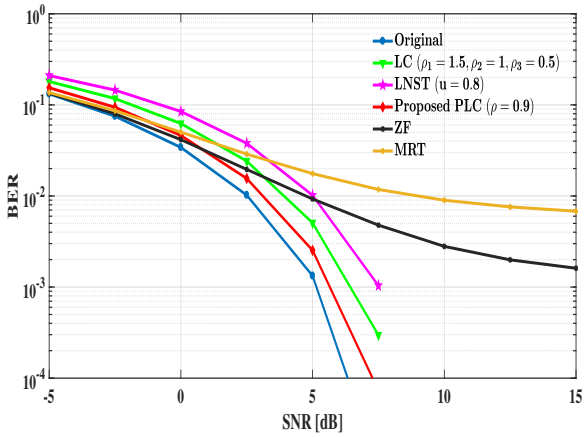

Figure 6.10: BER curves of the proposed nonlinear SQUID precoding 1-bit quantized massive MIMO-UFMC signal and various companding schemes for QPSK with SSPA.

proposed PLC are analyzed by including a solid state power amplifier with p_a of 2 and IBO of 5 dB, as illustrated in Fig. 6.10. The SSPA is one of the widely accepted models of HPA and is more advantageous due to the utilization of Gallium Arsenide (GaAs) device technology. It is concluded from Fig. 6.10 that the performance does not change much even in the presence of SSPA.

The BER curves of the massive MIMO-UFMC signal, LNST, LC, and the proposed PLC schemes for 8-PSK and 16-QAM are illustrated in Fig. 6.11 and Fig. 6.12, respectively. The proposed nonlinear SQUID precoding 1-bit quantized massive MIMO-UFMC with PLC transform offers better BER characteristics than LC and LNST schemes.

The PSD characteristics of the proposed massive MIMO-UFMC model and the proposed massive MIMO-UFMC model with various companding schemes, such as LNST, LC, μ-law, and the proposed PLC are described in Fig. 6.13. The proposed model with PLC offers less side-lobe levels than other companding schemes, whereas the conventional μ-law produces both OOB and in-band distortions.

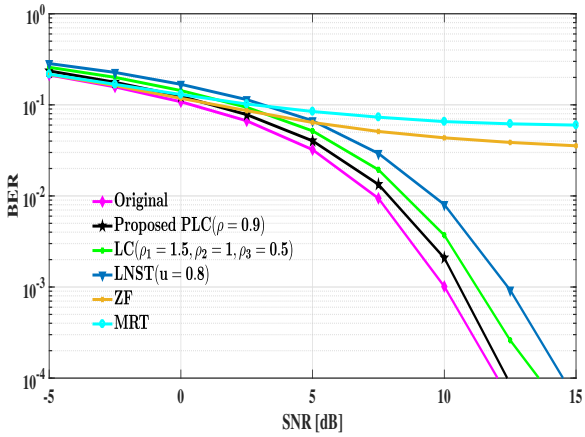

Figure 6.11: BER curves of the proposed nonlinear SQUID precoding 1-bit quantized massive MIMO-UFMC signal and various companding schemes for 8-PSK.

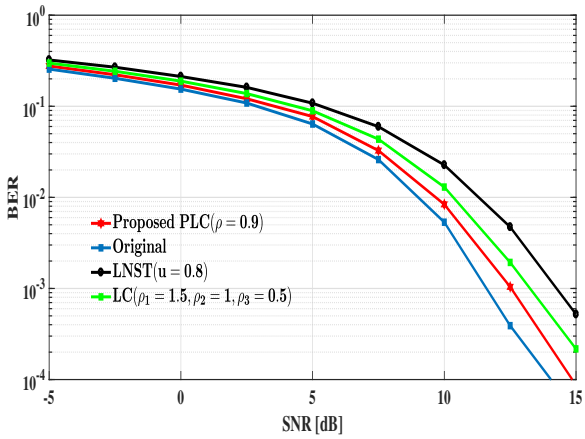

Figure 6.12: BER curves of the proposed nonlinear SQUID precoding 1-bit quantized massive MIMO-UFMC signal and various companding schemes for 16-QAM.

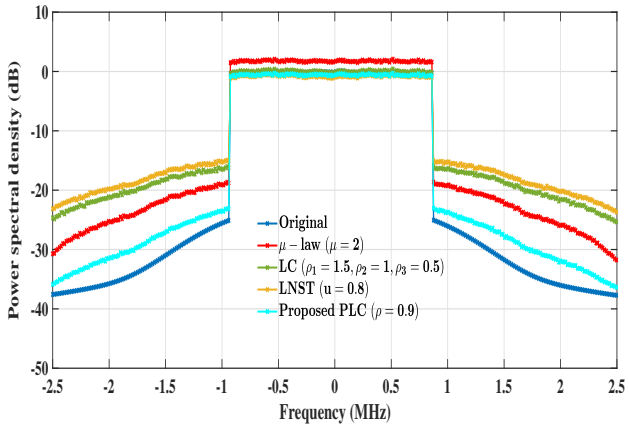

Figure 6.13: PSD curves of the proposed nonlinear SQUID precoding 1-bit quantized massive MIMO-UFMC signal and various companding schemes.

Table 6.4: Comparison of performance analysis of the proposed schemes with the state-of-art schemes

Companding Transform	PAPR reduction improvement at CCDF=10^{-3}	Additional SNR required at BER=10^{-3}	net-gain (PAPR reduction improvement-Additional SNR)
LC (ρ_1=1.5,ρ_2=1,ρ_3=0.5)	3.7	1.1	2.6
LNST (u=0.8)	3.2	2.1	1.1
Proposed PLC (ρ=0.9)	4.7	0.5	4.2
ALC (M=1,s=1.2,v=1.8) [116]	4.7	1.7	3
EC (d=0.7) [116]	4.8	1.9	2.9

The performance analysis of the proposed quantized massive MIMO-UFMC with PLC scheme is compared with the literature, as shown in Table 6.4. The proposed PLC transform is compared with EC and amplitude-limiting companding (ALC) of OFDM system. The net gain of the quantized massive MIMO-UFMC with PLC scheme is 4.2 dB, which is higher than other companding transforms.

6.7 Conclusion

In this contribution, we have proposed quantized MU precoding and companding schemes for PAPR reduction of massive MIMO-UFMC system. Also, a nonlinear phase-quantized low resolution SQUID precoder, which reduces the MUI and enhances the power efficiency of the massive MIMO-UFMC system, has been proposed. The SQUID-UFMC precoder is an iterative scheme that solves the convex optimization problems effectively. Simulation results confirm that the proposed UFMC based massive MIMO system with 1-bit SQUID precoder provides better PAPR reduction. Besides, the use of 1-bit DACs simplifies the hardware design of the proposed massive MIMO based UFMC system. Also, the nonlinear precoders minimize the MSE between the transmitted symbols and received symbols. Hence, the BER characteristics of the proposed UFMC based massive MIMO system with 1-bit nonlinear SQUID precoder outperform linear 1-bit ZF and MRT precoders. Additionally, a PLC scheme that further reduces the PAPR of the proposed UFMC based massive MIMO system with 1-bit SQUID precoder has been proposed. Simulation results show that 1-bit quantized massive MIMO-UFMC with the proposed PLC scheme provides enhanced PAPR reduction of 4.7 dB, which is higher than LNST and LC schemes. Moreover, the proposed PLC scheme offers better BER characteristics than LNST and LC schemes. The theoretical analysis has confirmed that the proposed PLC scheme without decompanding provides better BER characteristics than with decompanding.

Finally, it has been concluded that the proposed MU precoding with PLC scheme improves the energy efficiency of the UFMC based massive MIMO systems.

Chapter 7

Conclusions and Future Scope

7.1 Conclusions

The thesis mainly reports the performance analysis of the UFMC system. Initially, channel estimation has been employed to analyze the performance of UFMC system in terms of MSE and BER. A comb type pilot structure has been employed to insert the pilots in all UFMC symbols. Afterwards, LS and MMSE estimation techniques have been employed to estimate and compensate the channel at the receiver structure. The interpolation techniques, such as linear and spline have been applied to estimate the channel at data subcarriers. The estimation accuracy of LS technique is poor as MSE is inversely proportional to SNR. Since LS method is simple, it is widely used for channel estimation. Whereas MMSE provides better accuracy when compared to LS technique. However, the computational complexity of MMSE is high due to the requirement of knowledge of channel statistics (KCS) parameters. Finally, it is concluded that the proposed UFMC system with channel estimation offers better BER performance when compared to UFMC system without channel estimation.

An exponential companding scheme, which transforms rayleigh distributed UFMC signals into uniform distribution, has been presented for UFMC system. Simulation results have illustrated that EC technique provides better PAPR reduction with degradation in BER when compared to original UFMC signal and μ-law scheme. Further, we have proposed a new NCT called "modified exponential companding", which alters the large and small amplitudes of UFMC signals depending on two companding levels based on a threshold parameter. Simulation results have proven that MEC-NDC scheme provides improved BER of 9.1×10^{-4} at SNR=15 dB than

EC technique. Moreover, by properly choosing companding factors d_1, d_2, and α, the system becomes more flexible and can be used in various applications. The theoretical analysis has proven that the proposed MEC scheme with no decompanding operation offers an enhanced BER performance than with decompanding at the receiver. Furthermore, by properly choosing the clipping ratio of 1.5, an optimal hybrid scheme provides enhanced PAPR reduction of 8.02 dB and the net gain of 7.72 dB. In addition to this, the BER performance of various companding techniques has been analyzed over a multipath fading channel. Moreover, the experimental results show that a significant PAPR reduction has been attained by using the proposed hybrid scheme. Finally, it is concluded that the proposed hybrid schemes improve the efficiency of the UFMC system performance.

A hybrid transform that combines the NCT based on error function and clipping technique has been proposed for UFMC system. Moreover, the performance evaluation of various NCTs have been presented. The simulations have shown that the proposed hybrid transform with CR of 1.6 offers improved PAPR reduction of 8.1 dB. Also, the proposed hybrid transform with CR of 1.4 provides enhanced PAPR reduction of 8.5 dB with a slight degradation in BER when compared to the μ-law and the companding scheme based on error function. Additionally, proper selection of various factors, such as β_1, β_2, and CR ensure the system flexibility and more freedom. Besides, the proposed hybrid scheme with CR of 1.4 offers enhanced net gain of 8.9 dB. The theoretical study has confirmed that the proposed hybrid scheme without decompanding provides better BER characteristics than with decompanding at the UFMC receiver. Also, the performance of the proposed hybrid schemes and various companding transforms have been investigated by considering the HPA. Besides, the BER characteristics of several companding transforms have been evaluated over a multipath rician channel. Additionally, the experimental outcomes describe that better PAPR reduction has been achieved by employing the proposed hybrid transform. It has been concluded that the proposed hybrid technique enhances the performance of UFMC system.

A joint pilot-based time domain CE with hybrid PAPR reduction scheme has been proposed for UFMC system. In the proposed time domain CE, the CSI, which has been employed to enhance the performance of CE, is obtained in advance. Moreover, the proposed CE does not need the length of UFMC symbol to be much larger than the maximum delay spread of the channel. Hence, the computational complexity of the proposed time domain CE is less and adaptable to rapid channel variations. Also, LC scheme that improves the PAPR performance with more design flexibility by using two inflexion points has been proposed. Simulation results show that the proposed LC scheme offers improved PAPR reduction of 6.2 dB at a CCDF of 10^{-4} and the BER is 0.3875×10^{-4} at a SNR of 14 dB. Moreover, a hybrid scheme with

proper clipping ratio has been proposed. The proposed LC+clipping with a CR of 1.4 offers improved PAPR reduction of 8.8 dB and the net gain of 7.3 dB. Besides, the proposed hybrid transforms have been compared with the DFT-ARCT and ICF-ENC schemes. Additionally, the proposed time domain CE with hybrid scheme has been validated and the experimental results have concluded that the PAPR performance has been improved by employing the proposed hybrid method. Eventually, it is concluded that the proposed channel estimation along with PAPR reduction method enhances the performance of UFMC system.

A quantized MU precoding and companding schemes for PAPR reduction of massive MIMO-UFMC system has been proposed. Also, a nonlinear phase-quantized low resolution SQUID precoder, which reduces the MUI and enhances the power efficiency of the massive MIMO-UFMC system, has been proposed. The SQUID-UFMC precoder is an iterative scheme that solves the convex optimization problems effectively. Simulation results confirm that the proposed UFMC based massive MIMO system with 1-bit SQUID precoder provides better PAPR reduction. Besides, the use of 1-bit DACs simplifies the hardware design of the proposed massive MIMO based UFMC system. Also, the nonlinear precoders minimize the MSE between the transmitted symbols and received symbols. Hence, the BER characteristics of the proposed UFMC based massive MIMO system with 1-bit nonlinear SQUID precoder outperform linear 1-bit ZF and MRT precoders. Additionally, a PLC scheme that further reduces the PAPR of the proposed UFMC based massive MIMO system with 1-bit SQUID precoder has been proposed. Simulation results show that 1-bit quantized massive MIMO-UFMC with the proposed PLC scheme provides enhanced PAPR reduction of 4.7 dB, which is higher than LNST and LC schemes. Moreover, the proposed PLC scheme offers better BER characteristics than LNST and LC schemes. The theoretical analysis has confirmed that the proposed PLC scheme without decompanding provides better BER characteristics than with decompanding. Finally, it is concluded that the proposed MU precoding with PLC scheme improves the energy efficiency of the UFMC based massive MIMO systems.

7.2 Future scope

In this thesis, various channel estimation schemes and PAPR reduction schemes have been employed for UFMC system. Moreover, the performance of UFMC based massive MIMO has been analyzed. This work can be further extended as follows.

- Joint channel estimation and noise variance estimation in UFMC can be investigated.

- PAPR reduction in UFMC systems for massive MIMO applications using different coding techniques can be investigated.
- Impact of carrier frequency offset on different PAPR reduction techniques can be investigated.
- Further, there are many aspects of UFMC signals not addressed in this thesis that would be worth investigating.

References

[1] W. Y. Y. Yong Soo Cho, Jaekwon Kim and C. G. Kang, "MIMO-OFDM Wireless Communications with MATLAB," *John Wiley and Sons (Asia) Pte Ltd.*, 2010.

[2] J. Bingham, "Multicarrier modulation for data transmission: an idea whose time has come," *IEEE Communications Magazine*, vol. 28, no. 5, pp. 5–14, 1990.

[3] J. Bingham, " ADSL, VDSL, and Multicarrier Modulation ," *John Wiley and Sons, Inc., New York* ., 2000.

[4] G. Cherubini, E. Eleftheriou, and S. Olcer, "Filtered multitone modulation for very high-speed digital subscriber lines," *IEEE Journal on Selected Areas in Communications*, vol. 20, no. 5, pp. 1016–1028, 2002.

[5] T. Wang, J. G. Proakis, and J. R. Zeidler, "Interference Analysis of Filtered Multitone Modulation Over Time-Varying Frequency- Selective Fading Channels," *IEEE Transactions on Communications*, vol. 55, no. 4, pp. 717–727, 2007.

[6] Y. Wu and W. Y. Zou, "Orthogonal frequency division multiplexing: a multi-carrier modulation scheme", *IEEE Transactions on Consumer Electronics*, vol. 41, no. 3, pp. 392–399, 1995.

[7] A. R. S. Bahai and B. R. Saltzberg, " Multi-Carrier Digital Communications:Theory and Applications of OFDM ," *New York: Kluwer Academic Publishers.*, 2002.

[8] R. van Nee and R. Prasad, " OFDM for Wireless Multimedia Communications:," *Artech House.*, 2000.

[9] T. Hwang, C. Yang, G. Wu, S. Li, and G. Ye Li, "OFDM and Its Wireless Applications: A Survey," *IEEE Transactions on Vehicular Technology*, vol. 58, no. 4, pp. 1673–1694, 2009.

[10] J. G. Andrews, S. Buzzi, W. Choi, S. V. Hanly, A. Lozano, A. C. K. Soong, and J. C. Zhang, "What Will 5G Be?" *IEEE Journal on Selected Areas in Communications*, vol. 32, no. 6, pp. 1065–1082, 2014.

[11] G. Wunder, P. Jung, M. Kasparick, T. Wild, F. Schaich, Y. Chen, S. T. Brink, I. Gaspar, N. Michailow, A. Festag, L. Mendes, N. Cassiau, D. Ktenas, M. Dryjanski, S. Pietrzyk, B. Eged, P. Vago, and F. Wiedmann, "5GNOW: non-orthogonal, asynchronous waveforms for future mobile applications," *IEEE Communications Magazine*, vol. 52, no. 2, pp. 97–105, 2014.

[12] Y. Liu, X. Chen, Z. Zhong, B. Ai, D. Miao, Z. Zhao, J. Sun, Y. Teng, and H. Guan, "Waveform design for 5G networks: Analysis and comparison," *IEEE Access*, vol. 5, pp. 19 282–19 292, 2017.

[13] R. Nissel, S. Schwarz, and M. Rupp, "Filter Bank Multicarrier Modulation Schemes for Future Mobile Communications," *IEEE Journal on Selected Areas in Communications*, vol. 35, no. 8, pp. 1768–1782, 2017.

[14] F. Schaich and T. Wild, "Waveform contenders for 5G-OFDM vs. FBMC vs. UFMC," in *2014 6th International Symposium on Communications, Control and Signal Processing (ISCCSP)*, 2014, pp. 457–460.

[15] H. Nam, M. Choi, S. Han, C. Kim, S. Choi, and D. Hong, "A New Filter-Bank Multicarrier System With Two Prototype Filters for QAM Symbols Transmission and Reception," *IEEE Transactions on Wireless Communications*, vol. 15, no. 9, pp. 5998–6009, 2016.

[16] B. Farhang-Boroujeny, "OFDM Versus Filter Bank Multicarrier," *IEEE Signal Processing Magazine*, vol. 28, no. 3, pp. 92–112, 2011.

[17] S. Wei, H. Li, W. Zhang, and W. Cheng, "A Comprehensive Performance Evaluation of Universal Filtered Multi-Carrier Technique," *IEEE Access*, vol. 7, pp. 81 429–81 440, 2019.

[18] X. Chen, L. Wu, Z. Zhang, J. Dang, and J. Wang, "Adaptive modulation and filter configuration in universal filtered multi-carrier systems," *IEEE Transactions on Wireless Communications*, vol. 17, no. 3, pp. 1869–1881, 2018.

[19] V. Vakilian, T. Wild, F. Schaich, S. Ten Brink, and J. F. Frigon, "Universal-filtered multi-carrier technique for wireless systems beyond LTE," *2013 IEEE Globecom Workshops*, pp. 223–228, 2013.

[20] F. Schaich, T. Wild, and Y. Chen, "Waveform contenders for 5G - Suitability for short packet and low latency transmissions," *IEEE Vehicular Technology Conference*, vol. 2015-January, pp. 1–5, 2014.

[21] F. Schaich and T. Wild, "Relaxed synchronization support of universal filtered multi-carrier including autonomous timing advance," in *2014 11th International Symposium on Wireless Communications Systems (ISWCS)*, 2014, pp. 203–208.

[22] T. Wild, F. Schaich, and Y. Chen, "5G air interface design based on Universal Filtered (UF)-OFDM," vol. 2014, 08 2014, pp. 699–704.

[23] H. Cho and Y. Yan and G. Chang and X. Ma,"Asynchronous multi-user uplink transmissions for 5G with UFMC waveform," *IEEE Wireless Communications and Networking Conference, WCNC*, pp. 1–5, 2017.

[24] X. Wang, "Channel Estimation and Equalization for 5G Wireless Communication Systems," Ph.D. dissertation, 2014.

[25] M. K. Ozdemir and H. Arslan, "Channel estimation for wireless OFDM systems," *IEEE Communications Surveys Tutorials*, vol. 9, no. 2, pp. 18–48, 2007.

[26] O. Simeone and U. Spagnolini, "Pilot-Based Channel Estimation for OFDM Systems by Tracking the Delay-Subspace," *IEEE Transactions on Wireless Communications*, vol. 3, pp. 315 – 325, 02 2004.

[27] F. Tufvesson and T. Maseng, "Pilot assisted channel estimation for OFDM in mobile cellular systems," in *1997 IEEE 47th Vehicular Technology Conference. Technology in Motion*, vol. 3, 1997, pp. 1639–1643.

[28] R. Heath and G. Giannakis, "Exploiting input cyclostationarity for blind channel identification in OFDM systems," *IEEE Transactions on Signal Processing*, vol. 47, no. 3, pp. 848–856, 1999.

[29] S. Halford and G. Giannakis, "Direct blind equalization for transmitter induced cyclostationarity," in *First IEEE Signal Processing Workshop on Signal Processing Advances in Wireless Communications*, 1997, pp. 117–120.

[30] C. Ho, B. Farhang-Boroujeny, and F. Chin, "Added pilot semi-blind channel estimation scheme for OFDM in fading channels," in *GLOBECOM'01. IEEE Global Telecommunications Conference (Cat. No.01CH37270)*, vol. 5, 2001, pp. 3075–3079 vol.5.

[31] J.-J. van de Beek, O. Edfors, M. Sandell, S. Wilson, and P. Borjesson, "On channel estimation in OFDM systems," in *1995 IEEE 45th Vehicular Technology Conference. Countdown to the Wireless Twenty-First Century*, vol. 2, 1995, pp. 815–819.

[32] O. Edfors, M. Sandell, J.-J. van de Beek, S. Wilson, and P. Borjesson, "OFDM channel estimation by singular value decomposition," *IEEE Transactions on Communications*, vol. 46, no. 7, pp. 931–939, 1998.

[33] M.-H. Hsieh and C.-H. Wei, "Channel estimation for OFDM systems based on comb-type pilot arrangement in frequency selective fading channels," *IEEE Transactions on Consumer Electronics*, vol. 44, no. 1, pp. 217–225, 1998.

[34] R. Steele, " Mobile Radio Communications, London, England: ," *Pentech Press Limited*, 1992.

[35] S. Coleri, M. Ergen, A. Puri, and A. Bahai, "Channel estimation techniques based on pilot arrangement in OFDM systems," *IEEE Transactions on Broadcasting*, vol. 48, no. 3, pp. 223–229, 2002.

[36] B. Muquet, M. de Courville, and P. Duhamel, "Subspace-based blind and semi-blind channel estimation for OFDM systems," *IEEE Transactions on Signal Processing*, vol. 50, no. 7, pp. 1699–1712, 2002.

[37] W. Yang, Y. Cai, and Y. Xun, "Semi-blind Channel Estimation for OFDM Systems," in *2006 IEEE 63rd Vehicular Technology Conference*, vol. 1, 2006, pp. 226–230.

[38] Y. Li, L. Cimini, and N. Sollenberger, "Robust channel estimation for OFDM systems with rapid dispersive fading channels," *IEEE Transactions on Communications*, vol. 46, no. 7, pp. 902–915, 1998.

[39] Y. Li, "Pilot-symbol-aided channel estimation for OFDM in wireless systems," *IEEE Transactions on Vehicular Technology*, vol. 49, no. 4, pp. 1207–1215, 2000.

[40] K. F. Lee and D. B. Williams, "Pilot-Symbol-Assisted Channel Estimation for Space-Time Coded OFDM Systems," *EURASIP Journal on Applied Signal Processing*, vol. 2002, p. 374703, Dec. 2002.

[41] F. Said and H. Aghvami, "Linear two dimensional pilot assisted channel estimation for OFDM systems," in *6th IEE Conference on Telecommunications 1998 (Conf. Publ. No. 451)*, 1998, pp. 32–36.

[42] M. Garcia, S. Zazo, and J. Paez Borrallo, "Pilot patterns for channel estimation in OFDM," *Electronics Letters*, vol. 36, pp. 1049 – 1050, 07 2000.

[43] J. K. Moon and S. I. Choi, "Performance of channel estimation methods for OFDM systems in a multipath fading channels," *IEEE Transactions on Consumer Electronics*, vol. 46, no. 1, pp. 161–170, 2000.

[44] P. Hoeher, S. Kaiser, and P. Robertson, "Two-dimensional pilot-symbol-aided channel estimation by Wiener filtering," in *1997 IEEE International Conference on Acoustics, Speech, and Signal Processing*, vol. 3, 1997, pp. 1845–1848.

[45] J.-W. Choi and Y.-H. Lee, "Optimum pilot pattern for channel estimation in OFDM systems," *IEEE Transactions on Wireless Communications*, vol. 4, no. 5, pp. 2083–2088, 2005.

[46] M. Zhu, A. B. Awoseyila, and B. G. Evans, "Low complexity time-domain channel estimation for OFDM using training symbols," in *2010 5th Advanced Satellite Multimedia Systems Conference and the 11th Signal Processing for Space Communications Workshop*, 2010, pp. 203–207.

[47] A. M. Khan, V. Jeoti, and M. A. Zakariya, "Pilot based Pre FFT channel estimation for OFDM systems in rayleigh-fading channel," in *2014 5th International Conference on Intelligent and Advanced Systems (ICIAS)*, 2014, pp. 1–5.

[48] D. Kong, D. Qu, and T. Jiang, "Time Domain Channel Estimation for OQAM-OFDM Systems: Algorithms and Performance Bounds," *IEEE Transactions on Signal Processing*, vol. 62, no. 2, pp. 322–330, 2014.

[49] W. Rong, J. Cai, and X. Yu, "Low-complexity PTS PAPR reduction scheme for UFMC systems," *Cluster Computing*, vol. 20, no. 4, pp. 3427–3440, 2017.

[50] M. El Ghzaoui, A. Hmamou, J. Foshi, and J. Mestoui, "Compensation of Non-linear Distortion Effects in MIMO-OFDM Systems Using Constant Envelope OFDM for 5G Applications," *Journal of Circuits, Systems and Computers*, vol. 29, no. 16, p. 2050257, 2020.

[51] F. M. H. A. F. J. Mestoui Jamal, El Ghzaoui Mohammed, "Performance analysis of CE-OFDM-CPM Modulation using MIMO system over wireless channels," *Journal of Ambient Intelligence and Humanized Computing*, vol. 11, no. 10, pp. 3937–3945, 2020.

[52] H. G. Myung and D. J. Goodman, "Single carrier FDMA: A new air interface for long term evolution," *Chichester, UK: John Wiley & Sons, Ltd.*, 2008.

[53] S. L. Miller and R. J. O'Dea, "Peak power and bandwidth efficient linear modulation," *IEEE Trans. Commun.*, vol. 46, pp. 1639–1648, 1998.

[54] S. C. Cripps, "RF power amplifiers for wireless communications," *Artech House*, 2006.

[55] C. Rapp, "Effects of HPA-Nonlinearity on a 4-DPSK/OFDM-Signal for a Digital Sound Broadcasting System." in *Second European Conf. on Sat. Comm., 22. - 24.10.91, Liege, Belgium.*, 1991, pp. 179–184.

[56] Y. Rahmatallah and S. Mohan, "Peak-to-average power ratio reduction in OFDM systems: A survey and taxonomy," *IEEE Communications Surveys and Tutorials*, vol. 15, no. 4, pp. 1567–1592, 2013.

[57] T. Jiang and Y. Wu, "An Overview: Peak-to-Average Power Ratio Reduction Techniques for OFDM Signals," *IEEE Transactions on Broadcasting*, vol. 54, no. 2, pp. 257–268, 2008.

[58] S. H. Han and J. H. Lee, "An overview of peak-to-average power ratio reduction techniques for multicarrier transmission," *IEEE Wireless Communications*, vol. 12, no. 2, pp. 56–65, 2005.

[59] X. Zhu, W. Pan, H. Li, and Y. Tang, "Simplified approach to optimized iterative clipping and filtering for PAPR reduction of OFDM signals," *IEEE Transactions on Communications*, vol. 61, no. 5, pp. 1891–1901, 2013.

[60] K. R. Panta and J. Armstrong, "Effects of Clipping on the Error Performance of OFDM in Frequency Selective Fading Channels," *IEEE Transactions on Wireless Communications*, vol. 3, no. 2, pp. 668–671, 2004.

[61] R. van Nee and A. de Wild, "Reducing the peak-to-average power ratio of OFDM," *VTC '98. 48th IEEE Vehicular Technology Conference. Pathway to Global Wireless Revolution (Cat. No.98CH36151)*, vol. 3, pp. 2072–2076 vol.3, 1998.

[62] X. Huang, J. Lu, J. Chuang, and J. Zheng, "Companding transform for the reduction of peak-to-average power ratio of OFDM signals," in *IEEE VTS 53rd Vehicular Technology Conference, Spring 2001. Proceedings (Cat. No.01CH37202)*, vol. 2, 2001, pp. 835–839 vol.2.

[63] X. Huang, J. Lu, J. Zheng, J. Chuang, and J. Gu, "Reduction of peak-to-average power ratio of OFDM signals with companding transform," *Electronics Letters*, vol. 37, pp. 506 – 507, 05 2001.

[64] H.-B. Jeon, J.-S. No, and D.-J. Shin, "A New PAPR Reduction Scheme Using Efficient Peak Cancellation for OFDM Systems," *IEEE Transactions on Broadcasting*, vol. 58, no. 4, pp. 619–628, 2012.

[65] J. H. S.H. MÃijller, "OFDM with reduced peak-to-average power ratio by optimum combination of partial transmit sequences," *Electronics Letters*, vol. 33, pp. 368–369(1), February 1997.

[66] S. H. Han and J. Lee, "PAPR reduction of OFDM signals using a reduced complexity PTS technique," *Signal Processing Letters, IEEE*, vol. 11, pp. 887 – 890, 12 2004.

[67] Y. A. Jawhar, L. Audah, M. A. Taher, K. N. Ramli, N. S. M. Shah, M. Musa, and M. S. Ahmed, "A Review of Partial Transmit Sequence for PAPR Reduction in the OFDM Systems," *IEEE Access*, vol. 7, pp. 18 021–18 041, 2019.

[68] J.-H. Wen, S.-H. Lee, and C.-H. Cheng, "SLM-based PAPR reduction method using partial data circulation and side information insertion in OFDM systems," *International Journal of Communication Systems*, vol. 22, no. 1, pp. 87–100, 2009.

[69] J.-H. Wen, S.-H. Lee, and C.-H. Cheng, "SLM-based PAPR reduction method using partial data circulation and side information insertion in OFDM systems," *Int. J. Communication Systems*, vol. 22, pp. 87–100, 01 2009.

[70] J. Tellado, "Peak to average ratio reduction for multi-carrier modulation," *PhD Thesis, Stanford University, Stanford, CA, USA*, 1999.

[71] J.-C. Chen and C.-K. Wen, "PAPR Reduction of OFDM Signals Using Cross-Entropy-Based Tone Injection Schemes," *IEEE Signal Processing Letters*, vol. 17, no. 8, pp. 727–730, 2010.

[72] V. Sandeep and S. Anuradha, "Novel Peak-to-Average Power Ratio Reduction Methods for OFDM/OQAM Systems," *ETRI Journal*, vol. 38, no. 6, pp. 1124–1134, 2016.

[73] H. Liang, H.-C. Chu, and C.-B. Lin, "Peak-to-average power ratio reduction of orthogonal frequency division multiplexing systems using modified tone reservation techniques," *International Journal of Communication Systems*, vol. 29, no. 4, pp. 748–759, 2016.

[74] J. Davis and J. Jedwab, "Peak-to-mean power control in OFDM, Golay complementary sequences, and Reed-Muller codes," *IEEE Transactions on Information Theory*, vol. 45, no. 7, pp. 2397–2417, 1999.

[75] Y. Louet and A. Le Glaunec, “Peak-factor reduction in ofdm by reed-muller channel coding a new soft decision decoding algorithm,” in *2000 10th Mediterranean Electrotechnical Conference. Information Technology and Electrotechnology for the Mediterranean Countries. Proceedings. MeleCon 2000 (Cat. No.00CH37099)*, vol. 2, 2000, pp. 872–875.

[76] K. Anoh, C. Tanriover, B. Adebisi, and M. Hammoudeh, “A New Approach to Iterative Clipping and Filtering PAPR Reduction Scheme for OFDM Systems,” *IEEE Access*, vol. 6, pp. 17 533–17 544, 2018.

[77] G. Chen, R. Ansari, and Y. Yao, “Improved Peak Windowing for PAPR Reduction in OFDM,” in *VTC Spring 2009 - IEEE 69th Vehicular Technology Conference*, 2009, pp. 1–5.

[78] J. Song and H. Ochiai, “Performance Analysis for OFDM Signals With Peak Cancellation,” *IEEE Transactions on Communications*, vol. 64, no. 1, pp. 261–270, 2016.

[79] A. F. Almutairi, M. Al-Gharabally, and A. Krishna, “Performance Analysis of Hybrid Peak to Average Power Ratio Reduction Techniques in 5G UFMC Systems,” *IEEE Access*, vol. 7, pp. 80 651–80 660, 2019.

[80] A. Mattsson, G. Mendenhall, and T. Dittmer, “Comments on: "Reduction of peak-to-average power ratio of OFDM system using a companding technique",” *IEEE Transactions on Broadcasting*, vol. 45, no. 4, pp. 418–419, 2002.

[81] T. Jiang and G. Zhu, “Nonlinear companding transform for reducing peak-to-average power ratio of OFDM signals,” *IEEE Transactions on Broadcasting*, vol. 50, no. 3, pp. 342–346, 2004.

[82] Y. Wang, J. H. Ge, L. H. Wang, and B. Ai, “Nonlinear companding transform using hyperbolic tangent function in OFDM systems,” *2012 International Conference on Wireless Communications, Networking and Mobile Computing, WiCOM 2012*, 2012.

[83] Xiao Huang, Jianhua Lu, Junli Zheng, K. B. Letaief, and Jun Gu, “Companding transform for reduction in peak-to-average power ratio of OFDM signals,” *IEEE Transactions on Wireless Communications*, vol. 3, no. 6, pp. 2030–2039, Nov 2004.

[84] V. Sudha and D. Sriram Kumar, “Low complexity PAPR reduction in SLM-OFDM system using time domain sequence separation,” *Alexandria Engineering Journal*, vol. 57, no. 4, pp. 3111–3115, 2018.

[85] J.-Y. Woo, K.-S. Lee, D.-J. Shin, Y.-J. Cho, and J.-S. No, “Low-complexity PTS schemes using OFDM signal rotation and pre-exclusion of phase rotating vectors,” *IET Communications*, vol. 10, no. 5, pp. 540–547, 2016.

[86] B. Krongold and D. Jones, "Papr reduction in ofdm via active constellation extension," *IEEE Transactions on Broadcasting*, vol. 49, pp. 258 – 268, 10 2003.

[87] B. Krongold and D. Jones, "An active-set approach for OFDM PAR reduction via tone reservation," *IEEE Transactions on Signal Processing*, vol. 52, no. 2, pp. 495–509, 2004.

[88] S. H. Han, J. Cioffi, and J. H. Lee, "Tone injection with hexagonal constellation for peak-to-average power ratio reduction in OFDM," *IEEE Communications Letters*, vol. 10, no. 9, pp. 646–648, 2006.

[89] E. Hong, H. Kim, K. Yang, and D. Har, "Pilot-Aided Side Information Detection in SLM-Based OFDM Systems," *IEEE Transactions on Wireless Communications*, vol. 12, no. 7, pp. 3140–3147, July 2013.

[90] E. G. Larsson, O. Edfors, F. Tufvesson, and T. L. Marzetta, "Massive MIMO for next generation wireless systems," *IEEE Communications Magazine*, vol. 52, no. 2, pp. 186–195, 2014.

[91] H. Q. Ngo, E. G. Larsson, and T. L. Marzetta, "Energy and Spectral Efficiency of Very Large Multiuser MIMO Systems," *IEEE Transactions on Communications*, vol. 61, no. 4, pp. 1436–1449, 2013.

[92] D. Mercer, " Global connected and IoT device forecast update ," *Strategy Analytic research services, Tech. Rep*, 2019.

[93] A. L. d. A. T. M. Daniel C. Araujo, Taras Maksymyuk, "Massive MIMO: survey and future research topics," *IET Communications*, vol. 10, pp. 1938–1946(8), October 2016.

[94] M. A. M. Albreem, "5G wireless communication systems: Vision and challenges," in *2015 International Conference on Computer, Communications, and Control Technology (I4CT)*, 2015, pp. 493–497.

[95] T. L. Marzetta and H. Q. Ngo, " Fundamentals of massive MIMO ," *Cambridge University Press*, 2016.

[96] D. Jiang and B. Natarajan, "Hybrid precoding with compressive sensing based limited feedback in massive MIMO systems," *Transactions on Emerging Telecommunications Technologies*, vol. 27, no. 12, pp. 1672–1678, 2016.

[97] L. Zhao, K. Zheng, H. Long, and H. Zhao, "Performance analysis for downlink massive MIMO system with ZF precoding," *Transactions on Emerging Telecommunications Technologies*, vol. 25, no. 12, pp. 1219–1230, 2014.

[98] H. Yang and T. L. Marzetta, "Performance of Conjugate and Zero-Forcing Beamforming in Large-Scale Antenna Systems," *IEEE Journal on Selected Areas in Communications*, vol. 31, no. 2, pp. 172–179, 2013.

[99] S. K. Mohammed and E. G. Larsson, "Constant-Envelope Multi-User Precoding for Frequency-Selective Massive MIMO Systems," *IEEE Wireless Communications Letters*, vol. 2, no. 5, pp. 547–550, 2013.

[100] S. K. Mohammed and E. G. Larsson, "Per-Antenna Constant Envelope Precoding for Large Multi-User MIMO Systems," *IEEE Transactions on Communications*, vol. 61, no. 3, pp. 1059–1071, 2013.

[101] C. Mollen, E. G. Larsson, and T. Eriksson, "Waveforms for the Massive MIMO Downlink: Amplifier Efficiency, Distortion, and Performance," *IEEE Transactions on Communications*, vol. 64, no. 12, pp. 5050–5063, 2016.

[102] J. Guerreiro, R. Dinis, and P. Carvalho, "Use of 1-bit digital-to-analogue converters in massive MIMO systems," *Electronics Letters*, vol. 52, 02 2016.

[103] A. K. Saxena, I. Fijalkow, and A. L. Swindlehurst, "On one-bit quantized ZF precoding for the multiuser massive MIMO downlink," in *2016 IEEE Sensor Array and Multichannel Signal Processing Workshop (SAM)*, 2016, pp. 1–5.

[104] A. K. Saxena, I. Fijalkow, and A. L. Swindlehurst, "Analysis of One-Bit Quantized Precoding for the Multiuser Massive MIMO Downlink," *IEEE Transactions on Signal Processing*, vol. 65, no. 17, pp. 4624–4634, 2017.

[105] S. Jacobsson, G. Durisi, M. Coldrey, T. Goldstein, and C. Studer, "Quantized Precoding for Massive MU-MIMO," *IEEE Transactions on Communications*, vol. PP, 10 2016.

[106] C. Studer and E. G. Larsson, "PAR-Aware Large-Scale Multi-User MIMO-OFDM Downlink," *IEEE Journal on Selected Areas in Communications*, vol. 31, no. 2, pp. 303–313, 2013.

[107] J.-C. Chen, C.-K. Wen, and K.-K. Wong, "Improved Constant Envelope Multiuser Precoding for Massive MIMO Systems," *IEEE Communications Letters*, vol. 18, no. 8, pp. 1311–1314, 2014.

[108] A. Brihuega, L. Anttila, and M. Valkama, "Performance comparison of constant envelope and zero-forcing precoders in multiuser massive MIMO," in *2018 IEEE Wireless Communications and Networking Conference (WCNC)*, 2018, pp. 1–6.

[109] A. Li, C. Masouros, F. Liu, and A. L. Swindlehurst, "Massive MIMO 1-Bit DAC Transmission: A Low-Complexity Symbol Scaling Approach," *IEEE Transactions on Wireless Communications*, vol. 17, no. 11, pp. 7559–7575, 2018.

[110] Jun Hou, Jianhua Ge, Dewei Zhai, and Jing Li, "Peak-to-Average Power Ratio Reduction of OFDM Signals With Nonlinear Companding Scheme," *IEEE Transactions on Broadcasting*, vol. 56, no. 2, pp. 258–262, 2010.

[111] J. Kim and Y. Shin, "An effective clipped companding scheme for PAPR reduction of OFDM signals," *IEEE International Conference on Communications*, no. 1, pp. 668–672, 2008.

[112] M. Hu, Y. Li, Y. Liu, and H. Zhang, "Parameter-adjustable piecewise exponential companding scheme for peak-to-average power ratio reduction in orthogonal frequency division multiplexing systems," *IET Communications*, vol. 8, no. 4, pp. 530–536, 2014.

[113] B. Tang, K. Qin, and H. Mei, "A Hybrid Approach to Reduce the PAPR of OFDM Signals Using Clipping and Companding," *IEEE Access*, vol. 8, pp. 18 984–18 994, 2020.

[114] Mohamed Mounir and Mohamed Bakry El Mashade, "On the selection of the best companding technique for PAPR reduction in OFDM systems," *Journal of Information and Telecommunication*, vol. 3, no. 3, pp. 400–411, 2019.

[115] "WARPLab framework." [Online]. Available: http://warpproject.org/trac/wiki/WARPLab.

[116] Z. Xing, K. Liu, B. Tang, and Y. Liu, "Novel PAPR Reduction Scheme Based on Piecewise Nonlinear Companding Transform in OFDM Systems," *IEEE Communications Letters*, vol. 24, no. 8, pp. 1757–1761, 2020.

[117] Z. Xing, K. Liu, and Y. Liu, "Low-complexity companding function design for PAPR reduction in OFDM systems," *IET Communications*, vol. 14, no. 10, pp. 1581–1587, 2020.

[118] S. A. Aburakhia, E. F. Badran, and D. A. E. Mohamed, "Linear Companding Transform for the Reduction of Peak-to-Average Power Ratio of OFDM Signals," *IEEE Transactions on Broadcasting*, vol. 55, no. 1, pp. 155–160, March 2009.

[119] A. Noll, H. Jedda, and J. Nossek, "PSK Precoding in Multi-User MISO Systems," in *WSA 2017; 21th International ITG Workshop on Smart Antennas*, 2017, pp. 1–7.

List of Publications

International Journals

1 Vijaya Durga Chintala and Anuradha Sundru, "An optimal nonlinear companding transform with clipping scheme for universal filtered multicarrier systems", **International Journal of Communication Systems**, vol. 33, no. 16, p. e4587, 2020 (SCIE-Wiley)

2 Vijaya Durga Chintala and Anuradha Sundru, "A Joint Quantized Precoding and PAPR Reduction in UFMC based Massive MIMO downlink systems", **Transactions on Emerging Telecommunications Technologies**, e4344, 2021. (SCIE-Wiley)

3 Vijaya Durga Chintala and Anuradha Sundru, "A Joint time domain channel estimation with hybrid PAPR reduction scheme in UFMC systems", **Journal of Circuits, Systems, and Computers**, (SCIE-World Scientific) (Accepted)

4 Vijaya Durga Chintala and Anuradha Sundru, "Performance Analysis of Hybrid Transform for Universal Filtered Multi Carrier System", **Mobile Networks and Applications**, (SCIE-Springer) (Under Review)

International Conferences

1 Vijaya Durga Chintala and Anuradha Sundru, "On channel estimation in universal filtered multi-carrier (UFMC) system," in **2019 PhotonIcs Electromagnetics Research Symposium (PIERS)**, pp. 3708-3713, Italy, 2019. (IEEEXplore)

2 Vijaya Durga Chintala and Anuradha Sundru, "PAPR Reduction in Universal Filtered Multicarrier Systems with Companding Transform", 3^{rd} **IEEE conference (ICAECC-2020)**, December 11-12, Bangalore, 2020. (IEEEXplore)